UNIVERSITÀ DEGLI STUDI DI TRIESTE

XXIX CICLO DEL DOTTORATO DI RICERCA IN
INGEGNERIA CIVILE

MECHANICAL CHARACTERIZATION OF CONNECTIONS IN SEISMIC RESISTANT CROSS-LAMINATED TIMBER STRUCTURES

Settore scientifico-disciplinare: ICAR/09, Tecnica delle Costruzioni

Dottorando:
Ing. **Matteo IZZI**

Coordinatore:
Prof. **Diego MICHELI**

Supervisore di Tesi:
Prof. **Massimo FRAGIACOMO**

Co-supervisore di Tesi:
Dr. **Andrea POLASTRI**

Anno Accademico 2015-2016

With four parameters I can fit an elephant,
and with five I can make him wiggle his trunk.

Attributed to Johnny von Neumann by Enrico Fermi,
as quoted by Freeman Dyson[1]

[1] Dyson F (2004) A meeting with Enrico Fermi. *Nature*, **427**: 297, doi: 10.1038/427297a.

Abstract

Cross-Laminated Timber (CLT) structures are assembled with massive timber panels that are fastened together and to the horizontal elements (the foundations or the intermediate floors) with step joints and mechanical connections. Due to the high in-plane stiffness of CLT, the dynamic behaviour of those structures (e.g. under earthquake loading) markedly depends on the connections used.

The mechanical behaviour of lateral load-resisting systems made with CLT panels and typical connection systems for CLT structures was the focus of a large body of research. Shear and tension tests were carried out on several types of wall-to-floor connections with angle brackets and hold-downs, using different nail patterns and anchoring. Furthermore, racking tests were conducted on wall systems with different layouts of connections and openings. Finally, full-scale shaking table tests were performed on multi-storey buildings, demonstrating a significant energy dissipation.

In contrast with the significant findings associated to those research projects, specific calculation methods have not yet been included either in Eurocode 5 (static design) or in Eurocode 8 (seismic design). Nowadays, the design is done using force-based calculation methods that neglect the connections stiffness and introduce some simplifications on their mechanical behaviour.

The mechanical characterization of typical connection systems for CLT structures (e.g. angle brackets and hold-downs) is an expensive and time-consuming process, requiring the execution of a large number of tests. Therefore, to limit the need of tests to a minimum, significant effort should be devoted to develop numerical models capable to predict their load-displacement response and failure mechanisms.

In the scope of this PhD thesis, an extensive test programme is carried out on nailed steel-to-timber joints in CLT. The experimental strength capacities assessed from the tests are used to verify the reliability of currently available calculation methods and to develop capacity-based design principles for nailed steel-to-timber joints in CLT (the overstrength factor and the strength degradation factor). In addition, analytical methods and numerical

models capable to predict the mechanical behaviour and the energy dissipation at different building levels (single fastener joint, wall-to-floor connection, and CLT wall system) are developed. The experimental test results obtained in previous research projects served for calibration of the non-linear analyses, used to extend the data available to configurations of technical interest. Outcome of the numerical studies provided a better understanding of the seismic behaviour of typical connections and wall systems for CLT buildings.

It is concluded that the numerical models presented within this thesis are a sound basis to investigate the seismic behaviour of CLT structures. Nevertheless, future research is required to further verify and improve these predictive models.

KEYWORDS: Cross-Laminated Timber, annular-ringed shank nail, steel-to-timber joint, mechanical connection, CLT wall system, capacity-based design, hysteretic behaviour.

Acknowledgements

Many people and organizations contributed to the successful completion of this project.

The PhD research grant was funded by the University of Trieste (through the resources of the European Social Fund) and by CNR IVALSA (San Michele all'Adige, Italy). The financial support of both organizations is gratefully acknowledged.

The study periods as a visiting scholar at the Institute of Timber Engineering and Wood Technology, Graz University of Technology (Graz, Austria), were financially supported by the COST Actions FP1004 and FP1402. The Management Committees of both COST Actions and the representatives of COST Office are acknowledged for the research grants, which contributed to a successful outcome of this study.

Firstly, I would like to thank Professor Massimo Fragiacomo and Andrea Polastri; their experience and comments were extremely precious to the outcome of the research project. They granted me great academic freedom whilst giving me the necessary guidance to not stray off course.

Professor Gerhard Schickhofer and Georg Flatscher (Graz University of Technology) are sincerely thanked; they provided all the materials used in the tests and allowed me to carry out the experimental programme in their laboratory. Their hospitality, kindness, and professional guidance are deeply appreciated.

I owe a very special 'thank you' to Chiara Bedon (University of Trieste); she provided me with valuable piece of advice that helped to steer the (many) simulations in ABAQUS. Word of thanks are extended to Giovanni Rinaldin (University of Sassari) who shared the subroutine used in such simulations.

Finally, my deepest gratitude goes to my parents Lorena and Giovanni, my sister Ilaria, and Sara. I would not be here today without their endless love and support. Grazie.

Matteo

Trieste, May 25, 2017

List of publications

INTERNATIONAL JOURNALS

Izzi M, Flatscher G, Fragiacomo M, Schickhofer G (2016) Experimental investigations and design provisions of steel-to-timber joints with annular-ringed shank nails for Cross-Laminated Timber structures. *Construction and Building Materials*, **122**: 446-457, doi: 10.1016/j.conbuildmat.2016.06.072.

Izzi M, Rinaldin G, Polastri A, Fragiacomo M (2016) Numerical modelling of joints with dowel-type fasteners. *European Journal of Wood of Wood and Wood Products* (under review).

Izzi M, Polastri A, Fragiacomo M (2017) Modelling the mechanical behaviour of typical wall-to-floor connection systems for Cross-Laminated Timber structures. *Engineering Structures* (under review).

Izzi M, Polastri A, Fragiacomo M (2017) Investigating the hysteretic behaviour of Cross-Laminated Timber wall systems depending on connection properties. *Journal of Structural Engineering* (under review).

INTERNATIONAL CONFERENCES

Izzi M, Polastri A, Fragiacomo M (2016) Advanced modelling of CLT wall systems for earthquake resistant timber structures. *3rd International Network on Timber Engineering Research (INTER) Meeting*, Graz, Austria, Paper 49-15-6.

Izzi M, Rinaldin G, Fragiacomo M, Polastri A (2016) Numerical modelling of steel-to-timber joints and connectors for CLT structures. *World Conference on Timber Engineering (WCTE)*, Vienna, Austria.

NATIONAL CONFERENCES

Izzi M, Flatscher G, Rinaldin G, Fragiacomo M, Schickhofer G (2015) Experimental tests on annular-ringed shank nails for seismic resistant Cross-Laminated Timber (CLT) structures. *16th Conference of the Italian National Association of Earthquake Engineering (ANIDIS)*, L'Aquila, Italy.

Table of contents

List of notations

Latin upper case letters

COV	Coefficient of variation
$Duct$	Ductility ratio (ratio of V_u to V_y)
E_d	Design value of an action effect
E_{diss}	Dissipated energy per full hysteresis cycle
E_{pot}	Available potential energy, according to EN 12512:2001/A1 [26]
F_{ax}	Axial withdrawal capacity of a nail
F_h	Embedding capacity of timber
F_{lat}	Lateral dowel capacity of a nailed joint
F_{max}	Load-carrying capacity (maximum load)
F_u	Ultimate load, according to EN 12512:2001/A1 [26]
F_v	Shear capacity of a nailed joint
F_y	Yield load, according to EN 12512:2001/A1 [26]
K_{ax}	Withdrawal stiffness of a nail
K_{el}	Elastic stiffness of a connection
K_h	Embedding stiffness of timber
K_{pl}	Inelastic stiffness of a connection
K_{ser}	Instantaneous slip modulus
K_θ	Bending stiffness of a nail
M_y	Yield moment of a nail
V_{max}	Displacement at maximum load (F_{max})
V_u	Displacement at ultimate load (F_u)
V_y	Displacement at yield load (F_y)

Latin lower case letters

b_{CLT}	Width of a CLT wall panel
b_l	Effective penetration depth of a joint

d	Diameter of a nail
f_{ax}	Withdrawal parameter of a nail
f_h	Embedding strength of timber
f_u	Ultimate tensile strength of a nail
f_y	Yield strength of a nail
h_{CLT}	Height of a CLT wall panel
i_{scr}	Spacing between two consecutive screws in a vertical step joint
k_{eff}	Effective factor (to account for the 'group effect' in nailed joints)
k_{mod}	Modification factor for duration of load and moisture content
k_s	Dimensionless operator, according to EN 14358 [28]
l	Beam length
l_{thr}	Threaded length of a nail shank
n	Number of tests, or number of nails connected to the same metal plate
q_v	Vertical load applied on top of a CLT wall panel
t_l	Pointside penetration depth

Greek lower case letters

α	Load inclination, with respect to the symmetry axis of a metal connector
β_{Sd}	Reduction factor for strength degradation due to cyclic loading
γ_{an}	Approximation of a design model to predict a strength property
γ_{sc}	Scatter of strength properties in monotonic tests
γ_M	Partial factor for material properties
γ_{Rd}	Overstrength factor
θ_u	Ultimate rotation
μ , $\bar{\mu}$	Average value, average value of the natural logarithm
μ_{fr}	Friction coefficient
ν_{eq}	Equivalent viscous damping ratio, according to Flatscher *et al.* [39]
ρ	Average timber density
$\bar{\sigma}$	Corrected sample standard deviation of the natural logarithm

Subscripts

$x_{B\&U}$	Strength capacity determined according to Blaß and Uibel [3]
x_{EC5}	Strength capacity determined according to EN 1995-1-1:2004/A2 [24]
x_{ETA}	Strength capacity determined according to ETA-04/0013 [30]
$x_{ö}$	Strength capacity determined according to ÖNORM B 1995-1-1 [75]
$x_{brittle}$	Brittle element in the capacity-based design method
$x_{ductile}$	Ductile element in the capacity-based design method
x_i	Property evaluated at the *i*-th analysis step of a simulation
x_k , x_{Rk}	Characteristic value of a strength capacity
x_{Rd}	Design value of a strength capacity
$F_{\#5/\#30}$	Load at the transition point between branches #5 and #30 (see Figure 4.5)
$x_{0°}$	Load evaluated parallel to the superficial lamination of a CLT panel
$x_{90°}$	Load evaluated perpendicular to the superficial lamination of a CLT panel
x_{05}	5th percentile of a property
x_{95}	95th percentile of a property
$x_{(1st)}$	Property evaluated on the 1st envelope curve of a cyclic test
$x_{(3rd)}$	Property evaluated on the 3rd envelope curve of a cyclic test

1 Introduction

1.1 RESEARCH BACKGROUND AND MOTIVATION

As a structural product, Cross-Laminated Timber (CLT) exhibits a high in-plane stiffness and linear-elastic behaviour with the tendency to fail with brittle mechanisms. Therefore, mechanical connections should be designed to resist large cyclic displacements, ensuring the necessary strength, stiffness, and energy dissipation under seismic conditions.

The increasing use of CLT for the construction of medium to high-rise structures (the so-called 'tall buildings') requires connections with excellent mechanical properties and large ductility ratios. However, results of past research projects on typical connections for CLT structures highlighted some inappropriate failure mechanisms that might limit the application of the metal connectors currently available on the market.

Improving the mechanical behaviour of the connection systems currently available on the market and developing new solutions is an expensive and time-consuming process, which requires the consideration of several factors (e.g. thickness of the metal member, number/position of nails, and anchoring) and loading cases. Therefore, to limit the need of experimental testing to a minimum, great effort should be devoted to the development of advanced numerical models capable to predict their load-displacement response and failure mechanisms.

1.2 OBJECTIVES AND SCOPE

The focus of this PhD thesis is the mechanical characterization of typical connections for seismic resistant CLT structures. The research work includes experimental tests on nailed joints in CLT, comparison with existing analytical models, implementation of simplified design principles and numerical procedures at different building levels (single fastener joint, wall-to-floor connection, and wall system), which are supported by experimental and analytical results. To achieve these objectives, several milestones must be reached:

a. Experimental testing:
   - Execution of bending tests and tension tests on single nails.

- Execution of shear tests and withdrawal tests on nailed joints in CLT.
- Assessment of their mechanical behaviour under monotonic and cyclic loads.

b. Analytical modelling:

- Definition of simplified design principles for nailed joints in CLT.
- Derivation of a simplified design method for nailed joints in CLT.
- Implementation of a reliable hysteresis model for nailed joints in CLT.

c. Numerical modelling:

- Implementation of numerical procedures for single joints and connections.
- Implementation of numerical procedures for single and segment wall systems.
- Prediction of their mechanical behaviour under monotonic and cyclic loads.

1.3 THESIS STRUCTURE

The thesis is a collection of journal articles written during the last three years of research. It consists of four chapters and a list of references. Each chapter opens with a summary on the topic under discussion and provides some information on previous research in the same field. In the subsequent sections, experimental, analytical, and numerical results are compared and discussed. To keep the overall formatting simple, the references between two or more chapters are treated like external citations, in particular: [59] refers to Chapter 2, [60] to Chapter 3 and [61] to Chapter 4.

Chapter 2 describes the outcome of a test programme on nailed steel-to-timber joints in CLT. Average and characteristic strength values are assessed from the test data. Results are compared to the values determined using the formulas prescribed in current structural design codes and recommended in literature. To fulfil the requirements of the capacity-based design, the overstrength factor and the strength degradation factor are evaluated and conservative values are recommended.

Chapter 3 presents a numerical model able to reproduce the mechanical behaviour and the failure mechanisms of joints with dowel-type fasteners; the joint is schematized as an elasto-plastic beam in a non-linear embedment with a compression-only behaviour. Shear

tests are reproduced on nailed steel-to-timber joints in CLT and results are compared to the test data published in literature, showing limited differences.

Chapter 4 focuses on the mechanical behaviour and the failure mechanisms of typical wall-to-floor connection systems for CLT structures. A numerical model is proposed, in which the metal connector and the panels where is anchored are simulated using 3D solid bodies while the nailed joints are schematized as non-linear hysteretic springs. Shear and tension tests are reproduced on typical connections with angle brackets and hold-downs. Experimental and numerical results are compared and critically discussed.

In Chapter 5, the mechanical and hysteretic behaviour of single and segmented CLT wall systems is analysed. A numerical model is proposed, where the CLT wall is modelled as a 3D solid body and the mechanical connections are schematized as non-linear springs. Typical racking tests are reproduced on a series of walls by varying the assumptions used to schematize the behaviour of the connections and their layout in the wall system. Test data and numerical predictions are compared and results are discussed.

Finally, Chapter 6 summarizes the most important findings of this research project and outlines some recommendations for future research.

2 Experimental investigations and design provisions of steel-to-timber joints with annular-ringed shank nails for Cross-Laminated Timber structures

SHORT SUMMARY

The mechanical and the hysteretic behaviour of steel-to-timber joints with annular-ringed shank nails in Cross-Laminated Timber (CLT) is investigated. These fasteners are used in CLT structures to anchor typical metal connectors, e.g. hold-downs and angle brackets, to the wall and floor panels. The experimental programme presented in this chapter was carried out at the Institute of Timber Engineering and Wood Technology, Graz University of Technology (Graz, Austria). Average and characteristic values of the experimental strength capacities are evaluated and compared with the analytical predictions determined according to the current structural design codes and literature. Furthermore, to fulfil the requirements of the capacity-based design, the overstrength factor and the strength degradation factor are evaluated and conservative values are recommended.

All the materials used in the tests were provided by Professor Gerhard Schickhofer and Georg Flatscher, who are sincerely acknowledged. Georg Flatscher is further thanked for his invaluable contribution in the planning, preparation and execution of the tests.

2.1 INTRODUCTION

Ensuring an adequate ductility and a sufficient energy dissipation are two crucial aspects when designing seismic resistant multi-storey timber buildings made of Cross-Laminated Timber (CLT) panels. As a structural product, CLT has high in-plane stiffness and linear-elastic behaviour with tendency to fail with brittle mechanisms (except for compressive stresses). Therefore, mechanical connections between adjacent walls and between wall and floor panels represent the ductile zones of CLT structures, supplying the necessary strength, stiffness and energy dissipation in seismic conditions [46].

The hysteretic behaviour of single-joints and CLT wall systems (CLT wall panel and connections) was the focus of several experimental programmes. Shear and tension tests were performed on typical metal connectors, such as hold-downs and angle brackets, and on screwed panel-to-panel connections [39, 47, 48, 64, 99]. Furthermore, racking tests performed on walls with several layouts of connections and openings [15-17, 49, 56, 80] and full-scale shaking table tests [10, 38, 55] demonstrated significant energy dissipation.

Predicting the load-carrying capacity of joints with dowel-type fasteners in CLT is more complex than for traditional sawn timber or other engineered wood products (e.g. Glued Laminated Timber). Blaß and Uibel [3] developed a calculation model for the prediction of the fastening capacity in CLT. Specific rules for joints in CLT, derived from the works of Blaß and his collaborators, are prescribed in the Austrian National Annex to Eurocode 5 [75]. However, design formulas were not included in structural design codes of any other European country.

The experimental programme presented herein aims at investigating the behaviour of steel-to-timber joints with annular-ringed shank nails in CLT. These nails are used in CLT buildings to anchor typical metal connectors (such as hold-downs and angle brackets) to the wall and floor panels. Monotonic and cyclic single fastener joint shear tests were carried out in parallel and perpendicular to the face lamination of the CLT panels while nail withdrawal tests were performed from the side face of CLT panels. Moreover, the tensile strength and the yield moment of the fastener were measured via tension and bending tests, respectively.

Mechanical properties such as strength, stiffness, ductility and equivalent viscous damping ratio were assessed as prescribed in EN 12512:2001/A1 [26] and ISO 16670 [57]. Characteristic values of the experimental strength capacities were derived according to EN 14358 [28] and were compared to the analytical predictions prescribed in the current standards [24, 30, 75] and recommended in literature [3]. Finally, the overstrength factor and the strength degradation factor were evaluated and conservative values were recommended for nailed steel-to-timber joints in CLT.

2.2 CALCULATION MODELS

The current version of Eurocode 5 [24] prescribes design rules for traditional structural products (solid timber, glued laminated timber, etc.) and fasteners (smooth nails, dowels, bolts, etc.). However, the same standard does not include any design provision for CLT and typically used metal connectors (such as angle brackets and hold-downs) requiring the use of harmonized technical specifications like the European Technical Assessments (ETAs). Some specific rules for joints in CLT were included in the Austrian National Annex to Eurocode 5 [75]. Moreover, Blaß and Uibel [3] proposed a calculation model for joints with dowel-type fasteners in CLT, where the load-carrying capacity and the failure modes are influenced by the thickness and by the embedding strength of each board layer. It should be noticed that this model was validated on CLT panels made of board layers thinner than what are used nowadays and has not been included in structural design codes of any European country to date.

The calculation models considered in the study are described in the following sub-sections. The design rules included in Eurocode 5 [24] divide the steel-to-timber joints into two groups: joints with thin metal plates (i.e. plates with thickness less than $0.5\,d$, with d diameter of the fastener) and with thick metal plates (i.e. plates with thickness greater than d). The thickness of the metal plate influences the failure mechanism of the joint. Joints with thick plates have a ductile failure mechanism where the bending capacity of the fastener is attained with two plastic hinges together with embedding of timber. Joints with thin plates have a less ductile failure mechanism where the bending capacity is attained with one plastic hinge together with embedding of timber. It must be noticed that, due to their conical-shaped cap, annular-ringed shank nails do not have such strict distinction. ETA-13/0523 [35] (Rothoblaas nails) takes into account a similar distinction between thin and thick plates; however, compared to Eurocode 5 [24], the condition of thick plate is satisfied with a much thinner plate (1.5 mm thickness if d = 4.0 mm and 3.0 mm thickness if d = 6.0 mm). On the contrary, the design provisions included in ETA-04/0013 [30] (Simpson Strong-Tie nails, like those used in this testing programme)

refer only to thick plates and can be applied to any joint regardless the thickness of the metal plate. Therefore, for the sake of clarity, the following discussions are all referred to steel-to-timber joints with thick plates, whereas joints with thin plates were not included in the study.

2.2.1 Capacity-based design approach

The application of a capacity-based design procedure to CLT structures requires the definition of specific regions that must withstand large cyclic deformations and provide a stable energy dissipation. When it comes to ductile failure of timber structures, this is achieved with proper connection design and by ensuring that no other part (less ductile or brittle) exhibits anticipated failure. However, results of past experimental programmes on typical metal connectors and CLT wall systems have highlighted some inappropriate mechanisms at the connection level that may be associated to an incorrect design of the nailed steel-to-timber joints. In particular: (*a*) in wall-to-floor connections with angle brackets, failure due to withdrawal of the nails connected to the floor panel; (*b*) in wall-to-foundation connections with angle brackets, failure due to pull-through of the anchoring bolts; and (*c*) in wall-to-floor connections with hold-downs, tensile failure of the net cross-section of the metal sheet.

Such failure mechanisms can be avoided by applying a capacity-based design approach, both at the connection level and at the wall level. Using force-based design methods, the load flow is followed from the top to the foundation of the building and design values of the action effects are determined (E_d). At the connection level, those values are used as inputs for the ductile design of the dissipative elements. In particular and again focusing on commonly used angle brackets and hold-downs, capacity-based provisions may be employed to avoid the afore-mentioned failure mechanisms and to ensure the plasticization of laterally loaded steel-to-timber joints. Once inappropriate failures at connection level are prevented, similar provisions are applied at the wall level. Here, the strength of the CLT panel (around the connections and of the entire panel

considering, e.g., openings) is designed for the overstrength of the dissipative connections considering their strength degradation for cyclic loading.

As discussed in Follesa *et al.* [42], a structural element designed in accordance with the concept of dissipative behaviour is verified at the Ultimate Limit State if:

$$E_{\mathrm{d}} \leq \beta_{\mathrm{Sd}} F_{\mathrm{Rd,ductile}} \tag{2.1}$$

with E_{d} design value of the action effects, $F_{\mathrm{Rd,ductile}}$ design strength of the ductile element and β_{Sd} reduction factor for strength degradation for cyclic loading. The design strength of the ductile element is defined as $F_{\mathrm{Rd,ductile}} = k_{\mathrm{mod}} F_{\mathrm{Rk,ductile}} / \gamma_{\mathrm{M}}$, where $F_{\mathrm{Rk,ductile}}$ is its characteristic value while k_{mod} and γ_{M} represent the modification factor for duration of load and moisture content and the partial factor for material properties, respectively. Values of $F_{\mathrm{Rk,ductile}}$ should be determined either by theoretical considerations or from experimental results in monotonic conditions. It should be noticed that Eurocode 8 [25] sets the partial factor for material properties γ_{M} equal to 1.0 for ductile elements designed in accordance with the concept of dissipative behaviour.

Once the dissipative elements are verified at Ultimate Limit State, ductile mechanisms can be ensured by designing the strength of the brittle part ($F_{\mathrm{Rd,brittle}}$) so that it is greater than or equal to the strength of the ductile part ($F_{\mathrm{Rd,ductile}}$) multiplied by an overstrength factor γ_{Rd} and divided by a reduction factor for strength degradation due to cyclic loading β_{Sd} [42]:

$$\frac{\gamma_{\mathrm{Rd}}}{\beta_{\mathrm{Sd}}} F_{\mathrm{Rd,ductile}} \leq F_{\mathrm{Rd,brittle}} \tag{2.2}$$

with $F_{\mathrm{Rd,brittle}} = k_{\mathrm{mod}} F_{\mathrm{Rk,brittle}} / \gamma_{\mathrm{M}}$, where $F_{\mathrm{Rk,brittle}}$ is the characteristic strength of the brittle member while all the other symbols have the same meaning of those used before.

The strength degradation factor β_{Sd} takes into account the impairment of strength of the dissipative element due to cyclic loading. In the present contribution it is determined based on a statistical analysis of experimental results in cyclic conditions, i.e., as the 5$^{\mathrm{th}}$ percentile of the factor determined for every single test as follows:

$$\beta_{\mathrm{Sd}} = \frac{F_{\mathrm{max(3rd)}}}{F_{\mathrm{max(1st)}}} \tag{2.3}$$

where $F_{max(1st)}$ and $F_{max(3rd)}$ signify the strength capacities measured on the first and third envelope curves, respectively. Values of $F_{max(1st)}$ and $F_{max(3rd)}$ are assessed at the 'cycle group' (which includes three consecutive cycles at the same displacement amplitude) where the peak of the first envelope curve is achieved.

The overstrength factor γ_{Rd} accounts for all the factors that may increase the strength of the ductile element (e.g. higher-than-specified material strength, strain hardening at large deformations, commercial sections larger than what resulting from the design). It is defined as the ratio of the 95th percentile of the experimental strength capacity $F_{max,95}$ (in monotonic tests) to the characteristic strength of the same element $F_{Rk,ductile}$ [63]:

$$\gamma_{Rd} = \frac{F_{max,95}}{F_{Rk,ductile}} = \frac{F_{max,95}}{F_{max,05}} \cdot \frac{F_{max,05}}{F_{Rk,ductile}} = \gamma_{sc} \cdot \gamma_{an} \tag{2.4}$$

The equation above shows that γ_{Rd} can be expressed as function of two factors. The first (γ_{sc}) accounts for the scatter of strength properties in monotonic tests and is defined as the $F_{max,95}$ over $F_{max,05}$ ratio (95th and 5th percentiles of the strength property, respectively). The second factor (γ_{an}) measures the quality of the analytical model to predict the strength property and is defined as the $F_{max,05}$ over $F_{Rk,ductile}$ ratio, where $F_{max,05}$ and $F_{Rk,ductile}$ have the same meaning of those used before. Values of γ_{an} close to one means that the analytical model provides a reliable prediction of the strength property; on the contrary, ratios far from one means an analytical prediction less representative of the characteristic experimental strength.

Equation 2.4 clearly highlights that two different cases should be considered. Firstly, when $F_{Rk,ductile}$ is determined using general rules such as those included in Eurocode 5 [24], the overstrength factor should be determined as given in Equation 2.4. In this situation the calculation model fully neglects some specific features of the ductile element (e.g. the profiled shank in threaded nails); therefore, it is important to consider both the approximation of the analytical model (γ_{an}) and scatter of strength properties (γ_{sc}). On the other hand, when distinct design rules are available or if the design process is based on characteristic strength capacities determined from test results, γ_{an} can be assumed equal to one and Equation 2.4 leads to $\gamma_{Rd} = \gamma_{sc}$.

2.2.2 Load-carrying capacity of a nailed steel-to-timber joint

Eurocode 5 [24] defines the characteristic load-carrying capacity ($F_{v,Rk}$) of a nailed steel-to-timber joint as the sum of two contributions:

$$F_{v,Rk} = F_{lat,Rk} + 0.25F_{ax,Rk} \tag{2.5}$$

The first term in Equation 2.5 signifies the lateral dowel capacity of the joint $F_{lat,Rk}$ according to the Johansen's yield theory; the second term represents the contribution due to the rope effect and is equal to 25% the withdrawal capacity of the nail $F_{ax,Rk}$. Characteristic values of $F_{lat,Rk}$ and $F_{ax,Rk}$ are obtained with theoretical considerations and by calibration on past experimental results. The contribution due to the rope effect depends upon the connector type and is taken into account at a maximum percentage of the lateral dowel capacity $F_{lat,Rk}$. For round nails with smooth shank, Eurocode 5 [24] limits the rope effect to 15% of $F_{lat,Rk}$ while for other nails it is increased up to 50% of the lateral dowel capacity. The relationship presented in Equation 2.5 is proposed also by Blaß and Uibel [3] while ETA-04/0013 [30] increases the rope effect to 60% of the withdrawal capacity.

2.2.3 Lateral dowel capacity of a nailed steel-to-timber joint

Eurocode 5 [24] and ETA-04/0013 [30] adopt the European Yield Model (EYM), originally proposed by Johansen [62], to define the lateral dowel capacity of a nailed steel-to-timber joint. An ideal rigid-plastic behaviour is assumed for both the fastener's yield moment and the embedment behaviour of timber. The equations derived from this model predict the load-carrying capacity of a single fastener joint loaded in shear depending upon its geometry, the embedding strength of timber, and the yield moment of the fastener.

The characteristic lateral dowel capacity ($F_{lat,Rk}$) of a nailed steel-to-timber joint made with a thick metal plate is defined by the lowest value among those in Equation 2.6. The derivation of the equations has been described by Hilson [53]. The equation giving the lowest load-carrying capacity identifies the actual failure mechanism.

$$F_{\text{lat,Rk}} = \min \begin{cases} f_{\text{h,k}} t_1 d & \text{(a)} \\ f_{\text{h,k}} t_1 d \left[\sqrt{2 + \dfrac{4 M_{\text{y,Rk}}}{f_{\text{h,k}} t_1^2 d}} - 1 \right] & \text{(b)} \\ 2.3 \sqrt{M_{\text{y,Rk}} f_{\text{h,k}} d} & \text{(c)} \end{cases} \tag{2.6}$$

In the previous equations, $f_{\text{h,k}}$ signifies the characteristic embedding strength of timber, t_1 indicates the penetration depth while d and $M_{\text{y,Rk}}$ denote the diameter and the characteristic yield moment of the fastener, respectively. Equation 2.6a describes a failure mechanism where the fastener behaves as a rigid element and there is only embedding of the timber member; moreover, the rope effect is not activated and has to be neglected. Equation 2.6b and 2.6c denote two failure mechanisms where the bending capacity of the fastener is attained (with one and two plastic hinges, respectively) together with embedding of the timber around the fastener. The calculation model developed by Blaß and Uibel [3] leads to formulations similar to those showed in Equation 2.6 where it is assumed that the CLT panels are manufactured with timber boards of the same density.

2.2.4 Embedding strength of timber

The embedding strength of timber depends upon several factors such as the size and cross-section shape of the fastener, the timber density and the relative orientation between applied load and timber grain [105]. Nevertheless, due to the limited size of the nail cross-section, the models discussed below do not take into the account this last variable.

Eurocode 5 [24] and ETA-04/0013 [30] define the characteristic embedding strength of timber $f_{\text{h,k}}$ depending upon the characteristic density of the timber ρ_{k} and the diameter of the fastener d; the model (Equation 2.7) was derived by Whale *et al.* [101] for a smooth nail embedded in a solid timber element without predrilled hole.

$$f_{\text{h,k}} = 0.082 \rho_{\text{k}} d^{-0.3} \tag{2.7}$$

The other two models considered in the study were derived by Uibel and Blaß [100] from the results of embedment tests in CLT panels. The first one provides a general formulation for the prediction of the embedding strength (Equation 2.8); the latter one (Equation 2.9) is used in the Austrian National Annex to Eurocode 5 [75] for profiled

nails placed in CLT and is derived from Equation 2.8 by considering a characteristic density $\rho_k = 400$ kg/m^3 :

$$f_{h,k} = 0.112 \rho_k^{1.05} d^{-0.5} \tag{2.8}$$

$$f_{h,k} = 60 d^{-0.5} \tag{2.9}$$

2.2.5 Yield moment of the nail

The yield moment of the nail is an important parameter in the design of steel-to-timber joints according to Eurocode 5 [24]. Johansen [62] assumed it as the elastic moment capacity of the circular cross-section; the possible increase of capacity associated to plastic deformations was disregarded. However, an ideal rigid-plastic behaviour was adopted in the subsequent developments of his theory.

The first model considered in the study has been proposed by Blaß and Colling [5] and defines the yield moment of the fastener as the plastic moment capacity of the circular cross-section:

$$M_{y,Rk} = f_{y,k} d^3 / 6 \tag{2.10}$$

In the previous equation the symbol $f_{y,k}$ indicates an 'equivalent' yield strength, estimated as 90% the characteristic ultimate tensile strength $f_{u,k}$ while d is the diameter of the nail. The ultimate tensile strength $f_{u,k}$ depends upon the quality of the wire from which the fastener was manufactured and has to be evaluated with experimental tests.

Based on the results of an experimental programme on joints with dowel-type fasteners, Blaß *et al.* [2] reported that most of the failures occurred for low values of the fasteners' bending angle (significantly below 45°). Therefore, the plastic capacity of the dowel's cross-section was not attained and the yield moment was lower than according to EN 409 [21]. Hence, Blaß *et al.* [2] proposed a calculation model which is currently prescribed in Eurocode 5 [24], ETA-04/0013 [30] and Blaß and Uibel [3]. The model is based on a theoretical derivation of the fastener's bending angle at a joint slip of 15 mm and defines the yield moment as given in Equation 2.11, depending upon the diameter d and a minimum tensile strength $f_{u,k} = 600$ N/mm^2.

$$M_{y,Rk} = 0.30 f_{u,k} d^{2.6} \tag{2.11}$$

Due to strain hardening and the varying effects of profiling, calculation models for threaded nails have not been derived; for a realistic joint design, the actual yield moment of those fasteners has to be determined with experimental tests, carried out as prescribed in EN 409 [21].

2.2.6 Axial withdrawal capacity

Eurocode 5 [24] and ETA-04/0013 [30] define the axial withdrawal capacity ($F_{ax,Rk}$) of a nailed joint depending upon the withdrawal parameter $f_{ax,k}$, the diameter of the fastener d and the profiled length of the shank l_{thr} :

$$F_{ax,Rk} = f_{ax,k} l_{thr} d \tag{2.12}$$

The current version of the Eurocode 5 [24] does not provide any rule for predicting the withdrawal parameter of threaded nails and the use of harmonized technical specifications is required. Specific rules for Simpson Strong-Tie connector nails have been included in ETA-04/0013 [30] and estimate $f_{ax,k}$ as in Equation 2.13, depending upon the geometry of the nail (threaded length and diameter) and the characteristic density of timber.

$$f_{ax,k} = \min \begin{cases} 6.125 \left(1 + \dfrac{1.5d}{l_{thr}}\right)\left(\dfrac{\rho_k}{350}\right) \\ \left(10.92 - 0.0158d - 0.0968 l_{thr}\right)\left(\dfrac{\rho_k}{320}\right)^2 \end{cases} \tag{2.13}$$

The other two models considered in the study were derived by Blaß and Uibel [3] for a profiled nail embedded in the side face of a CLT panel. The first one provides a general formulation for the prediction of the withdrawal capacity (Equation 2.14). The latter one (Equation 2.15) is currently included in the Austrian National Annex to Eurocode 5 [75] and is obtained from Equation 2.14 by assuming a characteristic density $\rho_k = 400$ kg/m^3.

$$F_{ax,Rk} = 0.117 d^{0.6} l_{thr} \rho_k^{0.8} \tag{2.14}$$

$$F_{ax,Rk} = 14 d^{0.6} l_{thr} \tag{2.15}$$

2.2.7 Slip modulus of a nailed joint

Eurocode 5 [24] provides a calculation model for the prediction of the instantaneous slip modulus of a timber-to-timber joint (K_{ser}). The derivation of the model is described in Ehlbeck and Larsen [18]. Therein, the instantaneous slip modulus is defined as the secant modulus of the load-displacement curve at approximately 40% of the characteristic load-carrying capacity of the joint. For nailed steel-to-timber joints, based on mechanical relationships, Eurocode 5 [24] suggests that the slip modulus of a similar timber-to-timber joint may be doubled up. The resulting model predicts the instantaneous slip modulus K_{ser} depending upon the average density of timber ρ and the diameter of the nail d:

$$K_{ser} = 2\rho^{1.5} d^{0.8} / 30 \tag{2.16}$$

2.3 EXPERIMENTAL PROGRAMME

Tests were performed using annular-ringed shank nails produced by Simpson Strong-Tie [30] (Figure 2.1a). Each nail has a total length of 60 mm and a penetration depth t_1 = 54 mm. The threaded shank, of length l_{thr} = 44 mm, increases the withdrawal strength under axial loads while the conical-shaped cap enhances the clamping to the metal plate and enforces a ductile failure mechanism with two plastic hinges. The nails are cold-formed from a steel wire with nominal diameter d = 4.0 mm; due to the profiling, the inner diameter of the threaded shank is 3.6 mm whereas the outer diameter is equal to 4.2 mm.

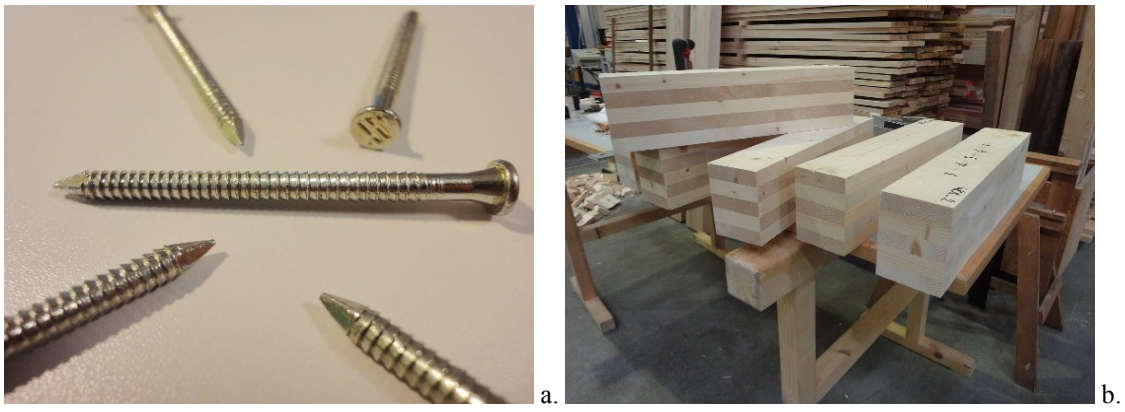

a. b.

Figure 2.1. Materials: (a) annular-ringed shank nails and (b) CLT elements used for withdrawal tests.

Solid timber panels made of five crosswise laminated board layers (CLT) and a total thickness of 134 mm (**26**-27-**28**-27-**26**) were used in the tests (Figure 2.1b). The numbers

in brackets denote the thickness of each board layer; the bold notation was used to mark the layers with boards parallel to the face lamination of the panel. As prescribed in EN 1380 [22], the panels were conditioned at 20°C and 65% relative humidity (RH) before performing the tests.

2.3.1 Tension tests and bending tests

The ultimate tensile strength and the yield moment of the fasteners were investigated with five tension tests and ten bending tests, respectively. The tension tests were carried out in displacement control until failure (Figure 2.2a); due to the small cross-section of the fastener, a thin metal pipe was placed around the nail shank to increase the clamping to the testing machine and to avoid issues with the experimental setup. The bending tests were performed in displacement control until a rotation of 45° (Figure 2.2b); the experimental setup was similar to the configuration depicted in Appendix A of EN 409 [21]. A free bending length of three times the diameter was ensured in all the tests.

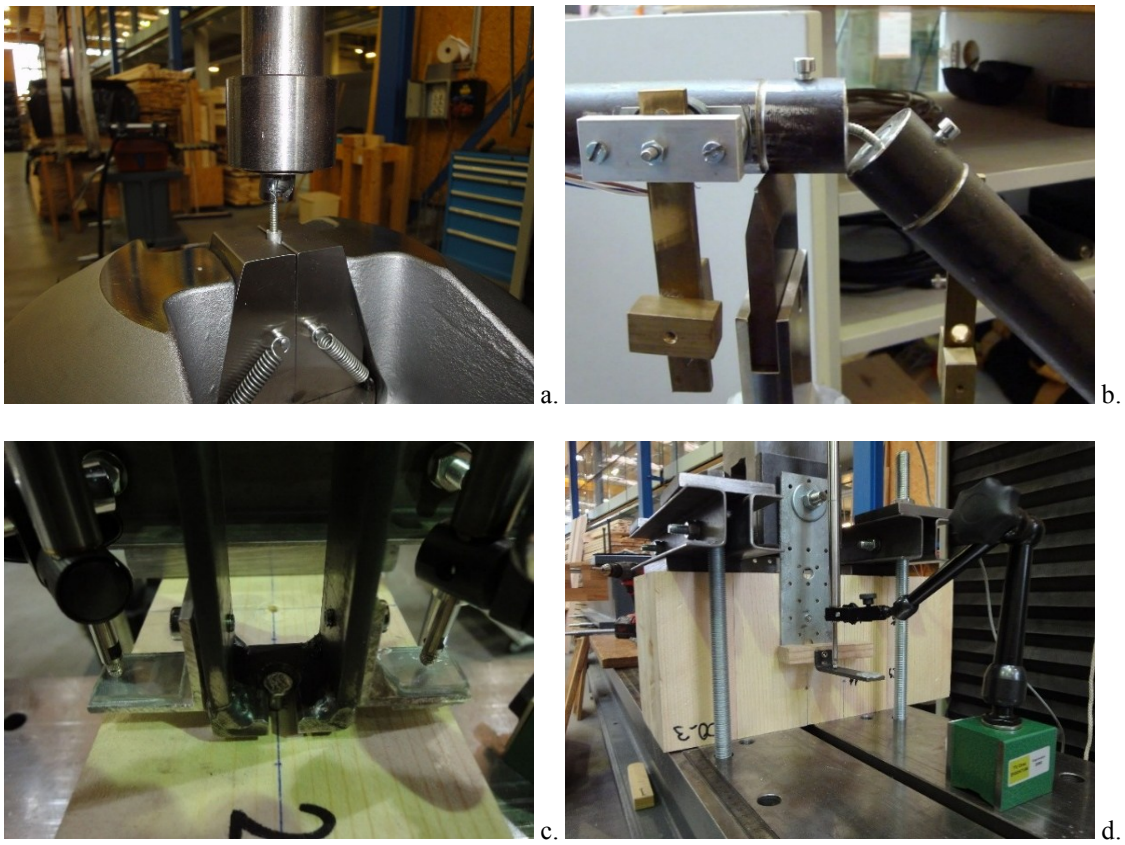

Figure 2.2. Experimental setups: (a) tension tests, (b) bending tests, (c) withdrawal tests, and (d) shear tests.

2.3.2 Nail withdrawal tests

The withdrawal capacity of the nailed joint was investigated with twenty-two nail withdrawal tests, carried out in accordance with EN 1382 [23]. The experimental setup consists of a nail embedded in the side face of a CLT panel and clamped to the testing machine (Figure 2.2c). The load bearing capacity was measured with a load cell, placed between the moving crosshead of the testing machine and the clamp which the nail was restrained to; the local displacements of the nail were measured with two linear variable displacement transducers (LVDTs) in the proximity of the nail cap (Figure 2.3a). Tests were carried out in displacement control at a rate of 2 mm/min and were stopped after a 40% loss of the maximum load bearing capacity.

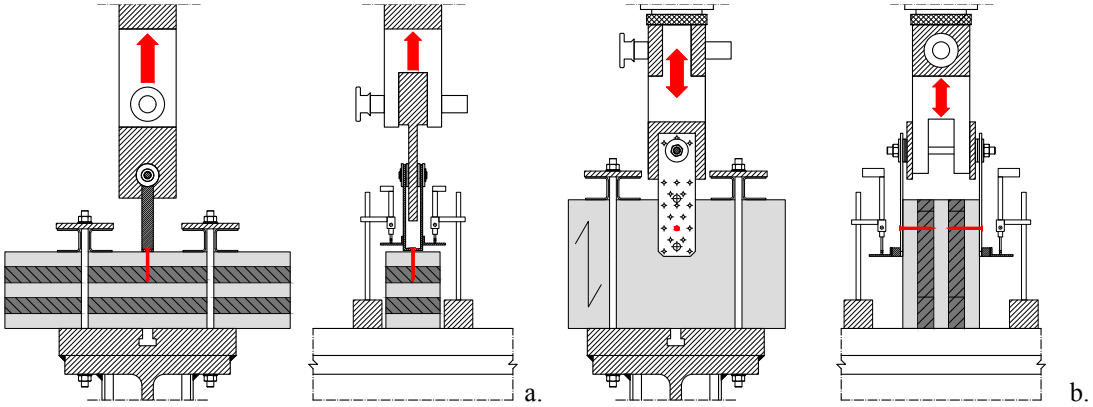

Figure 2.3. Test configurations for single fastener joint tests: (a) nail withdrawal tests (left: front view, right: side view) and (b) joint shear tests (left: front view, right: side view).

2.3.3 Single fastener joint shear tests

The lateral load bearing capacity and the hysteretic behaviour of the nailed steel-to-timber joint were investigated with shear tests. Six monotonic tests plus fifteen cyclic tests (labelled series ‘SH00’ and ‘SH00-C’, respectively) were carried out parallel to the face lamination of the CLT panel; furthermore, five monotonic tests plus fifteen cyclic tests (labelled series ‘SH90’ and ‘SH90-C’, respectively) were performed in the perpendicular direction. Tests were carried out in accordance with EN 1380 [22]; a symmetric setup was adopted, with two nails embedded at the same location in the opposite side faces of the CLT panel (Figure 2.2d). The load was applied to the nails cap with two 4 mm thick

metal plates obtained by cutting the shoulders of two hold-downs; to minimize the initial friction between the metal plates and the timber surfaces, thin metal blades were interposed among those elements while driving the nails into the CLT panel and removed just before testing. The load bearing capacity of the nailed joint was measured with a load cell, incorporated between the moving crosshead of the testing machine and the steel element to which the metal plates were restrained; the local displacements of the nails were measured with two LVDTs, located in correspondence of the nail caps (Figure 2.3b).

The loading protocol of the monotonic tests was defined in accordance with EN 26891 [29]; an estimated maximum load of 9.0 kN (4.5 kN for each nail) was assumed in both series. Load control with a loading rate of 1.8 kN/min was used up to 70% of the estimated maximum load; displacement control at a rate of 4 mm/min was used afterwards.

The displacement histories of the cyclic tests were defined according to ISO 16670 [57], acquiring the average ultimate displacements of each monotonic test series. The method proposed by ISO 16670 [57] was preferred to the one prescribed in EN 12512:2001/A1 [26] to avoid issues related to the lack of a standardized definition of the yield displacement [73, 74]. For each series, the first eleven tests were performed with the displacement levels prescribed by ISO 16670 [57] (one single cycle for 1.25-2.50-5.00-7.50-10% of the ultimate displacement; three cycles from 20% to 100% of the ultimate displacement, with 20% steps). To generate suitable data for calibration of the hysteresis models, the last four tests of each series were carried out with a modified set of displacement levels (same schedule for the single cycles; from 20% to 100% of the ultimate displacement, with 10% steps where three cycles at the same target displacement are applied). A displacement rate varying from 1 to 2 mm/min was used in all the tests.

2.3.4 Assumptions on data analysis

The mechanical properties of the joint tests were assessed according to EN 12512:2001/A1 [26] and ISO 16670 [57]. Figure 2.4 shows the model given in EN 12512:2001/A1 [26], used to evaluate the mechanical properties from the monotonic tests and from the first envelope curves of the cyclic tests.

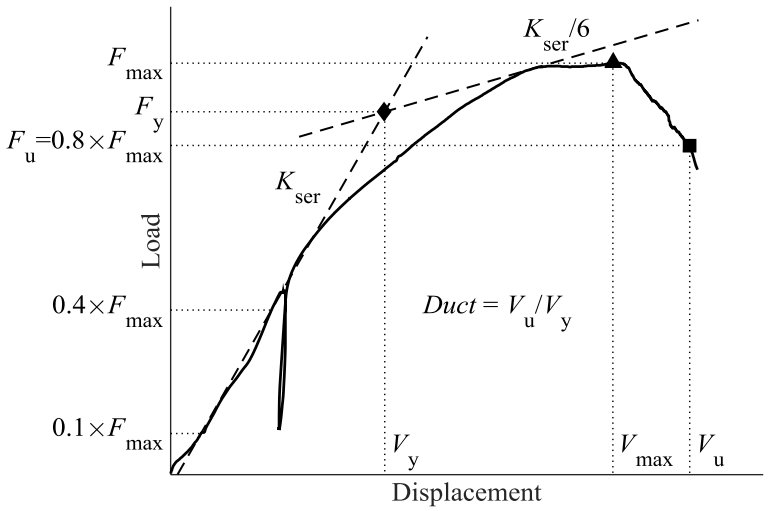

Figure 2.4. Model given in EN 12512:2001/A1 [26], used to evaluate the mechanical properties from the monotonic tests and from the first envelope curve of the cyclic tests.

In the monotonic tests (Figure 2.4), the maximum load bearing capacity (peak strength) and the displacement at which this is attained are denoted with F_{max} and V_{max}. The symbol K_{ser} signifies the instantaneous slip modulus of the joint, given by the slope of the line drawn through the points of the loading curve at 10% and 40% of F_{max}; F_y and V_y denote the yield load and its displacement while the ultimate load and its displacement are denoted with F_u and V_u, respectively. The yield point is determined by the intersection of the line used to define K_{ser} and the tangent line to the loading curve with slope equal to $K_{ser}/6$; the ultimate displacement is taken as either the displacement at failure or the displacement at 80% of F_{max}, whichever occurs first. Finally, the ductility ratio of the joint (denoted as $Duct$) is evaluated as the V_u to V_y ratio.

In the cyclic tests, the envelope curves of the hysteresis loops are derived by connecting the points at maximum load in the first, second and third cycles, respectively; however, in the first five single cycles the same values of the maximum load are taken for all the envelope curves. The maximum load bearing capacity, the slip modulus and the other mechanical properties mentioned for the monotonic tests are derived from the first envelope curve. Moreover, the peak strength is extracted from the third envelope curve ($F_{max(3rd)}$). The strength degradation factor due to cyclic loading (β_{Sd}) is assessed at the cycle group where the maximum strength of the first envelope curve is achieved and is determined as the ratio of the strength on the third envelope curve to its corresponding

value on the first envelope curve. If the strength on the third envelope curve is not available for that cycle group, β_{Sd} is evaluated on the preceding cycle group. The equivalent viscous damping ratio is calculated as $\nu_{eq} = E_{diss} / (4\pi E_{pot})$, with E_{diss} dissipated energy per full cycle and E_{pot} available potential energy as given in EN 12512:2001/A1 [26]. This method is preferred to the one included in EN 12512:2001/A1 [26] as it can be used for different curve shapes in the negative part of the loading curve. As suggested by Flatscher *et al.* [39], the available potential energy E_{pot} is derived from a second set of envelope curves obtained by connecting the points of maximum displacement per cycle. The equivalent viscous damping ratio at the first ($\nu_{eq(1st)}$) and third loop ($\nu_{eq(3rd)}$) is determined as the average values of all entire cycle groups before the ultimate displacement V_u was attained.

Average values (μ) and the coefficients of variation ($COV[\mu]$) are derived for all the mechanical properties; furthermore, the characteristic values of the experimental strength capacities (5th percentile) are calculated in accordance with EN 14358 [28] (Equation 2.17) assuming a log-normal distribution.

$$x_{05} = \exp(\bar{\mu} - k_s \cdot \bar{\sigma}) \tag{2.17}$$

In the equation above, the average value and the corrected sample standard deviation of the natural logarithm distribution are denoted with $\bar{\mu}$ and $\bar{\sigma}$, respectively. The k_s factor is an operator associated to the 5th percentile (x_{05}); its value depends upon the number of data available and is given in a tabular form in EN 14358 [28]. The 95th percentiles of the strength capacities (x_{95}) were obtained by inverting the sign of k_s.

2.3.5 Moisture content and density of CLT

Measurements of moisture content (MC) and density (ρ) of the CLT panels were taken either in the proximity (shear tests) or at the location (withdrawal tests) of the nail in the tests. The MC is measured with the oven dry method [27] by analysing altogether 59 test specimens (5 for series SH00, 12 for SH00-C, 5 for SH90, 15 for SH90-C and 22 for the withdrawal tests). For each series, average values of density at 12% MC are determined

in accordance with EN 384 [20] while characteristic values of density are determined by means of Equation 2.17.

2.4 RESULTS AND DISCUSSIONS

2.4.1 Tension tests and bending tests

Table 2.1 lists average values and coefficients of variation of the strength capacities obtained from the tension tests and from the bending tests; results are expressed in terms of ultimate tensile strength f_u and yield moment M_y.

Table 2.1. Mechanical properties of nails from tension tests and bending tests (the symbol n denotes the number of tests performed).

Property	Nail		
	μ	$COV[\mu]$	n
f_u [N/mm^2]	722.70	0.81%	5
M_y [Nmm]	6042.84	12.26%	10

Table 2.2 presents the characteristic strength capacities computed from the test results and a comparison with the calculated values of the yield moment. The subscript 05 is used to denote the 5th percentile of the strength whereas 95 identifies its 95th percentile. The characteristic strength values were assessed from the test data as prescribed in EN 14358 [28] assuming $k_s = 2.460$ for the tension tests and $k_s = 2.100$ for the bending tests.

Table 2.2. Characteristic strength capacities of nails from tension tests and bending tests, and comparison with calculation models.

Property	Nail
$f_{u,05}$ [N/mm^2]	639.04
$f_{u,95}$ [N/mm^2]	817.26
$M_{y,05}$ [Nmm]	4599.72
$M_{y,95}$ [Nmm]	7827.60
$M_{y,Rk\ B\&C}$ [Nmm]	5760.00
$M_{y,Rk\ EC5}$ [Nmm]	6616.50

All the fasteners used in the tension tests (Figure 2.5a) failed in a brittle manner in correspondence of the inner diameter of the profiled shank; however, to be consistent

with Eurocode 5 [24], the ultimate tensile strength f_u was defined as the maximum load to the nominal area of the shank (diameter d) ratio. As visible in Table 2.2, the tensile strength $f_{u,05}$ is slightly higher than the value suggested in the reference standards [24, 30, 75] and literature [3] (i.e. $f_{u,k}$ = 600 N/mm^2).

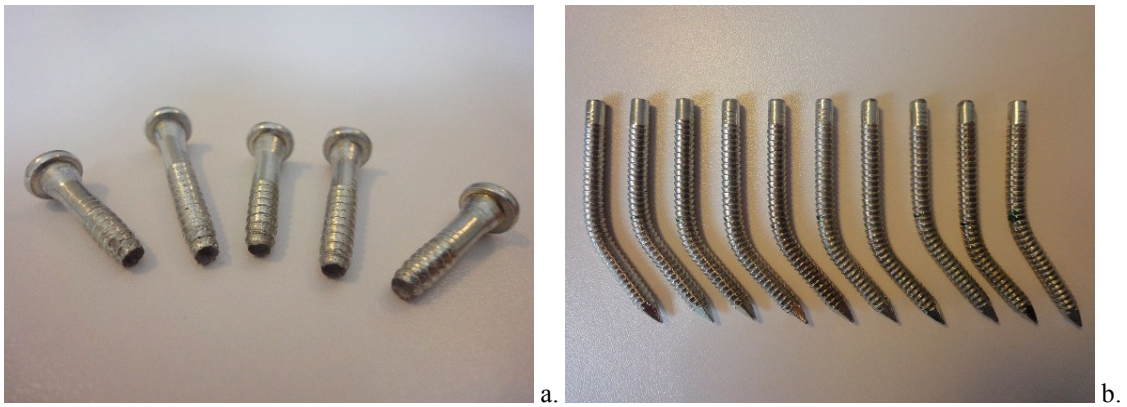

a. b.

Figure 2.5. (a) Failure modes of the tension tests and (b) deformed fasteners after bending tests.

Evident signs of failure were not visible in any of the fasteners tested in bending; a fully developed plastic hinge was recognised on some specimens while others showed a partially grown plastic hinge and a distributed plastic deformation (Figure 2.5b). As prescribed in EN 409 [21], the yield moment M_y should be determined either as the peak of the experimental moment-rotation relationship or as the moment at 45° rotation angle. However, due to some issues with the experimental setup, some tests were stopped between 40° and 45° and the yield moment was assessed assuming an ultimate rotation of 40°. The afore-mentioned issues were caused by the deformed shape of the fastener, which limited the rotational capacity of the test setup. This is clearly visible in Figure 2.2b, where the moving part of the setup touched its fixed section before reaching a rotation of 45°. However, since the peak strength of the moment-rotation relationship was generally attained before 40°, the results were not affected by this issue.

Calculated values of the yield moment were determined assuming $f_{u,k}$ = 600 N/mm^2. The model proposed by Blaß and Colling [5] ($M_{y,Rk\ B\&C}$) provided a more reliable prediction compared to the Eurocode 5 [24] model ($M_{y,Rk\ EC5}$). Nevertheless, calculated values are much higher compared to the experimental result (more than 25%). As pointed out in Section 2.2.4, specific calculation models to predict the yield moment of fasteners

with profiled shank have not been derived yet; therefore, the comparison given in Table 2.2 is of particular interest, as it gives an insight into the reliability of current design rules for the prediction of the yield moment of an annular-ringed shank nail. It should be noticed that the scatter of results in the bending tests is approximately ten times higher than in the tension tests; this suggests that the residual stresses produced by cold forming might have an influence on the bending behaviour of the nail. Results might be affected by the number of tests performed. Consequently, future studies should consider a wider set of tests and should investigate the bending behaviour under cyclic conditions.

2.4.2 Nail withdrawal tests

The mechanical properties resulting from the nail withdrawal tests are summarized in Table 2.3 while Figure 2.6 provides a comparison among all the experimental results (grey solid lines) and the trilinear approximating curve (red dashed line) determined by the average values given in Table 2.3; the trilinear approximating curve connects origin, yield, peak and ultimate strength. The experimental loading curves show a linear fashion until the yield load, a clear maximum, and a distinct load decrease after the displacement corresponding to the peak strength.

Table 2.3. Mechanical properties of joints from nail withdrawal tests and physical properties of the CLT specimens used in the tests (the symbol n denotes the number of tests performed).

Property	Withdrawal (n = 22)	
	μ	$COV[\mu]$
K_{ser} [N/mm]	1283.01	23.52%
V_y [mm]	1.73	24.18%
F_y [N]	2018.13	15.05%
V_{max} [mm]	2.41	12.82%
F_{max} [N]	2148.66	14.76%
V_u [mm]	3.74	10.41%
F_u [N]	1718.45	14.75%
Duct [-]	2.27	23.82%
ρ [kg/m^3]	460.95	5.88%

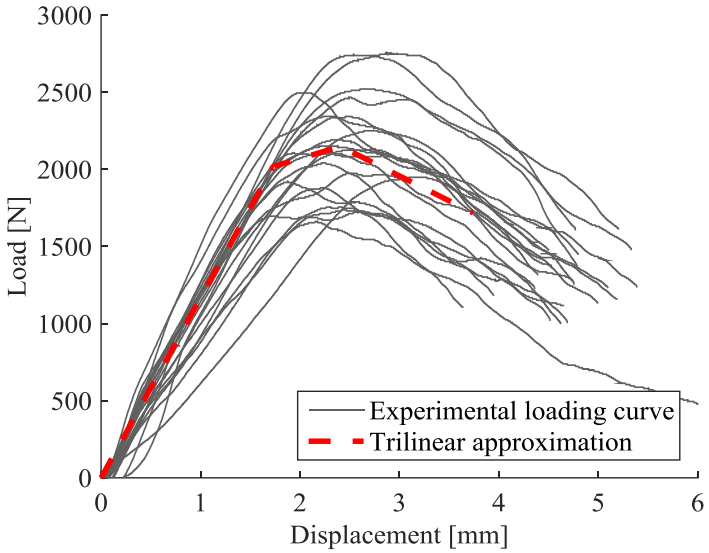

Figure 2.6. Nail withdrawal tests: comparison among all the experimental results (grey solid lines) and trilinear approximating curve (red dashed line).

Characteristic strength values from the tests and the characteristic density of the CLT panels (used as input parameter in the analytical models) were assessed as prescribed in EN 14358 [28] assuming k_s = 1.918. A comparison with the calculated values is given in Table 2.4.

Table 2.4. Characteristic strength capacities of joints from nail withdrawal tests and comparison with calculation models (with ρ_k = 410.85 kg/m^3).

Property	Withdrawal
$F_{max,05}$ [N]	1604.94
$F_{max,95}$ [N]	2817.93
$F_{ax,Rk\ ETA}$ [N]	1437.99
$F_{ax,Rk\ ..}$ [N]	1415.20
$F_{ax,Rk\ B\&U}$ [N]	1458.22

The model developed by Blaß and Uibel [3] gave the best agreement with the test results ($F_{ax,Rk\ B\&U}$). ETA-04/0013 [30] ($F_{ax,Rk\ ETA}$) led to slightly less accurate values while the rules included in the Austrian National Annex to Eurocode 5 [75] ($F_{ax,Rk\ ..}$) provided a more conservative prediction of the load-carrying capacity. In this context it must be noticed that, for design purposes, the Austrian National Annex to Eurocode 5 [75] suggests the use of only 80% of $F_{ax,Rk}$ if d is smaller than 6 mm. Furthermore, Eurocode 5 [24] and ETA-04/0013 [30] adopt the same model for the prediction of the axial

withdrawal capacity; however, the former does not provide any information on the withdrawal parameter and the use of harmonized technical specifications is required.

Based on the results presented in Table 2.4, values of γ_{sc} and γ_{an} were evaluated for nailed joints loaded in withdrawal. The first parameter (γ_{sc}) was determined as the $F_{max,95}$ to $F_{max,05}$ ratio and is equal to 1.76. The latter parameter (γ_{an}) was defined as the $F_{max,05}$ over $F_{ax,Rk,..}$ ratio, where $F_{ax,Rk,..}$ is the calculated strength capacity according to the Austrian National Annex to Eurocode 5 [75], and is equal to 1.13. Therefore, an overstrength factor γ_{Rd} = 2.0 is recommended for nailed joints with annular-ringed shank nails loaded in withdrawal when $F_{ax,Rk}$ is defined using general rules (e.g. those included in the above-mentioned standard) while γ_{Rd} = 1.8 is recommended if the design is based on the characteristic strength capacities determined from test results. It should be noticed that the overstrength factors determined on the results of single nails loaded in withdrawal are not necessarily valid for a group of nails. In particular, they could be even lower for, e.g., a metal connector that is anchored to the CLT panel with several nails that bear simultaneously the load.

The load bearing mechanism of the nailed joint loaded in withdrawal depends upon the friction between threaded shank and the surrounding timber. This mechanism is activated when the steel plate (to which the nail is clamped) is lifted from the CLT panel (in which the nail is embedded). Once the nail is extracted from the CLT panel, it cannot be pushed back by the steel plate; this suggests that the load bearing mechanism in withdrawal is effective as long as the joint is subjected to monotonic loads while is very weak in cyclic conditions and, if possible, it should be avoided. As already mentioned, applying the capacity-based design approach and over-strengthening this part of the connection (via, e.g., the use of more nails or by equipping it with screws instead of nails) might be a proper solution.

2.4.3 Single fastener joint shear tests

Average values and coefficients of variation of the mechanical properties obtained from the shear tests are listed in Table 2.5 (monotonic) and in Table 2.6 (cyclic), respectively.

Results are presented both in parallel and in perpendicular direction to the face lamination of the CLT panels.

Table 2.5. Mechanical properties of steel-to-timber joints from monotonic shear tests, in parallel and perpendicular direction to face lamination, and physical properties of the CLT specimens used in the tests (the symbol n denotes the number of tests performed).

Property	SH00 (n = 6)		SH90 (n = 5)	
	μ	$COV[\mu]$	μ	$COV[\mu]$
K_{ser} [N/mm]	483.69	17.81%	549.82	19.97%
V_y [mm]	7.63	27.67%	7.01	24.79%
F_y [N]	3508.51	5.39%	3916.14	9.66%
V_{max} [mm]	13.17	13.89%	12.90	9.83%
F_{max} [N]	3907.46	4.20%	4405.73	8.84%
V_u [mm]	22.66	27.23%	15.59	14.75%
F_u [N]	3275.26	4.32%	3877.99	12.06%
$Duct$ [-]	3.13	37.95%	2.38	36.26%
ρ [kg/m^3]	477.44	1.46%	455.01	3.11%

Table 2.6. Mechanical properties of steel-to-timber joints from cyclic shear tests, in parallel and perpendicular direction to face lamination, and physical properties of the CLT specimens used in the tests (the symbol n denotes the number of tests performed).

Property	SH00-C (n = 15)		SH90-C (n = 15)	
	μ	$COV[\mu]$	μ	$COV[\mu]$
K_{ser} [N/mm]	545.55	32.04%	515.78	27.90%
V_y [mm]	6.66	26.50%	5.45	31.77%
F_y [N]	3393.21	14.80%	2735.23	11.06%
V_{max} [mm]	10.73	11.63%	8.62	23.97%
F_{max} [N]	3756.32	17.12%	3007.93	13.21%
$F_{max(3rd)}$ [N]	2411.62	14.88%	2268.71	9.49%
V_u [mm]	10.94	7.98%	9.94	24.98%
F_u [N]	3667.64	19.88%	2562.63	17.00%
$Duct$ [-]	1.75	25.87%	2.01	44.78%
$\nu_{eq(1st)}$ [%]	20.20%	16.94%	16.92%	10.82%
$\nu_{eq(3rd)}$ [%]	10.66%	17.77%	10.44%	13.82%
β_{Sd} [-]	0.71	7.73%	0.72	13.32%
ρ [kg/m^3]	472.66	4.35%	481.13	6.36%

Figures 2.7a-7b show a comparison among the results of the monotonic tests (grey solid lines) and the trilinear approximating curve determined by the average quantities given in Table 2.5 (red dashed line connecting origin, yield, peak and ultimate strength). The same figures show also the instantaneous slip modulus of the steel-to-timber joint (dark grey dashed line), determined according to Equation 2.16.

Figures 2.8a-8b show a comparison among the first envelope curves extracted from the cyclic tests (grey solid lines) and the trilinear approximating curve determined by the average values given in Table 2.6 (red dashed line). For comparison with the monotonic tests, the same figures show also the trilinear approximating curves determined by the quantities given in Table 2.5 (dark grey dashed line).

The peak strength of both monotonic series was achieved at approximately 13 mm of displacement. The instantaneous slip modulus and the peak strength in perpendicular direction are slightly higher than in the parallel direction whereas the ultimate displacement and the ductility are lower. Moreover, the peak strengths of the cyclic tests are lower than the quantities determined in monotonic conditions. It should be noticed that some tests have failed prior to the cycle group where the maximum strength of the monotonic tests was achieved (as visible in Figures 2.8a-8b).

Two plastic hinges can be recognised in all the fasteners, one under the cap and another one in the shank (10 to 15 mm below). In the monotonic tests, failures always occurred for tearing of the cap in one fastener due to a combination of tension and bending (Figure 2.9a). In the cyclic tests, four different failure mechanisms can be recognised (Figure 2.9b): (*a*) tearing of the cap, (*b*) failure in bending, (*c*) failure in bending with a partially torn cap, (*d*) failure in bending with tearing of the cap. CLT panels tested in parallel direction to the face lamination failed for excess of embedment while local splitting occurred in some specimens loaded in perpendicular direction.

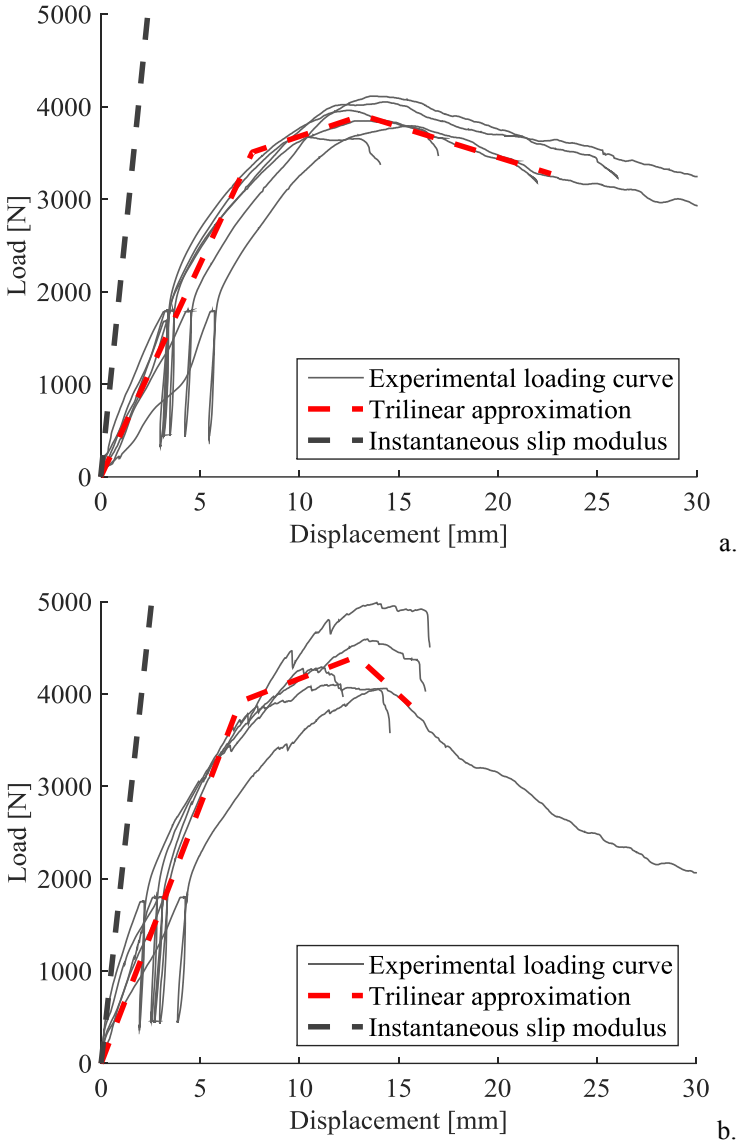

Figure 2.7. Monotonic shear tests: comparison among all the experimental results (grey solid lines), trilinear approximating curve (red dashed line) and instantaneous slip modulus (dark grey dashed line) according to Equation 2.16 (a) of specimens loaded in parallel to the face lamination of the CLT panel and (b) in perpendicular direction.

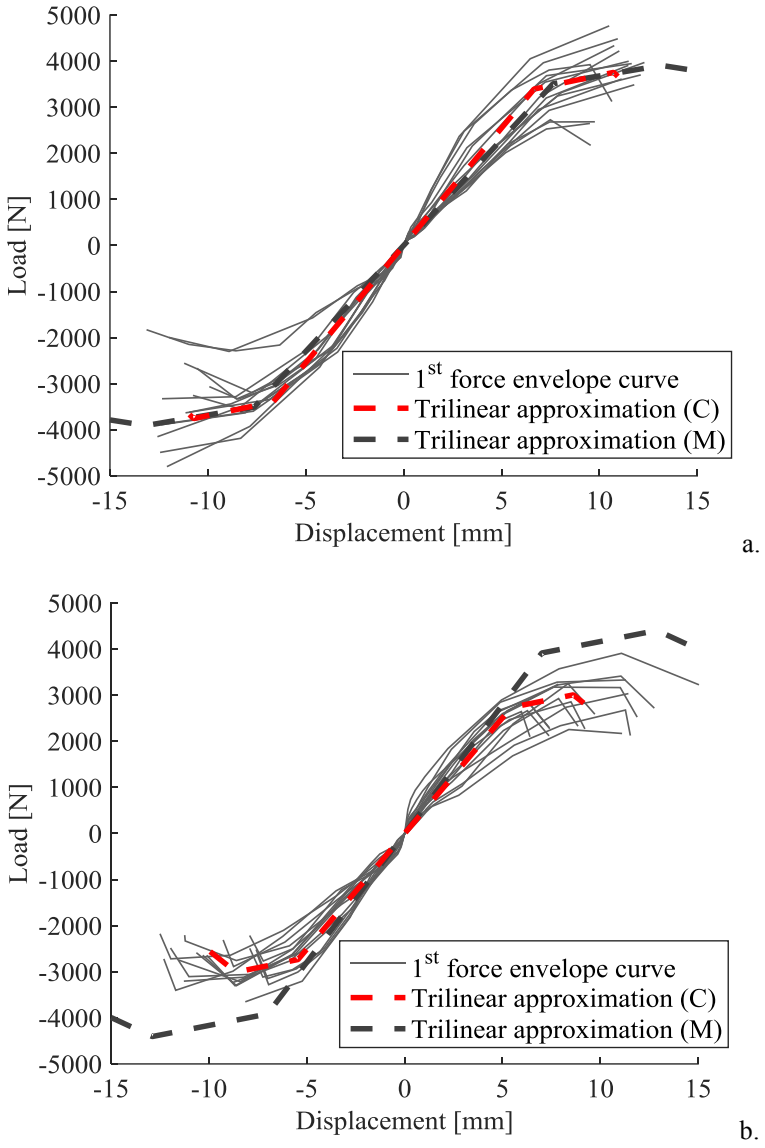

Figure 2.8. Cyclic shear tests: comparison among all the first envelope curves (grey solid lines), trilinear approximating curve determined from the cyclic tests (red dashed line) and from the monotonic tests (dark grey dashed line) (a) of specimens loaded in parallel to the face lamination of the CLT panel and (b) in perpendicular direction.


a.

b.

Figure 2.9. Single fastener joint shear tests: deformed fasteners (a) after monotonic and (b) after cyclic tests.

Table 2.7 presents the characteristic strength capacities computed from the monotonic tests and a comparison with the analytical models. The characteristic strength values were computed from the experimental data in accordance with EN 14358 [28] assuming k_s = 2.388 for series SH00, k_s = 2.460 for series SH90 and k_s = 1.990 for both series SH00-C and SH90-C. Furthermore, the characteristic densities of the CLT panels used in test series SH00 and SH90 (required as input parameter for the analytical models) were determined according to the same standard assuming k_s = 2.460.

Table 2.7. Characteristic strength capacities of steel-to-timber joints from monotonic shear tests and comparison with calculation models (with ρ_k = 422.14 kg/m^3 for test series SH00 and ρ_k = 402.19 kg/m^3 for test series SH90).

Property	Shear	
	Parallel	Perpendicular
$F_{max,05}$ [N]	3465.12	3549.46
$F_{max,95}$ [N]	4399.75	5435.40
$F_{v,Rk\ ETA}$ [N]	2674.63	2589.98
$F_{v,Rk\ EC5}$ [N]	2157.51	2097.29
$F_{v,Rk\ ..}$ [N]	2403.23	2403.23
$F_{v,Rk\ B\&U}$ [N]	2488.63	2421.38

All the calculation models led to conservative predictions of the load-carrying capacity. The rules included in ETA-04/0013 [30] ($F_{v,Rk\ ETA}$) provided the best agreement with the test results. The Austrian National Annex to Eurocode 5 [75] ($F_{v,Rk\ ..}$) and the model by Blaß and Uibel [3] ($F_{v,Rk\ B\&U}$) led to slightly less accurate values while

Eurocode 5 [24] ($F_{v,Rk\,EC5}$) gave the most conservative predictions. It is important to note that the load-carrying capacity of ETA-04/0013 [30] and Eurocode 5 [24] were computed using the same input values. However, Eurocode 5 [24] considers a contribution due to the rope effect equal to 25% of the withdrawal capacity (Equation 2.5) while ETA-04/0013 [30] increases that effect up to 60% of $F_{ax,Rk}$.

The 5th and 95th percentiles of the strength degradation factor were assessed from the experimental data as prescribed in EN 14358 [28]; $\beta_{Sd,05}$ is equal to 0.60 and $\beta_{Sd,95}$ to 0.83 parallel to the superficial lamination of the CLT panel whereas $\beta_{Sd,05}$ = 0.54 and $\beta_{Sd,95}$ = 0.94 in the perpendicular direction. Based on the statistical analysis, a conservative strength degradation factor β_{Sd} = 0.6 is recommended for laterally loaded steel-to-timber joints in parallel to the face lamination of the CLT panel while β_{Sd} = 0.5 is recommended in the perpendicular direction.

Once more, it should be noticed that both the overstrength factors and the strength degradation factors were determined using results of laterally loaded steel-to-timber joints equipped with one single nail and could be even lower as each connector is usually anchored to a CLT panel with several fasteners that bear simultaneously the load.

Finally, the experimental slip moduli of the monotonic tests (given in Table 2.5) are compared to the analytical values determined according to Equation 2.16. The predicted instantaneous slip modulus in parallel direction to the superficial lamination of the CLT panel is equal to 2108 N/mm while in perpendicular direction is equal to 1962 N/mm; the discrepancy between the calculated values depends upon the mean densities of the respective samples. However, the results computed from the experimental data are significantly lower than the analytical predictions. This suggests that the assumption of a rigid metal plate, which is the basis for doubling the stiffness of steel-to-timber joints according to Eurocode 5 [24], might not be valid for the conducted tests, especially at low load levels.

2.5 CONCLUDING REMARKS

This chapter investigates the mechanical behaviour of steel-to-timber joints with annular-ringed shank nails in CLT. Monotonic and cyclic shear tests were performed on single fastener joints loaded in parallel and perpendicular direction to the face lamination of the CLT panels; furthermore, withdrawal tests were carried out on single nails embedded in the side face of CLT panels. Finally, the ultimate tensile strength and the yield moment of the nail were determined by performing tension tests and bending tests, respectively. Characteristic values of the strength capacities were assessed from the experimental data and compared to the values calculated according to the current design models.

The best agreement with the experimental results was obtained with the design provisions included in the European Technical Assessment (ETA) of the fasteners tested [30]. The model developed by Blaß and Uibel [3] led to slightly less accurate values while the rules included in Eurocode 5 [24] and in the Austrian National Annex to Eurocode 5 [75] provided more conservative predictions of the load-carrying capacity. Finally, it was shown that the model included in Eurocode 5 [24] for the prediction of the slip modulus of a nailed steel-to-timber joint significantly overestimates the experimental results.

Based on the statistical analysis, the overstrength and strength degradation factors of the joints with annular-ringed shank nails were evaluated. For each configuration, two overstrength factors were determined: one is recommended when the characteristic load-carrying capacity is defined based on general rules (e.g. those included in the Austrian National Annex to Eurocode 5 [75]); the other is recommended when the design is based on the characteristic strength capacities determined from test results. Consequently:

- $\gamma_{Rd} = 2.0$ and $\gamma_{Rd} = 1.8$ are recommended for nailed joints with annular-ringed shank nails loaded in withdrawal;
- $\gamma_{Rd} = 1.8$ and $\gamma_{Rd} = 1.3$ are recommended for laterally loaded steel-to-timber joints parallel to the face lamination of the CLT panel;
- $\gamma_{Rd} = 2.3$ and $\gamma_{Rd} = 1.5$ are recommended for laterally loaded steel-to-timber joints perpendicular to the face lamination of the CLT panel.

The strength degradation factors were determined for the laterally loaded steel-to-timber joints and conservative values of β_{Sd} = 0.6 and β_{Sd} = 0.5 are recommended in parallel and perpendicular direction to the face lamination of the CLT panel, respectively. The overstrength and the strength degradation factors significantly depend on the scatter of mechanical properties observed in the tests and were determined on the results of single fastener joints. Due to the group effect, this scatter might be lower for, e.g., a metal connector anchored to the CLT panel with a group of nails. Therefore, in these situations, both factors may be even lower.

3 Numerical modelling of joints with dowel-type fasteners

SHORT SUMMARY

Predicting the mechanical behaviour and the failure mechanism of joints with dowel-type fasteners requires to consideration of several factors, which include the geometrical and mechanical properties of the fastener, the physical properties of timber and the interaction among such elements. This chapter proposes a numerical model where a joint is simulated as an elasto-plastic beam in a non-linear medium with a compression-only behaviour. In contrast with the differential approach adopted by most of the hysteresis models published in literature, this model predicts the load-displacement response using simple mechanical relationships and basic input parameters. Shear tests are reproduced on a nailed steel-to-timber joint in Cross-Laminated Timber. Firstly, the behaviour of the model is validated by comparing the numerical predictions of the lateral dowel capacity with the analytical values obtained employing a calculation model proposed by Hilson. The influence of the embedment behaviour of timber and the withdrawal behaviour of the nail on the response of the joint are then analysed via a parametric numerical study. Results are compared to the test data published in literature, showing limited differences.

The experimental results taken from Casagrande et al. were obtained in the framework of the Seismic X-REV research project, funded by Rothoblaas (Cortaccia, Italy) and by the Autonomous Province of Bolzano (Italy). Tests were carried out by the Timber Group of the University of Trento (Italy), which is gratefully acknowledged.

3.1 INTRODUCTION

Timber structures are made of 1D (e.g. beams and studs) and 2D elements (e.g. walls and floors) fastened together with mechanical joints and connection systems that transmit the lateral shear and withdrawal loads. Due to the high strength-to-weight ratio of timber and the connections capacity to resist the load with ductile deformations and little impairment of strength, these structures showed satisfactory performances under seismic conditions.

Mechanical joints in timber structures are assembled using dowel-type fasteners (e.g. nails, staples, screws, bolts, and dowels). Their load-displacement response depends on several factors, including the yield moment and the withdrawal behaviour of the fastener, the embedment behaviour of timber, and the interaction between fastener and timber.

Eurocode 5 [24] predicts the load-carrying capacity of joints with dowel-type fasteners according to the European Yield Model (EYM), originally proposed by Johansen [62]. The rope effect is included into the design equations and some limiting factors, expressed at a maximum percentage of the lateral dowel capacity of the joint, are introduced to avoid relying on the withdrawal of the fastener. One of the limitations of the EYM is the lack of indications regarding the load-displacement response of the joints, which are assumed to behave in a rigid-plastic manner.

Alternative calculation methods were proposed since the early ’50s to overcome the limits of the EYM. Ivanov [58] developed a second-order equation to relate the strength of a nailed joint to its displacement. Mack [71] proposed a calculation model where the load-displacement response is determined as the product of a series of independent factors. Finally, Kuenzi [67] reproduced a single-shear or double-shear joint as a beam on an elastic foundation. Using a fourth-order differential equation, this model estimated the pressure, shear, moment, and deflection at any point of the joint; however, it had little applications since it could be used only in the elastic range of the loading curve [13, 82].

In recent years, many research projects focused on developing hysteresis models able to predict both the elastic and inelastic response of joints with dowel-type fasteners. Three approaches were followed: the first one aimed at improving the results obtained with the beam on an elastic foundation, by reproducing the mechanical behaviour of timber with non-linear springs [12, 45, 69, 78]. In the second approach, the non-linear response of the joint was concentrated into non-linear hysteretic springs or simple elasto-plastic systems [41, 43, 52, 65, 86, 102]. These models were used to analyse the behaviour of light-frame shear walls or full-scale structures, i.e. situations in which computationally efficient algorithms are needed. Finally, the third one focused on the development of accurate

schematizations of the joints where the elements of the model were assigned the actual mechanical properties [51, 54, 72, 76, 93]. Regarding this last approach, it should be noticed that significant efforts were devoted to the development of advanced material models able to predict the mechanical behaviour and the failure mechanisms of timber [36, 90, 91].

This study proposes a numerical model able to predict the load-displacement response and failure mechanisms of joints with dowel-type fasteners. This model is also capable to reproduce the effect of the cavity formed around the fastener by timber crushing, allowing the prediction of the mechanical behaviour under monotonic or cyclic conditions. The joint is simulated as an elasto-plastic beam in a non-linear medium with a compression-only behaviour. In contrast with the differential approach used in most of the hysteresis models published in literature, this model employs simple mechanical relationships and basic input parameters to reproduce the response of the steel and timber components of the joint. In fact, in addition to the geometrical data, the yield moment and the withdrawal behaviour of the fastener and the embedment behaviour of timber are the required input parameters. Such input values can be derived either from experimental tests (carried out, e.g., according to EN 409 [21], EN 383 [19] and EN 1382 [23]) or from the models given in Eurocode 5 [24] and published in literature.

The model proposed in this chapter can be used to predict the response of several types of joints. In fact, with minor modifications on the boundary conditions, the response of a timber-to-timber, a steel-to-timber, and a slotted-in steel plate joint can be simulated (Figure 3.1). Results obtained on single fastener joints can be used to analyse systems where many of these elements are present. For instance, the predicted load-displacement response of a nailed joint can be concentrated into a non-linear hysteretic spring and used to investigate the load-displacement response of a metal connector (e.g. an angle bracket or a hold-down) or of a light-frame shear-wall.

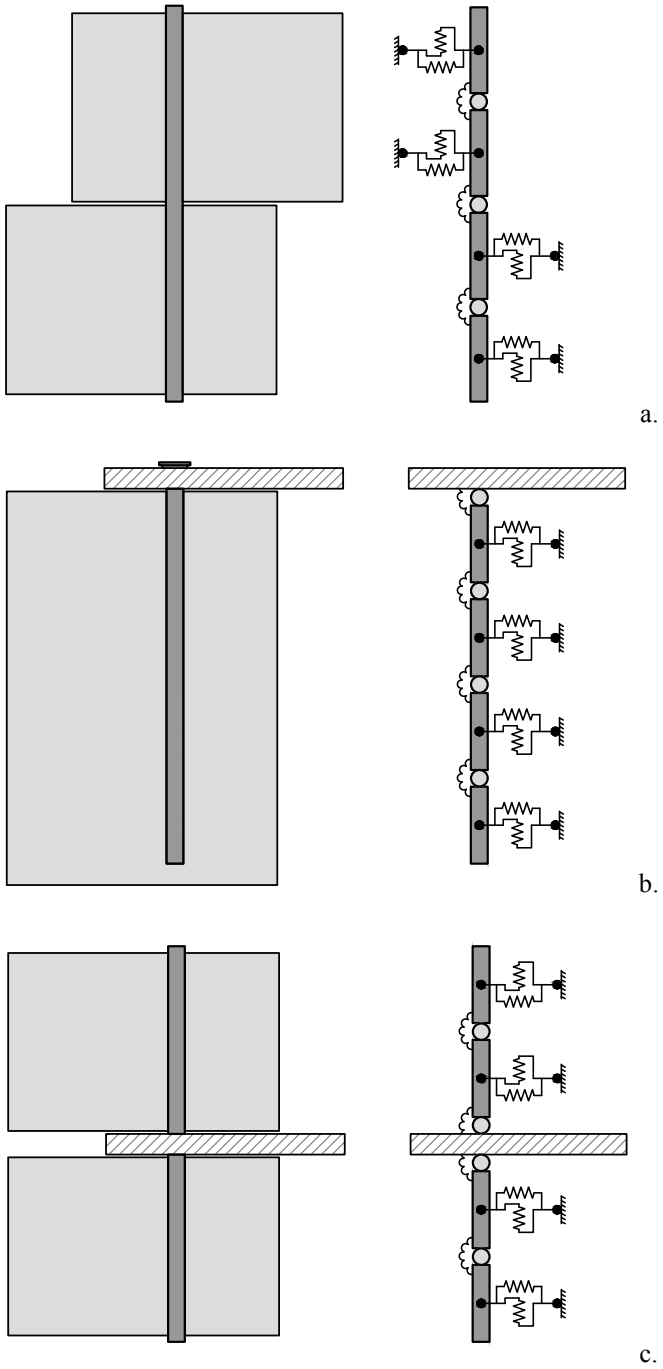

Figure 3.1. Schematics of (a) a timber-to-timber joint (left: according to the model prescribed in Eurocode 5 [24]; right: according to the proposed numerical model), (b) a steel-to-timber joint and (c) a joint with slotted-in steel plate.

Shear tests are reproduced on a steel-to-timber joint with an annular-ringed shank nail in Cross-Laminated Timber (CLT). The behaviour of the model is validated by comparing the numerical predictions of the lateral dowel capacity with the values determined using a calculation model proposed by Hilson [53]. The influence of the embedment behaviour of timber and the withdrawal behaviour of the fastener on the load-displacement response of the joint are subsequently analysed via a parametric numerical study. Numerical results are compared to the test data published in literature and differences are discussed. All the simulations are performed using ABAQUS software package [96].

3.2 MODEL DESCRIPTION

The numerical model proposed in this contribution schematizes a joint with a dowel-type fastener as an elasto-plastic beam in a non-linear medium with a compression-only behaviour. A key feature of this model is the use of non-linear springs able to reproduce the hysteretic behaviour of the steel and timber components of the joint. In this study, these springs are simulated with a user element subroutine taken from Rinaldin *et al.* [86, 87]; a preliminary version of this model was presented by Rinaldin [85].

3.2.1 Fastener schematization

The fastener shank is simulated with a series of non-linear beams interconnected with hinges and is equipped with a set of rotational springs, placed at the hinge locations, which control the bending behaviour in the plastic deformed configuration. Each beam (of length l, Figure 3.2) is characterized by an elastic behaviour in bending while a rigid behaviour is adopted in the axial direction. This uncoupled behaviour is used to keep the total length of the fastener constant and is attained by taking into account the 2nd order effects (i.e. by activating the non-linear geometry of the model).

Each rotational spring is restrained to the ends of two consecutive beams and has an elasto-plastic moment-rotation relationship with elastic stiffness K_θ and yield moment M_y. The elastic stiffness is determined by assuming that the yield moment M_y is attained

at a conventional rotation of 0.01°. The inelastic branch has a plastic behaviour until the ultimate rotation θ_u, which is set to 45° [21].

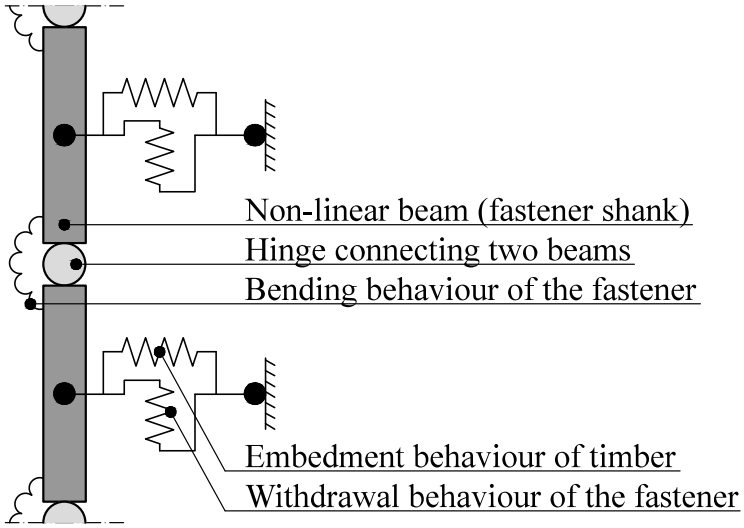

Figure 3.2. Schematics of the numerical model, with description of its components.

The piecewise-linear law governing the rotational springs is given in Figure 3.3a; the backbone curve (composed of branches #1, #2, #10, and #20) is assembled as discussed above. When the springs are unloaded from a positive rotation, branch #3 is followed. On the contrary, branch #40 is followed if the springs are unloaded from a negative rotation. The slope of branches #3 and #30 is the same of #1 and #10 while the load at the transition point between branches #3 and #5 is conventionally set to 2% of the load attained on the backbone curve at the current hysteresis cycle. Finally, the transition point between #5 and #30 is located in the origin of the axis.

The presence of supplementary boundary conditions can be accounted in the model by introducing additional springs. In a steel-to-timber joint (Figure 3.1b) the clamping of the fastener cap to the metal plate is simulated with an additional spring located between the upper beam and the metal member to which the cap is connected. On the contrary, in a joint with a slotted-in steel plate (Figure 3.1c) the clamping of the fastener shank to the plate is simulated with two additional spring elements located between the metal member and the beams to whom is connected.

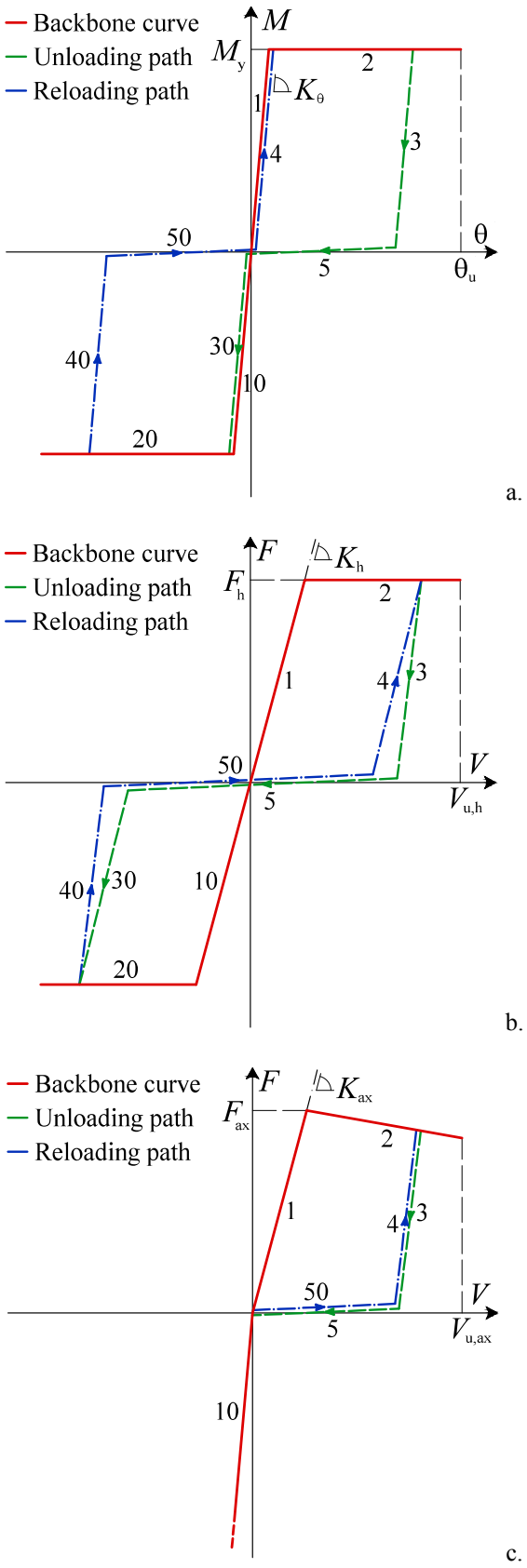

Figure 3.3. Piecewise-linear laws reproducing (a) the bending behaviour of the fastener, (b) the embedment behaviour of timber and (c) the withdrawal behaviour of the fastener (adapted from Rinaldin *et al.* [86, 87]).

3.2.2 Embedment behaviour of timber

The embedment behaviour of timber in compression is simulated with a set of non-linear hysteretic springs uniformly distributed along the fastener shank. Each spring is restrained to a master node located in the centre of the beam where it is attached and to a fixed point of the surrounding space (Figures 3.2). To limit the computational effort required by the simulations, the embedment behaviour in front of and behind each beam is simulated with a unique spring.

Each non-linear spring has an elasto-plastic load-displacement relationship with elastic stiffness K_{h} (in this study referred to as 'embedding stiffness') and embedding capacity F_{h}. The inelastic branch simulates the crushing of the fibres underneath the fastener and the associated densification of timber in the contact area [66]; it has a plastic behaviour until the ultimate displacement $V_{\mathrm{u,h}}$, conventionally set to 15 mm.

Generally, the embedment behaviour of timber depends on the relative orientation between applied load and grain direction. Fasteners loaded parallel to the grain direction have a high initial stiffness and a plastic plateau; fasteners loaded perpendicular to the grain are less stiff at lower loads but have a continuous load increase until failure [4, 50, 77, 94]. However, differences are negligible if d is smaller than 8 mm [54, 105].

The piecewise-linear law governing the non-linear springs is given in Figure 3.3b; the backbone curve (composed of branches #1, #2, #10, and #20) is assembled as discussed above. If the springs are unloaded from a positive displacement, branch #3 is followed until the attainment of zero load. On the contrary, branch #40 is followed if the unloading starts from a negative displacement. Branches #5 and #50 simulate the gap between the supporting medium and the fastener, caused by the cavity formed by timber crushing. Finally, branches #30 and #4 take to the opposite side of the backbone curve and simulate the embedment behaviour at increased displacement levels, when the fastener comes again into contact with the surrounding timber. The slopes of branches #3 and #4 are expressed as functions of the elastic stiffness K_{h}: the first one is set to $4K_{\mathrm{h}}$ while the latter one is equal to $2.5K_{\mathrm{h}}$ [11]. The transition point between branches #3 and #5 (and

between #50 and #4) depends on the load reached on the backbone curve and is updated at every hysteresis cycle.

3.2.3 Withdrawal behaviour of the fastener

The withdrawal behaviour of the fastener is simulated with a third set of hysteretic springs uniformly distributed along the fastener shank. Each spring is restrained to a master node, located in the centre of the corresponding beam, and to a fixed point of the surrounding space (Figures 3.2). The tangential stresses caused by the withdrawal of the fastener are assumed uniformly distributed along the shank and a unique calibration is used for all the springs. However, a non-uniform distribution might be considered in future developments of this research.

Each non-linear spring has a non-symmetric load-displacement relationship. If loaded in tension, an elasto-plastic behaviour is adopted with elastic stiffness K_{ax} (in this study referred to as 'withdrawal stiffness') and withdrawal capacity F_{ax}. The inelastic branch has a softening behaviour, determined by assuming that the load in correspondence of the ultimate displacement $V_{u,ax}$ is 60% of F_{ax} (with $V_{u,ax}$ conventionally set to 10 mm). If the spring is loaded in compression, based on the schematics given in Figure 3.1, the fastener cannot penetrate into the embedment and a rigid-elastic behaviour is adopted.

The piecewise-linear law governing the non-linear springs is given in Figure 3.3c; the backbone curve (composed of branches #1, #2, and #10) is assembled as discussed above. The hysteretic behaviour is similar to the one described in the previous sub-section, and should be specifically calibrated for the joint under analysis. For instance, in Figure 3.3c the typical hysteretic behaviour of a steel-to-timber joint is presented. Once extracted, the steel plate is not able to push the fastener backwards inside the timber element. Therefore, in cyclic conditions, branch #3 simulates the sudden reduction of load-carrying capacity due to the gap formed among the metal plate and the fastener cap. If the spring is reloaded (branch #4), the bearing mechanism under withdrawal loads is not activated until the gap between the metal plate and the fastener cap is closed. Based on this behaviour, the slope of branches #3 and #4 is conventionally set to 10 times K_{ax}.

3.2.4 Friction between fastener shank and timber

In laterally loaded joints, the friction between fastener shank and timber is caused by the slippage of the deformed fastener over the compressed timber. This interaction has minor effects on the overall behaviour of joint as long as the bearing mechanism is controlled by its lateral dowel capacity. However, it becomes significant at larger displacements, i.e. when the fastener is withdrawn from the timber embedment.

The friction between fastener shank and timber is schematized using two contributions. The first one simulates the indentation of the fastener shank into the timber embedment while the second one simulates the tangential stresses in the contact area between fastener shank and timber. The first contribution is taken into account in the model by increasing the stiffness of the springs that control the withdrawal behaviour of the fastener (K_{ax}). The second contribution is accounted by means of a concentrated load, applied to the non-linear springs that control the withdrawal behaviour of the fastener; its value is equal to the compression load of the timber embedment at the current analysis step multiplied by a friction coefficient μ_{fr}. The friction coefficient may vary between zero (smooth shank) to one (fully threaded shank). This approach has been confirmed by an independent study carried out by Domínguez *et al.* [14].

3.3 MODEL VALIDATION

The behaviour of the model is validated by comparing the numerical predictions of the lateral dowel capacity to the values determined according to a calculation model proposed by Hilson [53]. Simulations are carried out on steel-to-timber joints with annular-ringed shank nails in CLT. The discussion presented below focused on joints with thick plates. According to Eurocode 5 [24], the situation of 'thick plate' is achieved when the thickness of the metal member is greater than the diameter of the fastener. However, annular-ringed shank nails have a conical-shaped cap (Figure 3.4) that enforces a failure mechanism with two plastic hinges even with thinner plates [59].

Figure 3.4. Annular-ringed shank nails (reproduced from Izzi *et al.* [59]).

The calculation model proposed by Hilson [53] is given in Equation 3.1. The model does not take into account the rope effect; for this reason, both the withdrawal behaviour of the fastener and the friction between fastener shank and timber are disregarded.

$$F_{\text{lat,Rd}} = \min \begin{cases} f_{\text{h,d}} t_1 d & \text{(a)} \\ f_{\text{h,d}} t_1 d \left[\sqrt{2 + \dfrac{4 M_{\text{y,Rd}}}{f_{\text{h,d}} t_1^2 d}} - 1 \right] & \text{(b)} \\ 2.0 \sqrt{M_{\text{y,Rd}} f_{\text{h,d}} d} & \text{(c)} \end{cases} \tag{3.1}$$

In the expressions above, $F_{\text{lat,Rd}}$ denotes the design value of the lateral dowel capacity, d is the diameter of the fastener, t_1 the pointside penetration depth while $M_{\text{y,Rd}}$ and $f_{\text{h,d}}$ represent the design values of the yield moment of the nail and the embedding strength of timber, respectively. Values of $M_{\text{y,Rd}}$ and $f_{\text{h,d}}$ are assessed using the design models given Equation 3.2 and 3.3 [2, 100].

$$M_{\text{y,Rd}} = 0.30 \frac{f_{\text{u,k}}}{\gamma_{\text{S}}} d^{2.6} \tag{3.2}$$

$$f_{\text{h,d}} = \frac{k_{\text{mod}}}{\gamma_{\text{M}}} 0.112 \rho_{\text{k}}^{1.05} d^{-0.5} \tag{3.3}$$

In the equations above, $f_{\text{u,k}}$ is the characteristic ultimate tensile strength of the nail, ρ_{k} is the characteristic density of timber and k_{mod} is the modification factor for duration of load and moisture content. Finally, γ_{S} and γ_{M} represent the partial factors for material properties of steel and timber. Equation 3.2 is prescribed in Eurocode 5 [24] for dowel-

type fasteners with smooth shank while Equation 3.3 is included in the Austrian National Annex to Eurocode 5 [75] for threaded nails in CLT.

Following the assumptions adopted by Hilson [53], the non-linear springs used in the numerical model are characterized by a rigid-plastic behaviour and are calibrated on the strength capacities determined according to Equation 3.2 and 3.3. The stiffness properties (i.e. K_h, K_{ax} and the elastic modulus of the beams) are conveniently chosen to achieve a rigid behaviour while the embedding capacity of timber F_h is determined by multiplying the embedding strength $f_{h,d}$ by the tributary area of each beam (i.e. $d \times l$).

3.3.1 Results of the model validation

Simulations considered a nailed steel-to-timber joint with constant penetration depth t_1 = 60 mm and three diameters (d = 4.0 mm, 6.0 mm and 8.0 mm, respectively). The fastener shank is discretized into 20 beams of length l = 3 mm. According to Eurocode 5 [24], the ultimate tensile strength of the fastener is set to $f_{u,k}$ = 600 N/mm^2; the other factors used in Equation 3.2 and 3.3 are defined according to Hilson [53] as follows: k_{mod} = 0.9, γ_s = 1.1 and γ_m = 1.3. Analyses are performed by varying the characteristic density of timber ρ_k between 300 kg/m^3 and 500 kg/m^3.

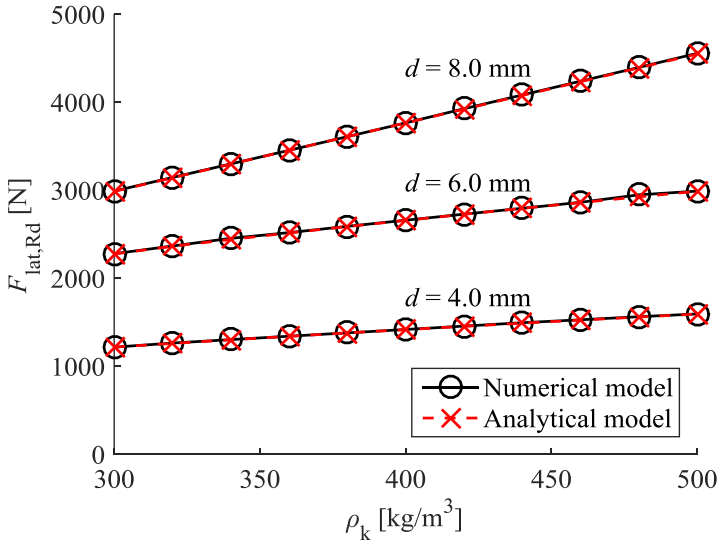

Figure 3.5. Mechanical validation of the model: comparison between the numerical predictions of the lateral dowel capacity (black solid lines with markers) and the analytical values determined according to Hilson [53] (red dashed lines with markers).

Results of this parametric study are summarized in Figure 3.5. Numerical predictions (black solid lines) provided an excellent match with the values determined according to Hilson [53] (red dashed lines). Analyses with d = 4.0 mm lead to a failure mechanism where the bending capacity of the nail is attained with two plastic hinges together with embedding of timber. Simulations performed with larger diameters lead to a mechanism where only one plastic hinge is attained together with embedding of timber.

3.4 PARAMETRIC STUDY

A parametric study is carried out to investigate how the response of the joint is influenced by the embedment behaviour of timber and the withdrawal behaviour of the fastener. The study is performed by considering a steel-to-timber joint in CLT and results are compared to the test data published by Casagrande *et al.* [7] and Izzi *et al.* [59].

Analyses are performed by defining the yield moment of the fastener M_{y} as the plastic moment capacity of the circular cross-section (Equation 3.4). The yield strength of the fastener f_{y}, which is an input parameter required by the model, is determined according to Equation 3.5 [92].

$$M_{\mathrm{y}} = \frac{1}{6} f_{\mathrm{y}} d^3 \tag{3.4}$$

$$f_{\mathrm{y}} = 1154 d^{-0.29} \tag{3.5}$$

The embedding capacity of timber F_{h} is determined by multiplying the embedding strength f_{h} by the tributary area of each beam ($d \times l$). Values of f_{h} are determined based on Equation 3.6, where ρ denotes the average density of the CLT panel [100].

$$f_{\mathrm{h}} = 0.13 \rho^{1.05} d^{-0.53} \tag{3.6}$$

Finally, the withdrawal capacity of the fastener F_{ax} is defined as given in Equation 3.7 [3], where l_{thr} is the threaded length of the shank. The withdrawal load attributed to each spring is determined as the ratio of F_{ax} to the number of beams used to discretize the fastener shank.

$$F_{\mathrm{ax}} = 0.155 \rho^{0.8} d^{0.6} l_{\mathrm{thr}} \tag{3.7}$$

Calculation methods to predict the embedment stiffness of timber and the withdrawal stiffness of the joint have not yet been derived; consequently, such stiffness properties are determined based on the test results published in the literature. The embedding capacity of timber F_h is usually attained at around 2.0 mm of displacement [54, 66, 77]; therefore, the embedment stiffness K_h is defined as the ratio of F_h to such value. The withdrawal capacity of a nail F_{ax} is usually attained at around 2.5 mm of displacement [59]; based on this, the withdrawal stiffness K_{ax} is defined as the ratio of the load attributed to each spring (i.e. F_{ax} divided by the number of beams used to discretize the shank) to such displacement. The influence of K_h and K_{ax} on the mechanical response of the joint is taken into account in the parametric study.

3.4.1 Results of the parametric study

Simulations considered a steel-to-timber joint with an annular-ringed shank nail in CLT. The nail has diameter d = 4.0 mm, threaded length l_{thr} = 44 mm and pointside penetration depth t_1 = 54 mm. The average density of CLT, measured from the specimen used in the test, is equal to 420 kg/m^3. Analyses are performed by assuming that the fastener shank is discretized into 18 beams of length l = 3 mm.

The embedding stiffness of timber is the first parameter taken into account in the study; analyses are carried out by varying the displacement at which F_h is attained between 1.0 mm and 3.0 mm, with 0.5 mm steps. The withdrawal stiffness is kept constant, assuming that F_{ax} is attained at 2.5 mm of displacement while the contribution due to the friction between fastener shank and timber is neglected.

Results obtained with the proposed numerical model (black lines) are compared to the test data published by Casagrande *et al.* [7] (solid red line) in Figure 3.6. The embedding stiffness of timber affects the response of the joint up to 3 mm of displacement. The loading curve obtained by assuming that F_h is attained at 2.0 mm of displacement (black dashed line) fits quite well with the test data. The withdrawal behaviour of the fastener is activated after 3 mm of displacement. Here, the difference between experimental and numerical results is due to the lack of friction in the contact area between fastener shank

and compressed timber. Nevertheless, the maximum load attained in the test is close to the numerical predictions, with a maximum error lower than 5%.

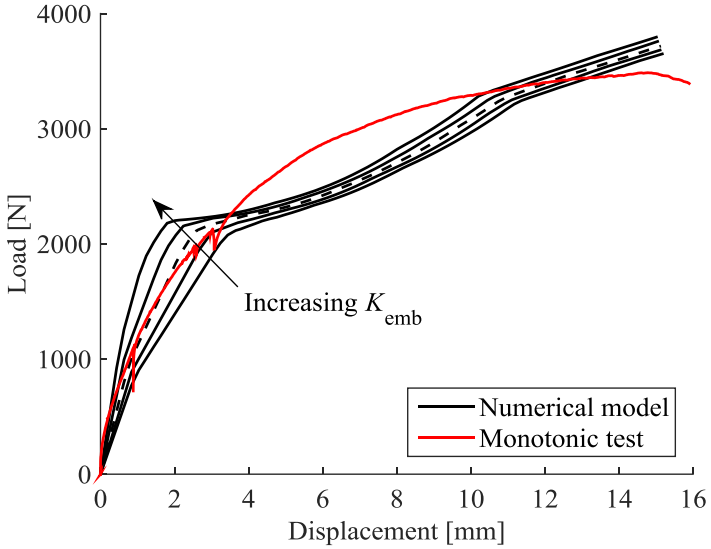

Figure 3.6. Influence of the embedding stiffness of timber: comparison between experimental data (from Casagrande *et al.* [7]) and numerical results obtained with the proposed model.

The stiffening contribution due to the friction between fastener shank and timber is the second parameter investigated in this study by varying the displacement at which F_{ax} is attained between 0.5 mm and 2.5 mm, with 0.5 mm steps. The embedding stiffness is kept constant, assuming that F_h is attained at 2.0 mm of displacement while the tangential stresses in the contact area between fastener shank and timber are disregarded.

Figure 3.7 shows a comparison between experimental and numerical results; it should be noticed that increasing the withdrawal stiffness of the nail has no evident effects before 3 mm of displacement; on the contrary, it reduces the difference between experimental and numerical results afterwards. Results highlight that the withdrawal stiffness has minor effects on the maximum load of the joint. The best fit between test and numerical results is obtained when the displacement at which F_{ax} is attained is reduced to 0.5 mm (black dashed line). It should be noticed that such value is much lower compared to the reference displacement discussed at the beginning of this section; however, that value is determined under pure withdrawal loads and might be lower when the joint is simultaneously loaded in shear and withdrawal.

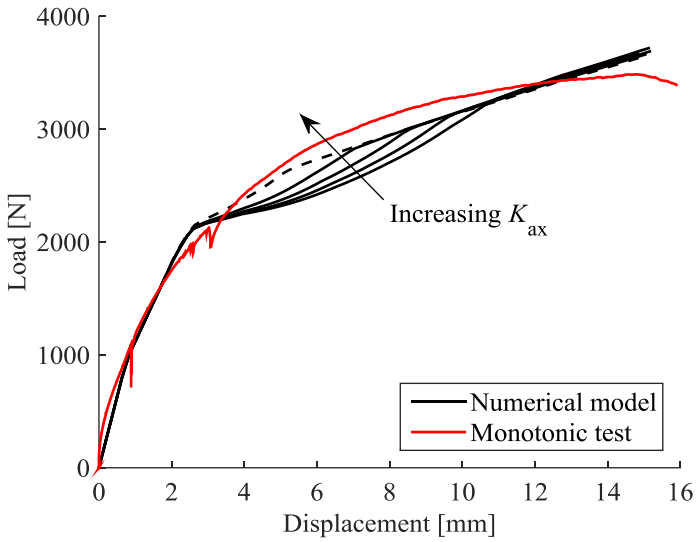

Figure 3.7. Influence of the withdrawal stiffness of the nail: comparison between experimental data (from Casagrande *et al.* [7]) and numerical results obtained with the proposed model.

The third set of simulations investigated the contribution of the tangential stresses in the contact area between fastener shank and compressed timber. Analyses are performed by varying the friction coefficient μ_{fr} between 0.0 and 0.4, with 0.1 steps. The embedding stiffness K_h is kept constant, assuming that F_h is attained after 2.0 mm of displacement. Similarly, K_{ax} is left unchanged, assuming that F_{ax} is attained at 0.5 mm of displacement.

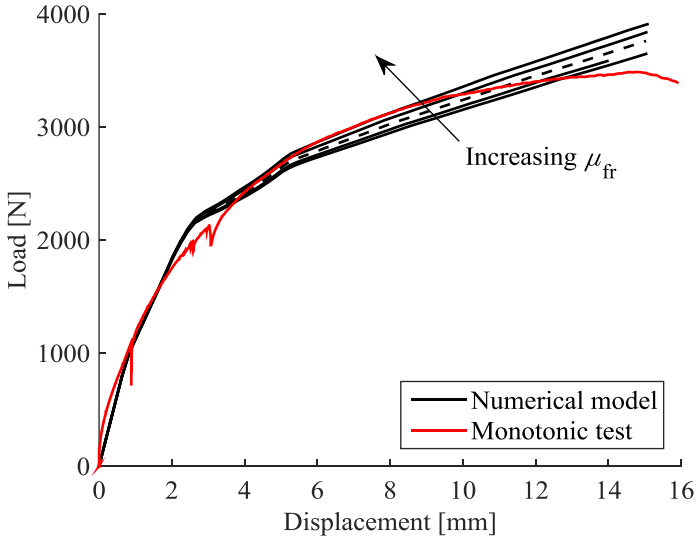

Figure 3.8. Influence of the tangential stresses in the contact area between nail shank and compressed timber: comparison between experimental data (from Casagrande *et al.* [7]) and numerical results obtained with the proposed model.

Results obtained with the numerical model are compared to the reference test data in Figure 3.8. The best fit between test and numerical results is obtained with μ_{fr} equal to

0.2 (black dashed line); in particular, considering such friction coefficient, the numerical results fit quite well the experimental loading curve up to 12 mm of displacement.

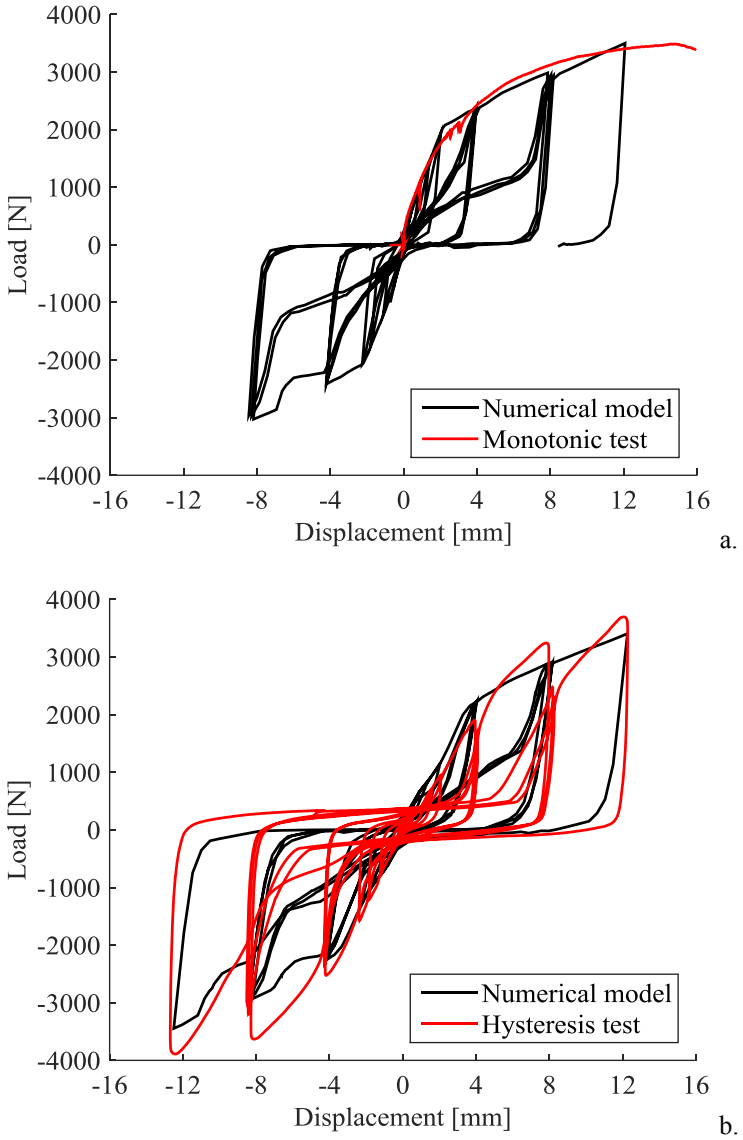

Figure 3.9. Load-displacement response under cyclic conditions: comparison between experimental data and numerical results, obtained by taking as a reference (a) the monotonic test performed by Casagrande *et al.* [7] and (b) a cyclic test carried out by Izzi *et al.* [59].

Finally, the load-displacement response under cyclic conditions is investigated. The numerical results are compared to the monotonic test carried out by Casagrande *et al.* [7] (Figure 3.9a) and to a cyclic test performed by Izzi *et al.* [59] (Figure 3.9b). In the first case, the same input parameters discussed above are adopted, i.e. F_{h} attained at 2.0 mm of displacement, F_{ax} attained at 0.5 mm of displacement, and μ_{fr} equal to 0.2. In the

second case, since the test showed a lower elastic stiffness, the embedding stiffness of timber is conveniently reduced to take into account the effect of small gaps between nail cap and metal plate that might have influenced the experimental loading curve. All the other input parameters are left unchanged. Both simulations were performed considering the displacement history used in the test done by Izzi *et al.* [59]. As visible in Figure 3.9, the model is capable to reproduce the cyclic response of the joints, leading to sufficiently accurate predictions of the hysteresis cycles. This applies even to the history of dissipated energy, with a final difference between experimental and numerical results equal to 5.3%.

3.5 CONCLUDING REMARKS

This chapter proposes a numerical model able to predict the load-displacement response and the failure mechanism of joints with dowel-type fasteners. The model reproduces the non-linear response of the steel and timber components of the joint employing basic input parameters and simple mechanical relationships.

Shear tests were reproduced on a nailed steel-to-timber joint in CLT. The mechanical behaviour of the joint was validated by comparing the numerical predictions of the lateral dowel capacity to the analytical values determined using a calculation model proposed by Hilson [53]. Moreover, the model was capable to identify the failure mechanism in all the cases analysed.

A parametric study investigated afterwards how the load-displacement response of the joint is influenced by the embedment behaviour of timber and the withdrawal behaviour of the fastener. Results obtained with the numerical model were compared to the test data published in literature. Simulations showed that the bearing mechanism is controlled by the lateral dowel capacity of the joint up to 3 mm of displacement while the withdrawal behaviour of the nail is activated afterwards. Analyses highlighted that the friction among the fastener shank and timber has a significant effect on the response of the joint, and is activated when the nail is withdrawn from the timber embedment. Finally, the hysteretic behaviour of the joint was investigated. Numerical results were compared to the test data published in literature leading to sufficiently accurate predictions of the hysteresis cycles.

4 Modelling the mechanical behaviour of typical wall-to-floor connection systems for Cross-Laminated Timber structures

SHORT SUMMARY

This chapter proposes a numerical model able to predict the mechanical behaviour and failure mechanisms of wall-to-floor connections for Cross-Laminated Timber structures. Such systems are assembled using metal connectors (e.g. angle brackets and hold-downs), anchored to the wall and floor panels with nailed and bolted joints. The connector and the panels to which it is restrained are simulated using 3D solid bodies while the nailed joints are schematized as non-linear hysteretic springs. Shear and tension tests are reproduced on typical wall-to-floor connection systems and results are compared to the experimental data obtained on similar test setups, leading to limited differences. Finally, the behaviour when shear and tension loads are applied simultaneously is investigated via a parametric numerical study. Analyses highlighted a quadratic interaction domain between shear and tension loads and showed that their coupled effect reduces the stiffness and the maximum load-carrying capacity of the connections.

The experimental results taken from Casagrande et al. were obtained in the framework of the Seismic X-REV research project, funded by Rothoblaas (Cortaccia, Italy) and by the Autonomous Province of Bolzano (Italy). Tests were carried out by the Timber Group of the University of Trento (Italy), which is gratefully acknowledged.

4.1 INTRODUCTION

As a structural product, Cross-Laminated Timber (CLT) exhibits a high in-plane stiffness and linear-elastic behaviour with the tendency to fail with brittle mechanisms (except for compressive stresses). Therefore, mechanical connections between walls and floor panels represent the ductile zones of CLT structures, supplying the necessary strength, stiffness, and energy dissipation under seismic conditions [46].

The mechanical behaviour of wall-to-floor connection systems for CLT structures was the focus of a large body of research. Shear and tension tests were carried out on several types of angle brackets and hold-downs, considering different nail patterns and anchoring [7, 39, 47, 99]. Recently, tests were even performed under the simultaneous application of shear and tension loads, highlighting that the coupled shear-tension action affects the stiffness, the load-carrying capacity and the energy dissipation [70, 83].

The increasing use of CLT for the construction of medium to high-rise structures (the so-called 'tall buildings') requires connections with excellent mechanical properties and large ductility ratios. However, the outcome of past test programmes highlighted some inappropriate failure mechanisms that might limit the application of the metal connectors currently available on the market. In particular (see Figure 4.1): in connections with angle brackets, (*a*) failure due to withdrawal of the nails connected to the floor panel or (*b*) due to pull-through of the anchoring bolts; (*c*) in connections with hold-downs, tensile failure in the net cross-section of the metal flange. Those failure mechanisms might be associated to an incorrect design of the nailed joints and could be avoided by employing a capacity-based design approach and by over-strengthening those parts of the connection [59].

Improving the mechanical behaviour of the connection systems currently available on the market and developing new solutions is an expensive and time-consuming process, since requires the consideration of several factors (e.g. thickness of the metal member, number and position of nails, anchoring) and loading cases. Therefore, to limit the need of experimental tests to a minimum, great effort should be devoted to develop advanced numerical models capable to predict their mechanical behaviour and failure mechanisms.


a.

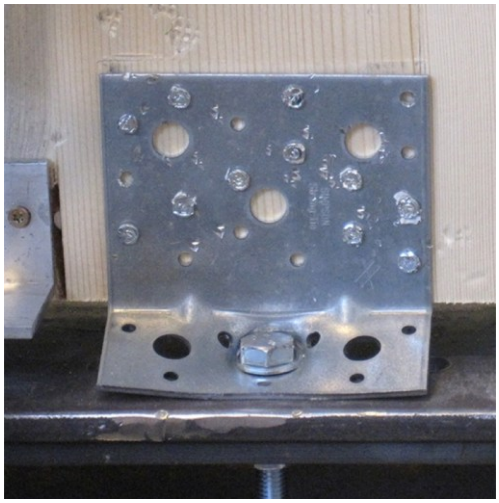
b.

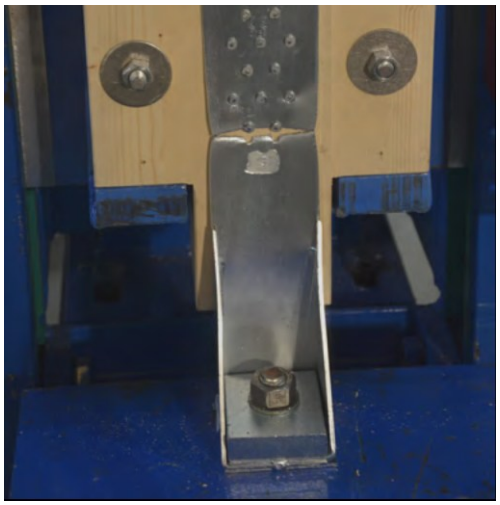
c.

Figure 4.1. Inappropriate failure mechanisms at the connection level: (a) failure due to withdrawal of the nails connected to the floor panel; (b) failure due to pull-through of the anchoring bolt, and (c) tensile failure of the net cross-section of the metal flange (courtesy of CNR IVALSA and University of Trento, Italy).

This chapter presents a numerical model that predicts the load-displacement response and failure mechanisms of wall-to-floor connections for CLT structures. The connector (e.g. an angle bracket or a hold-down) and the panels where it is anchored are modelled as 3D solid bodies while the nailed joints are simulated as non-linear hysteretic springs with a user element subroutine taken from Rinaldin *et al.* [86]. Shear and tension tests are reproduced on typical connections for CLT structures tested at the University of Trento (Italy) in the framework of the Seismic X-REV research project. Experimental data and numerical predictions are compared and discussed. Finally, the behaviour when shear and tension loads are applied simultaneously is investigated via a parametric numerical study. Simulations are carried out by varying the inclination of the external load, with respect to the axis of the metal connector, between 0° (pure axial load) and 90° (pure shear load). Analyses are subsequently repeated by varying the nail pattern used to anchor the metal connectors to the CLT panels, highlighting how the number of nailed joints influences the stiffness and the load-carrying capacity of the connections. All the simulations are performed using ABAQUS software package [96].

4.2 MODEL DESCRIPTION

The metal connector and panels where it is anchored are modelled as 3D solid bodies, meshed with cubic elements with reduced integration (C3D8R). The wall and floor panels are introduced in the analyses to account for the surface-to-surface contact interaction and do not influence the mechanical behaviour of the metal connector. Therefore, to limit the computational effort required by the simulations, only the top 10 mm thickness of those elements are modelled.

The metal connector has an elasto-plastic isotropic behaviour with elastic stiffness set to 210 GPa and Poisson's ratio equal to 0.3. The proof strength and the ultimate strength of the steel material cannot be set *a priori* and depend on the connector being analysed. In this chapter, such parameters are defined according the requirements included in the European Technical Assessments (ETAs) of the connectors considered in the simulations.

The CLT wall has an elastic orthotropic behaviour with material parameters taken from Fortino *et al.* [44] (*Picea abies*). The floor element can be either a rigid foundation (e.g. a steel profile or a concrete basement over which the ground floor is assembled) or another CLT panel (e.g. an intermediate floor). In the first situation, an elastic isotropic material is considered with the material properties defined above; in the second situation, the same material parameters of the CLT wall are used.

The nailed steel-to-timber joints are simulated as 2-node non-linear springs with three degrees of freedom. Two displacement components simulate the shear response parallel and perpendicular to the superficial lamination of the panel. The third one reproduces the withdrawal behaviour of the nail under axial loads. Each spring is pinned onto the metal connector (at the nail cap location) and onto the external surface of the CLT panel (at the nail point location), where the boundary conditions of the model are applied.

The displacement components that simulate the shear response of the nailed joints are coupled by means of the force-based strength domain with quadratic interaction given in Equation 4.1. In the expression below, F_{y} is the yield load of the joint while $F_{0°,i}$ and $F_{90°,i}$ are the shear loads parallel and perpendicular to the superficial lamination of the CLT panel at the *i*-th analysis step. Further information on this quadratic interaction and how it affects the response of the non-linear springs are given in Rinaldin *et al.* [86].

$$\left(\frac{F_{0°,i}}{F_{\mathrm{y}}}\right)^2+\left(\frac{F_{90°,i}}{F_{\mathrm{y}}}\right)^2\leq 1 \tag{4.1}$$

4.3 MECHANICAL PROPERTIES OF NAILED JOINTS

Nailed joints in CLT structures are assembled using annular-ringed shank nails (Figure 4.2). Compared to traditional round nails with smooth shank, the threaded shank increases the withdrawal capacity while the conical-shaped cap enhances the clamping to the metal plate and enforces a ductile failure mechanism with two plastic hinges.

In this study, the mechanical properties of nailed joints are determined based on the calculation models published in literature [3, 53, 89, 92]. Moreover, results are combined with the prescriptions included in the ETAs of nails currently available on the market.

Figure 4.2. Annular-ringed shank nails (reproduced from Izzi *et al.* [59]).

4.3.1 Load-carrying capacity

The load-carrying capacity of laterally loaded joints with annular-ringed shank nails F_{v} is defined as the sum of two contributions (Equation 4.2); the first term signifies the lateral dowel capacity of the joint F_{lat} while the second one denotes the rope effect and is equal to 50% of the withdrawal capacity of the nail F_{ax}.

$$F_{\mathrm{v}} = F_{\mathrm{lat}} + 0.5F_{\mathrm{ax}} \tag{4.2}$$

The contribution due to the rope effect is determined following the design provisions included in the ETAs of Rothoblaas [35] and Simpson Strong-Tie [30] annular-ringed shank nails. It must be noticed that the calculation model prescribed in Eurocode 5 [24] for nailed joints with smooth shank is similar to Equation 4.2. However, the standard sets the rope effect to $0.25F_{\mathrm{ax}}$ and limiting factors are introduced to avoid relying on the withdrawal of the fastener. In particular, the standard limits the rope effect of round nails with smooth shank to $0.15F_{\mathrm{lat}}$ while for other nails it is increased up to $0.5F_{\mathrm{lat}}$.

The lateral dowel capacity of the joint (F_{lat}) is defined based on the European Yield Model, originally proposed by Johansen [62]. The analytical model adopted in this study (Equation 4.3) was developed by Hilson [53] considering a nailed steel-to-timber joint with a thick metal plate. According to Eurocode 5 [24] the situation of 'thick plate' is attained when the thickness of the metal plate is greater than or equal to the diameter of the nail. However, as discussed by Izzi *et al.* [59], the conical-shaped cap enforces a

ductile failure mechanism with two plastic hinges even with thinner plates and Equation 4.3 is employed regardless the thickness of the metal sheet.

$$F_{\text{lat}} = \min \begin{cases} f_{\text{h}} t_1 d & \text{(a)} \\ f_{\text{h}} t_1 d \left[\sqrt{2 + \dfrac{4 M_{\text{y}}}{f_{\text{h}} t_1^2 d}} - 1 \right] & \text{(b)} \\ 2.0 \sqrt{M_{\text{y}} f_{\text{h}} d} & \text{(c)} \end{cases} \tag{4.3}$$

In the expressions above, d is the diameter of the fastener, t_1 the pointside penetration depth while M_{y} and f_{h} denote the yield moment of the nail and the embedding strength of timber, respectively. The equation giving the lowest lateral dowel capacity identifies the failure mechanism (Figure 4.3). Equation 4.3a is associated to a mechanism where there is only embedding of timber while the fastener behaves as a rigid element. Equation 4.3b-4.3c describe two mechanisms where the yield moment of the fastener is attained (with one and two plastic hinges) together with embedding of the timber around it.

The yield moment of the nail is defined as the plastic moment capacity of the circular cross-section (Equation 4.4); in the expression below, f_{y} denotes the yield strength of the nail, determined according to Equation 4.5 [92].

$$M_{\text{y}} = \frac{1}{6} f_{\text{y}} d^3 \tag{4.4}$$

$$f_{\text{y}} = 1154 d^{-0.29} \tag{4.5}$$

The embedding strength of timber is defined based on the calculation model given in Equation 4.6, with ρ average density of CLT [89]. Generally, the embedment behaviour of timber depends on the relative orientation among applied load and grain direction [4, 50, 77, 94]; differences can be neglected if d is smaller than 8 mm [54, 105]

$$f_{\text{h}} = 0.10 \rho d^{-0.3} \tag{4.6}$$

Finally, the withdrawal capacity of a nail F_{ax} is determined as shown in Equation 4.7, where l_{thr} is the threaded length of the nail shank [3].

$$F_{\text{ax}} = 0.155 \rho^{0.8} d^{0.6} l_{\text{thr}} \tag{4.7}$$

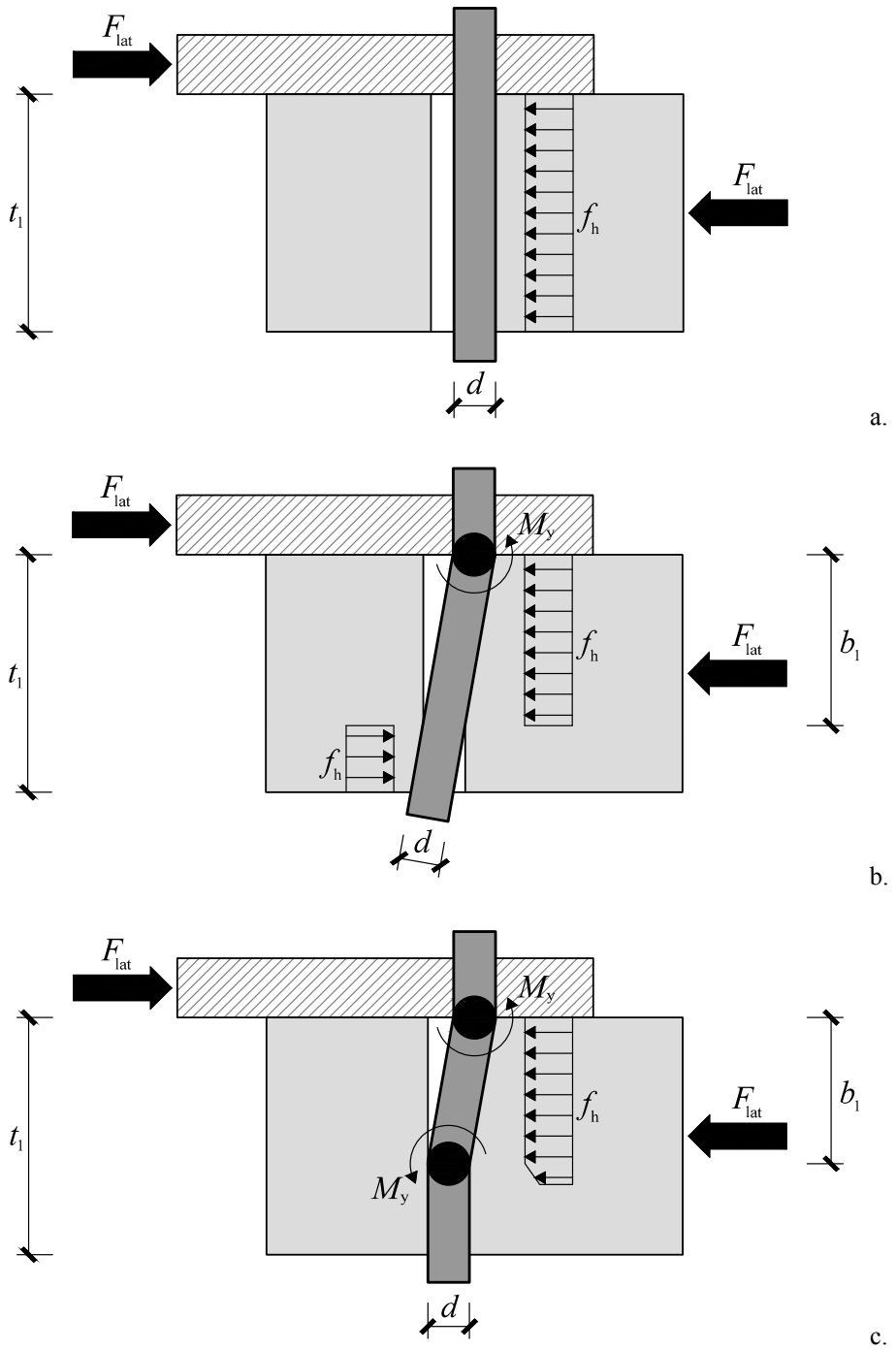

Figure 4.3. Failure mechanisms in nailed steel-to-timber joints with thick metal plates (adapted from Flatscher [37] and Hilson [53]).

4.3.2 Slip modulus

The slip modulus of laterally loaded nailed joints is predicted based on the calculation model included in Eurocode 5 [24]; such model was originally developed by Ehlbeck and Larsen [18] for a nailed timber-to-timber joint. Based on mechanical relationships, the

standard suggests that the slip modulus of a similar steel-to-timber joint may be doubled up, leading to Equation 4.8. It should be noticed that tests carried out by Izzi *et al.* [59] on single fastener joints highlighted that this expression overestimates the experimental slip moduli and suggested that the assumption of rigid plate, which is the basis for doubling the stiffness, might not be valid at low load levels.

$$K_{ser} = 2\rho^{1.5} d^{0.8} / 30 \tag{4.8}$$

4.4 LOAD-DISPLACEMENT RESPONSE OF NAILED JOINTS

The mechanical relationships used to schematize the shear response of a nailed joint are discussed in the following sub-sections. Since tests carried out on single and on a group of nailed joints showed slightly different load-displacement responses, such behaviour is schematized according to three methods (Figure 4.4). The first one (labelled 'Method I') uses a bilinear relationship with a plastic plateau. The second one (labelled 'Method II') adopts a bilinear relationship with a hardening branch; finally, the third one (labelled 'Method III') employs a trilinear elasto-plastic relationship.

The third displacement component of the non-linear springs simulates the withdrawal behaviour of the nail. Since the rope effect is already accounted into the shear components (Equation 4.2), this contribution is activated only under pure axial loads. Consequently, it is taken into account in the analyses as an elastic spring with a brittle failure mechanism after the attainment of the maximum load. The stiffness of the withdrawal component is set to 1250 N/mm based on the test results published by Izzi *et al.* [59] while the maximum load is determined as shown in Equation 4.7.

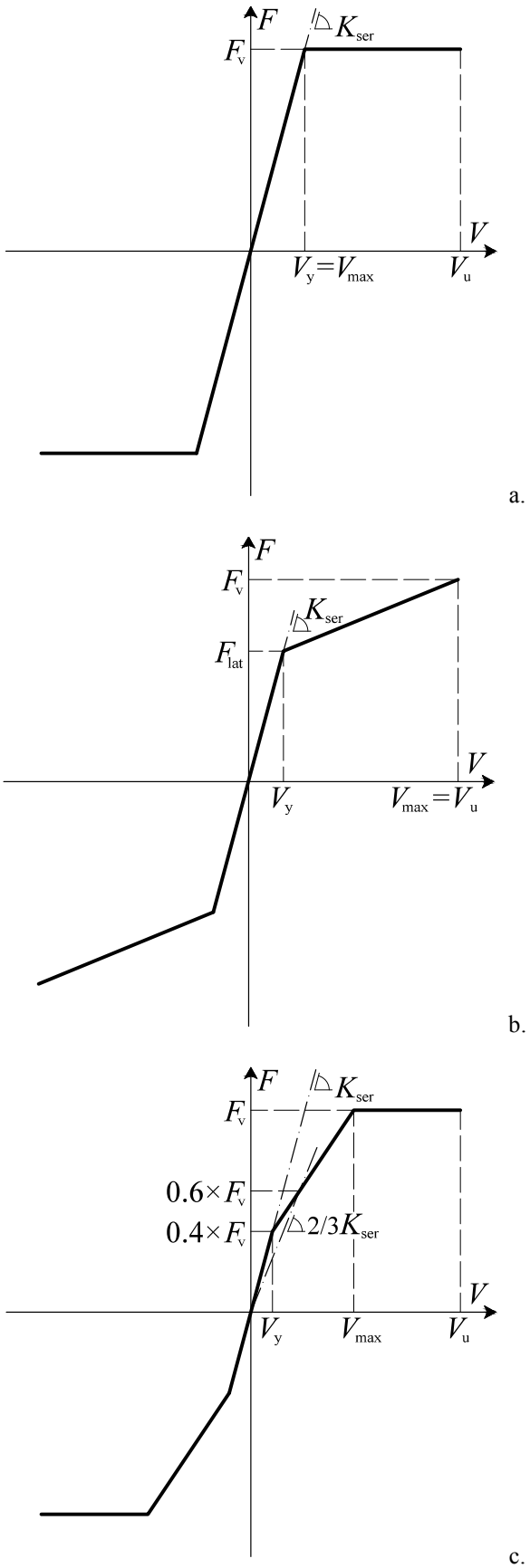

Figure 4.4. Load-displacement response of nailed steel-to-timber joints according to (a) Method I, (b) Method II, and (c) Method III.

4.4.1 Method I

The first method schematizes the shear response of a nailed joint with a bilinear elasto-plastic relationship (Figure 4.4a). The elastic stiffness is equal to the slip modulus of the joint K_{ser} while the load-carrying capacity F_v identifies the load at both the transition point between the elastic branch and the plastic plateau, and at the ultimate displacement V_u (conventionally set to 20 mm). In Figure 4.4a, V_y denotes the yield displacement and V_{max} the displacement at which F_v is attained, being $V_y = V_{max} = F_v / K_{ser}$.

The assumption of elastic behaviour until the attainment of F_v is acceptable since tests carried out by Izzi *et al.* [59] on single fastener joints showed a linear fashion until 90% of the maximum load-carrying capacity. However, the displacement at which F_v is attained in the tests is generally higher compared to the values obtained with this bilinear method, possibly leading to incorrect predictions of V_y (and V_{max}) in the analyses.

4.4.2 Method II

The second method schematizes the shear response of a nailed joint using an elasto-plastic relationship with a hardening branch (Figure 4.4b) and is derived from the tests carried out by Casagrande *et al.* [7]. The elastic stiffness is equal to the slip modulus of the joint K_{ser} while the load-carrying capacity F_v identifies both the maximum load and the load at the ultimate displacement ($V_{max} = V_u$). The yield load is equal to the lateral dowel capacity F_{lat}; this assumption has been confirmed via a parametric numerical study performed by Izzi *et al.* [60] on the same experimental data. Finally, the slope of the hardening branch is determined by assuming that F_v is attained at $V_{max} = V_u = 6V_y$, being $V_y = F_{lat} / K_{ser}$.

4.4.3 Method III

The third method schematizes the shear response of a nailed joint using a trilinear elasto-plastic relationship (Figure 4.4c) and is derived from the tests carried out by Ceccotti *et al.* [9]. The slope of the elastic branch is equal to the slip modulus K_{ser} while its maximum load is equal to 40% of F_v. The first inelastic branch has a hardening behaviour

and maximum load equal to F_v. Its slope is given by the line drawn through the points at 40% and 60% of F_v; the first point lays on the elastic branch while the second one belongs to the line drawn through the origin of the axis with stiffness equal to $2/3\,K_{ser}$. The second inelastic branch has a plastic behaviour until the ultimate displacement V_u (which is conventionally set to 20 mm) and is activated after the attainment of the maximum load, i.e. at $V_{max} = 1.9\,F_v / K_{ser}$.

4.4.4 Hysteretic behaviour

Nailed joints subjected to cyclic loads show pinching due to the reduction of stiffness at small displacement amplitudes when a cavity is formed around the fastener due to timber crushing. Stiffness increases at higher displacement levels when the nail comes again into contact with the surrounding timber [41].

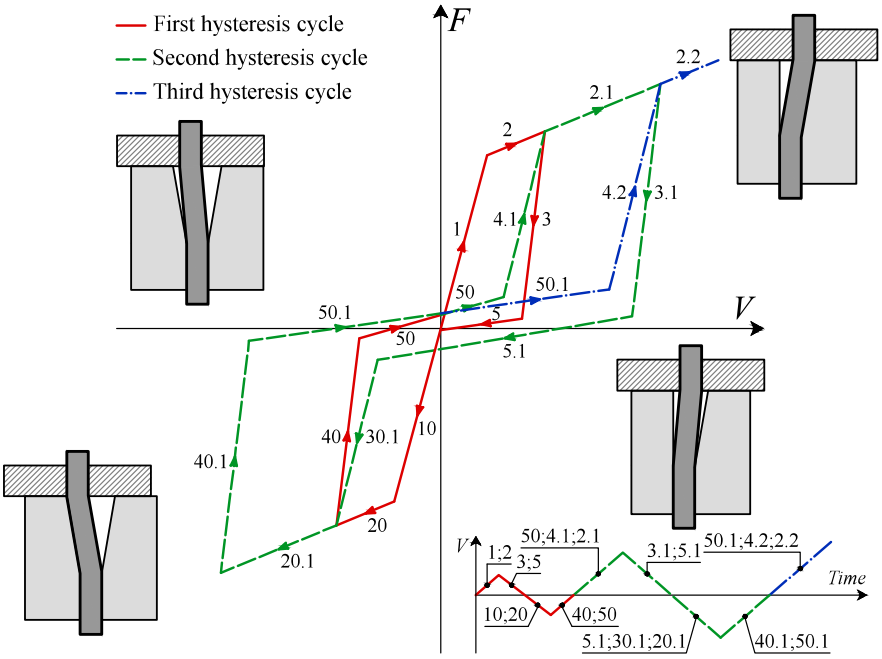

Figure 4.5. Hysteretic behaviour of a nailed steel-to-timber joint (adapted from Flatscher [37]).

The hysteretic behaviour of a nailed joint is schematized according to the piecewise-linear law given in Figure 4.5. The backbone curve (composed of branches #1, #2, #10, #20) is assembled based on the methods discussed above. If the joint is unloaded from a positive displacement, branch #3 is followed; on the contrary, branch #40 is followed if the unloading starts from a negative displacement. Branches #5 and #50 simulate the gap

between the fastener shank and the surrounding timber. Finally, branches #30 and #4 simulate the mechanical behaviour when the nail comes again into contact with timber.

The unloading (#3, #5, #30) and reloading (#40, #50, #4) paths depend on the plastic deformed configuration of the joint. Since nailed joints are too slender to attain a failure mechanism with only embedding of timber (Figure 4.3a), this situation is disregarded in the following discussion.

The slopes of branches #3 and #4 are defined based on the cyclic tests carried out by Izzi *et al.* [59] and are set to 5 and 2.5 times K_{ser}, respectively. Similarly, the load at the transition point between branches #3 and #5 is assessed from the same test data and is set to 5% of F_i, where F_i is the load attained on the backbone curve at the *i*-th analysis step. Finally, the load at the transition point between branches #5 and #30 is determined using an analytical procedure derived from Hilson [53] and is equal to $F_{\#5/\#30}/F_{\text{v}}$ times F_i, being $F_{\#5/\#30}$ the load taken by the deformed nail (in bending) at the hysteresis cycle where the load-carrying capacity F_{v} is attained (Equation 4.9).

$$F_{\#5/\#30} = M_{\text{y}}/b_1 \tag{4.9}$$

In the equation above, M_{y} denotes the yield moment of the nail while b_1 represents the effective penetration depth of the joint, which depends on its failure mechanism. In this study b_1 is determined according to Equation 4.10 when failure occurs for embedding of timber and yielding of the nail with one plastic hinge (Figure 4.3b) while Equation 4.11 is used when two plastic hinges have formed (Figure 4.3c).

$$b_1 = t_1\left[\sqrt{2+\frac{4M_{\text{y}}}{f_{\text{h}}t_1^2 d}}-1\right] \tag{4.10}$$

$$b_1 = 2\sqrt{\frac{M_{\text{y}}}{f_{\text{h}}d}} \tag{4.11}$$

The hysteresis model discussed above is validated by comparison with the cyclic tests carried out by Izzi *et al.* [59] on two nailed joints loaded parallel and perpendicular to the superficial lamination of a CLT panel, respectively. Results of this comparison are shown in Figure 4.6. Simulations employed the same displacement histories used in the reference

tests; moreover, the backbone curves of the non-linear springs are assessed from the first envelope curve of the experimental data according to EN 12512:2001/A1 [26]. Analyses highlighted that the hysteresis model is capable to predict with sufficient accuracy both load-displacement response and the energy dissipation, leading to less than 10% difference between experimental and numerical results.

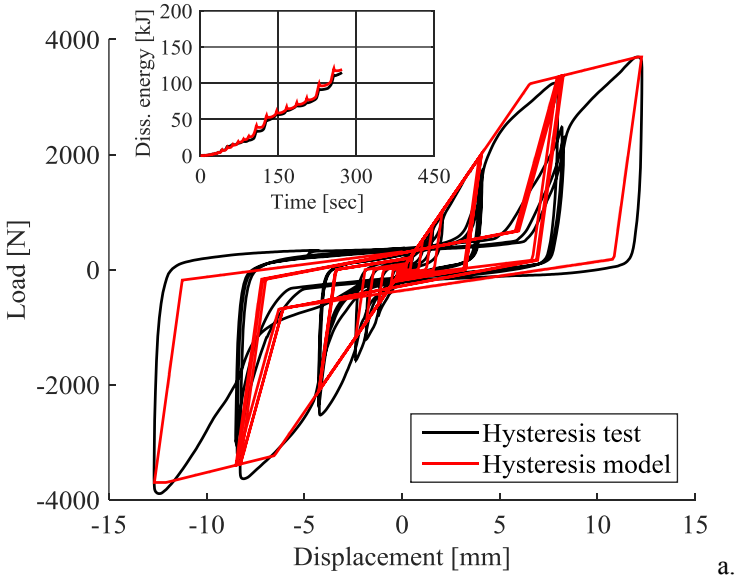

a.

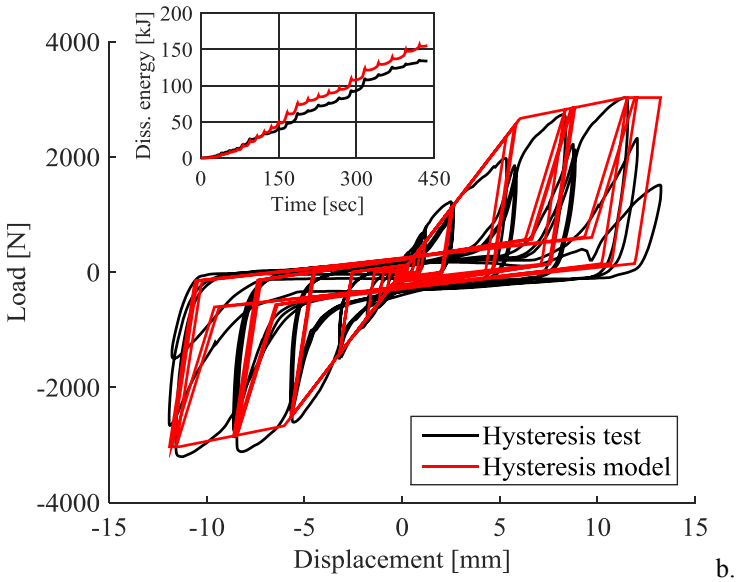

b.

Figure 4.6. Comparison between experimental (from Izzi *et al.* [59]) and numerical results obtained using the proposed hysteresis model for a nailed steel-to-timber joint loaded (a) parallel and (b) perpendicular to the superficial lamination of a CLT panel (with close-up on the history of dissipated energy).

4.5 GROUP EFFECT

The presence of several nails connected to the same metal plate at a very close distance requires the consideration of the mutual interaction among the fasteners, i.e. the so-called 'group effect'. Eurocode 5 [24] accounts for this interaction by considering the 'effective number of nails in a row', which depends on their spacing along the grain direction. Furthermore, the standard allows neglecting the group effect when the nails are staggered perpendicular to the grain by at least one diameter.

In this study, the mutual interaction among the nails is accounted by introducing the concept of 'effective load-carrying capacity'. In comparison with the approach given in the standard, the number of nails connected to the same metal plate is left unchanged. On the contrary, their load-carrying capacity F_{v} (Equation 4.3) is reduced by multiplying F_{lat} and F_{ax} by the effective factor k_{ef} defined in Equation 4.12.

$$k_{\mathrm{eff}} = n^{0.9}/n = n^{-0.1} \tag{4.12}$$

In the equation above, n denotes the total number of nails connected to the same metal plate while $n^{0.9}$ is their effective number, determined according to Eurocode 5 [24] when their spacing is in the range of $10d$ to $14d$ (which corresponds to the usual spacing on the metal connectors). Finally, similarly to what is assumed in the standard, no reduction is applied to the slip modulus of the nailed joints, which is calculated as in Equation 4.8.

4.6 NUMERICAL ANALYSES

Shear and tension tests are reproduced on two typical wall-to-floor connections systems tested at the University of Trento (Italy) and published by Casagrande *et al.* [7]. The first system is assembled with a Rothoblaas TTF200 angle bracket [34], anchored to two CLT panels with 60 nails (30 in each one). The second system is assembled with a Rothoblaas WHT620 hold-down [33], anchored to a Glue-Laminated Timber (GLT) panel with 52 nails and to a steel foundation with a bolt. In this second system, to prevent local buckling and to distribute the load over a larger surface, the anchoring to the steel foundation is strengthened with a 10 mm thick washer plate. Both setups used Rothoblaas annular-ringed shank nails [35] with d = 4.0 mm, t_1 = 54 mm and l_{thr} = 44 mm.

Based on the requirements given in the ETAs of the connectors, the angle bracket is made of S250GD steel with proof strength equal to 250 MPa and ultimate strength equal to 330 MPa. The hold-down is made of S355 steel with proof and ultimate strength equal to 355 MPa and 430 MPa, respectively. The average density of timber is measured from the test specimens and is ρ = 480 kg/m^3 for CLT and ρ = 420 kg/m^3 for GLT.

4.6.1 Simulations under monotonic loading conditions

The mechanical behaviour under monotonic conditions is investigated by considering the angle bracket subjected to a shear load and the hold-down to a tensile load. Analyses are carried out by applying a monotonic displacement history to the wall panel (up to 20 mm and 15 mm, respectively) while the floor element is restrained to its original position.

The first set of simulations neglected the reduction of strength due to the group effect. The load-displacement response of the nailed joints is defined based on Method I while their mechanical properties are determined as discussed in Section 4.3. As mentioned in Section 4.3.2, tests on single fastener joints highlighted that Equation 4.8 overestimates the experimental slip moduli; therefore, analyses are subsequently repeated by considering a factor 1 instead of the factor 2 prescribed in Eurocode 5 [24].

Figure 4.7 compares experimental data (solid grey line for the monotonic test and solid black line for the hysteresis) and numerical predictions when K_{ser} is calculated using a factor 2 (dash-dotted blue line) and a factor 1 (dashed red line), respectively. Furthermore, Figure 4.8 displays the stress distribution on the connectors after 15 mm of displacement. The angle bracket is characterized by local buckling while the hold-down shows a tensile failure in the lower part of the metal flange (which justifies the softening behaviour shown in Figure 4.7b). Analyses pointed out that the factor 1 provides accurate predictions of the elastic stiffness while the factor 2 leads to unrealistic stiff responses. Moreover, results showed higher load-carrying capacities compared to the reference test results.

Simulations are then repeated by considering even the other two methods discussed in Section 4.4 and by including the reduction of strength due to the group effect; all the slip moduli are calculated employing a factor 1 instead of the factor 2 given in Equation 4.8.

Figure 4.9 compares experimental and numerical results when the shear response of the nailed joints is defined according to Method I (dashed red line), II (solid orange line) and III (dash-dotted green line). Simulations showed that Method II and III provide reliable predictions of the mechanical behaviour of the connections; on the other hand, Method I leads to similar load-carrying capacities but provides less accurate identifications of the overall behaviour.

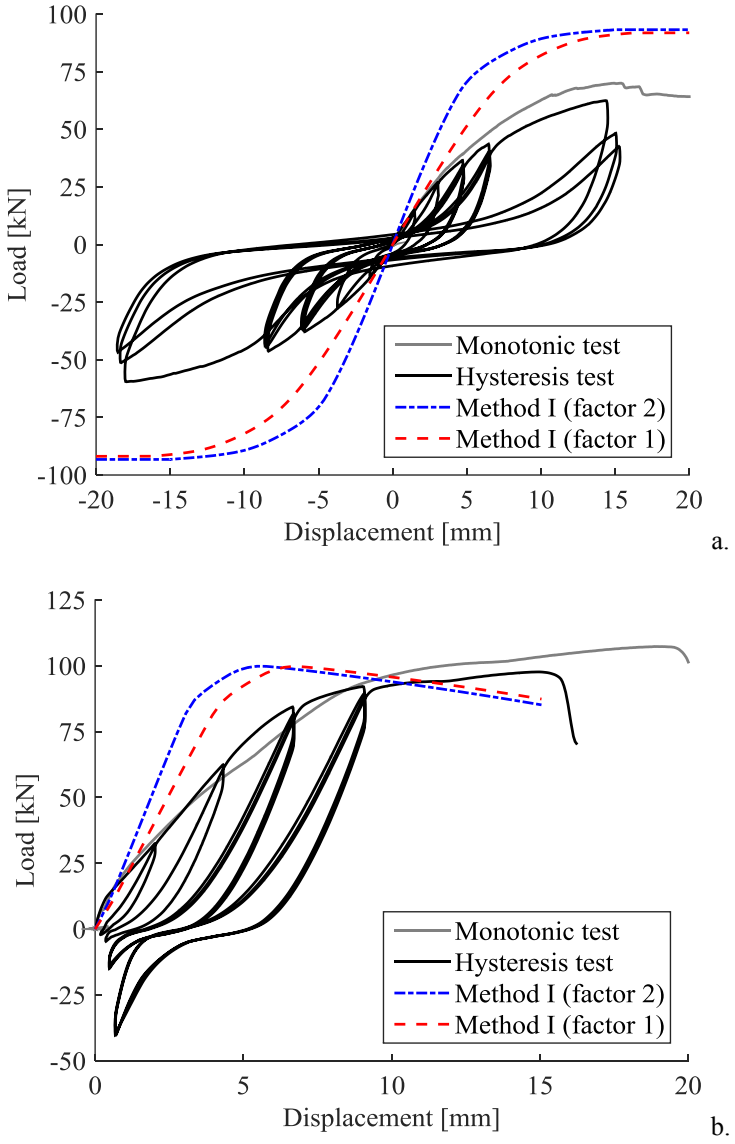

Figure 4.7. Comparison between experimental (from Casagrande *et al.* [7]) and numerical results (a) for the TTF200 angle bracket loaded in shear and (b) for the WHT620 hold-down loaded in tension using the actual mechanical properties of the nailed joints.

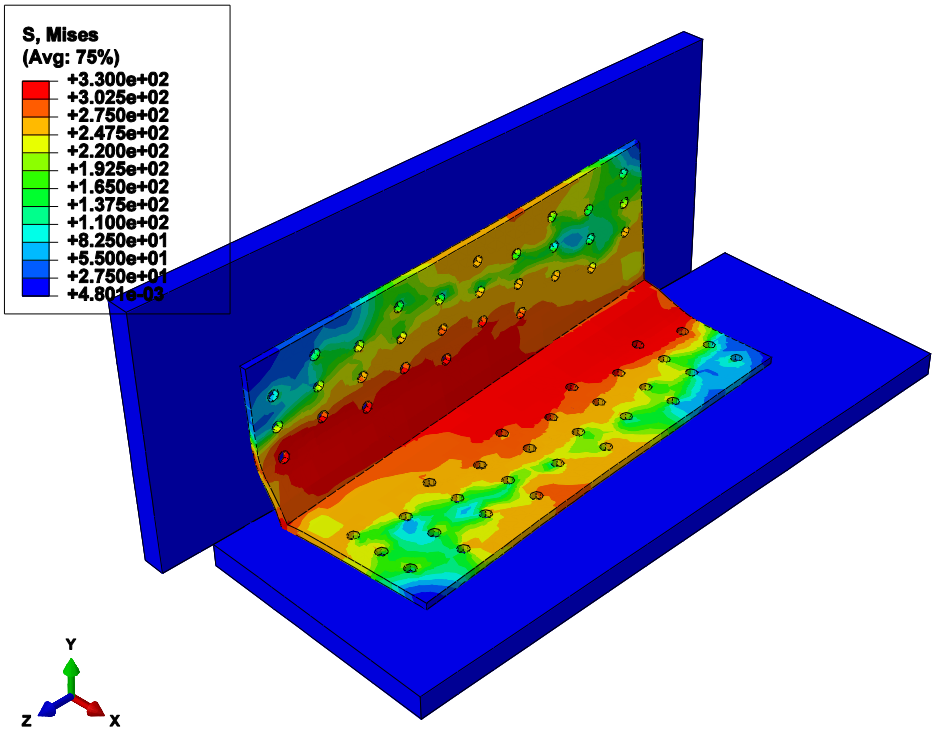

a.

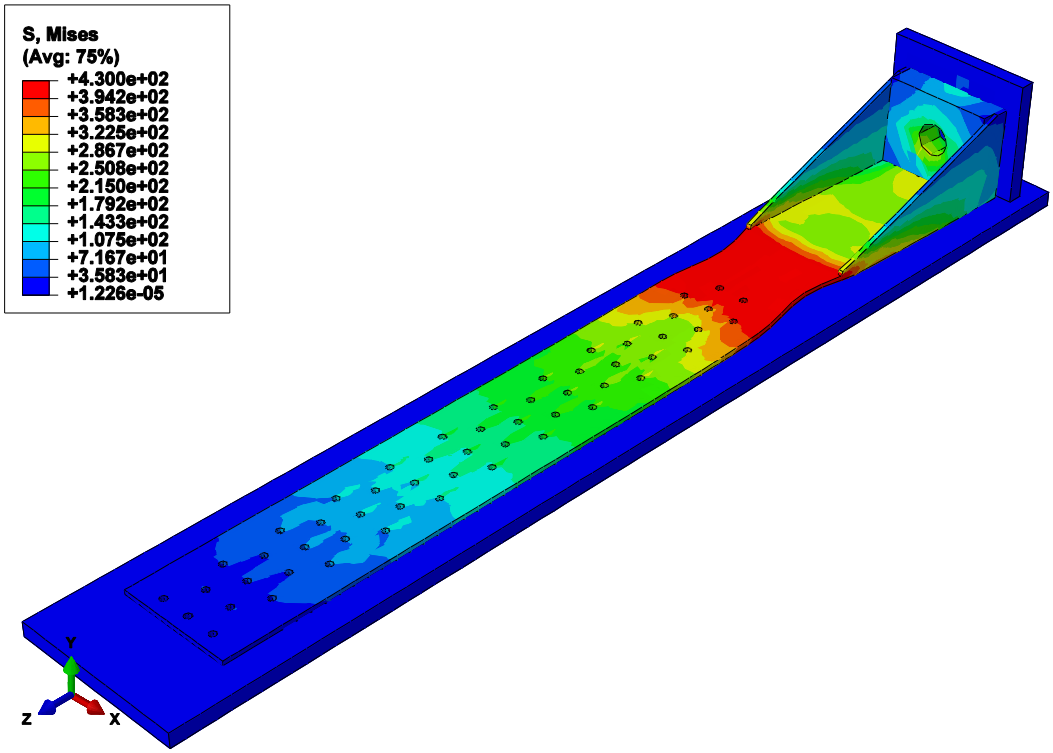

b.

Figure 4.8. Stress distribution in the metal connectors at 15 mm of displacement (a) for the TTF200 angle bracket loaded in shear and (b) for the WHT620 hold-down loaded in tension (displayed as contour of Von Mises stresses).

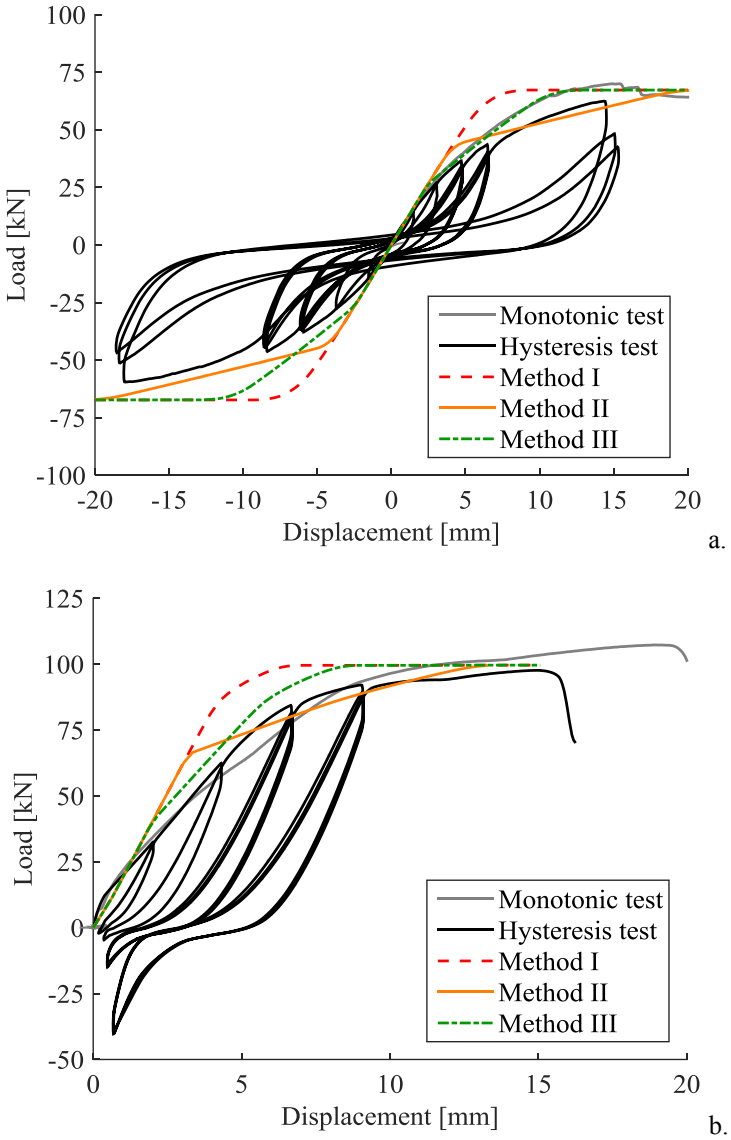

Figure 4.9. Comparison between experimental (from Casagrande *et al.* [7]) and numerical results (a) for the TTF200 angle bracket loaded in shear and (b) for the WHT620 hold-down loaded in tension when the load-carrying capacity of the nailed joints is reduced to account for the group effect.

4.6.2 Simulations under cyclic loading conditions

Cyclic shear and tension tests are reproduced on the previous numerical models, using the same input data of the monotonic analyses. Figures 4.10 and 4.11 compare test data (black line) and numerical results when the shear response of the nailed joints is defined according to Method II (orange line) and III (green line). Both methods provide reliable predictions of the hysteretic response and the energy dissipation. Method I is not taken into account in this comparison since it provides less accurate results and higher energy dissipations (about 10% higher than in the experimental tests).

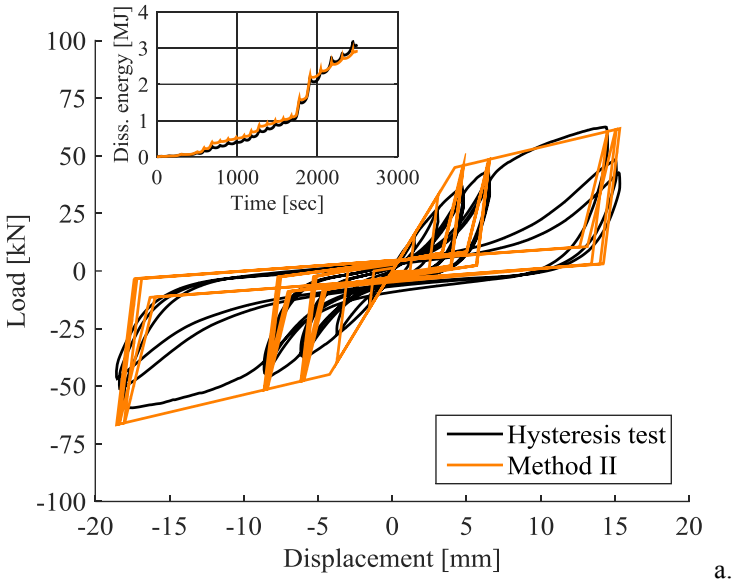

a.

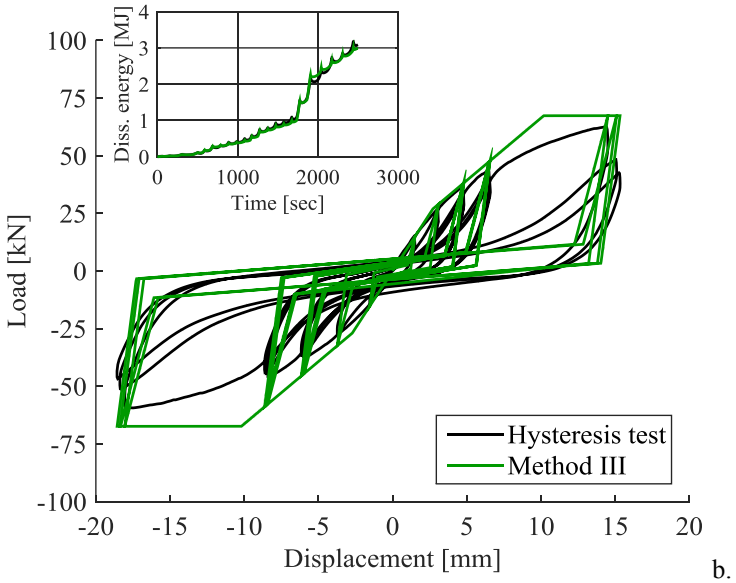

b.

Figure 4.10. Comparison between experimental hysteresis (from Casagrande *et al.* [7]) and numerical results for the TTF200 angle bracket when the load-displacement response of the nailed joints is defined according to (a) Method II and (b) Method III (with close-up on the history of dissipated energy).

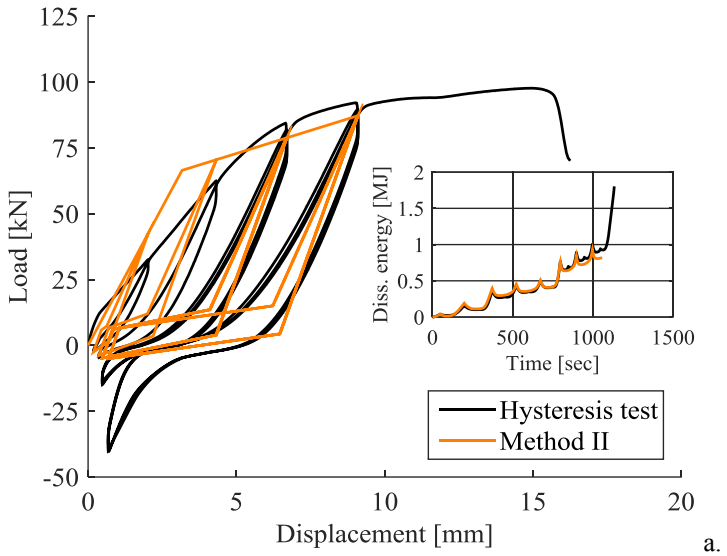

a.

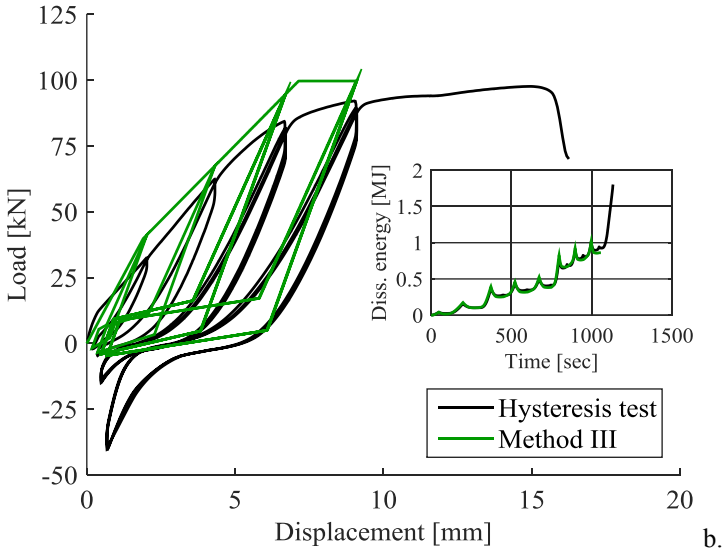

b.

Figure 4.11. Comparison between experimental hysteresis (from Casagrande *et al.* [7]) and numerical results for the WHT620 hold-down when the load-displacement response of the nailed joints is defined according to (a) Method II and (b) Method III (with close-up on the history of dissipated energy).

4.6.3 Simulations under bi-axial loading conditions

The mechanical behaviour under the simultaneous application of shear and tension loads (bi-axial loading condition) is investigated via a parametric numerical study. Simulations are carried out by varying the inclination of the external load, with respect to the axis of the metal connector, between 0° (only axial load) and 90° (only shear load). Analyses are subsequently repeated by reducing the number of nails used in the connections. For each metal connector, three nail patterns are considered: 30+30 (original pattern), 25+25, and 15+15 nails for the angle bracket; 52 (original pattern), 30 and 22 nails for the hold-down. Analyses are carried out by assuming an ultimate displacement equal to 15 mm [29]. For simplicity, the behaviour of the nailed joints is always defined according to Method II.

Figure 4.12 shows the load-displacement response of the angle bracket when $\alpha = 90°$ and $\alpha = 45°$ while Figure 4.13 presents similar results for the hold-down when $\alpha = 0°$ and $\alpha = 45°$. Finally, Figure 4.14 displays the stress distribution in the connectors at the end of the simulations when $\alpha = 45°$. Results highlighted that the loading direction affects the stiffness and the load-carrying capacity of the connections.

The maximum loads attained in the analyses are used to create the strength domains shown in Figure 4.15 (black lines); each point is determined as either the absolute maximum of the loading curve or the load at 15 mm of displacement, whichever occurs first. Results are then compared to the strength domains suggested in the ETAs of the metal connectors (Equation 4.13, red dashed lines).

$$\left(\frac{F_{0°,i}}{F_{0°,\max}}\right)^2 + \left(\frac{F_{90°,i}}{F_{90°,\max}}\right)^2 \leq 1 \tag{4.13}$$

In the equation above, $F_{0°,\max}$ and $F_{90°,\max}$ represent the maximum loads in the axial and shear direction while $F_{0°,i}$ and $F_{90°,i}$ are the corresponding loads at the *i*-th analysis step, respectively. Based on the comparisons presented in Figure 4.15, numerical results validate the strength domains suggested in the ETAs by confirming a quadratic interaction relationship between shear and tension load.

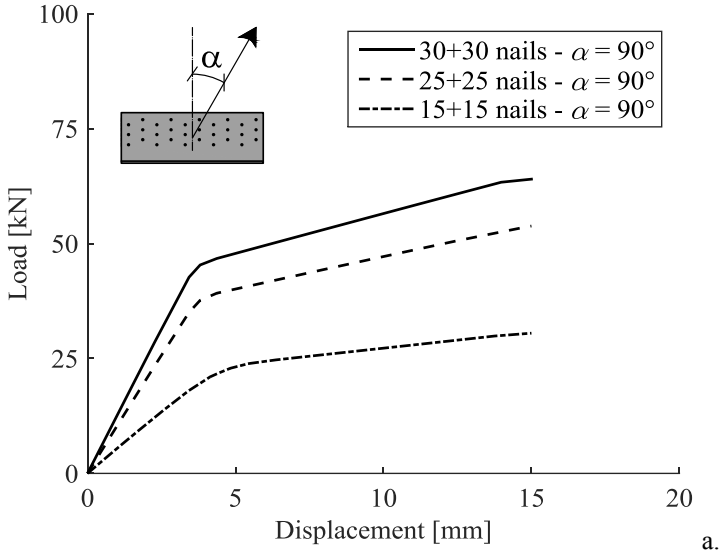

Figure 4.12. Load-displacement response of the TTF200 angle bracket loaded (a) with α =90° and (b) with α =45°, when the number of nails varies from 30+30 (solid line) to 15+15 (dash-dotted line).

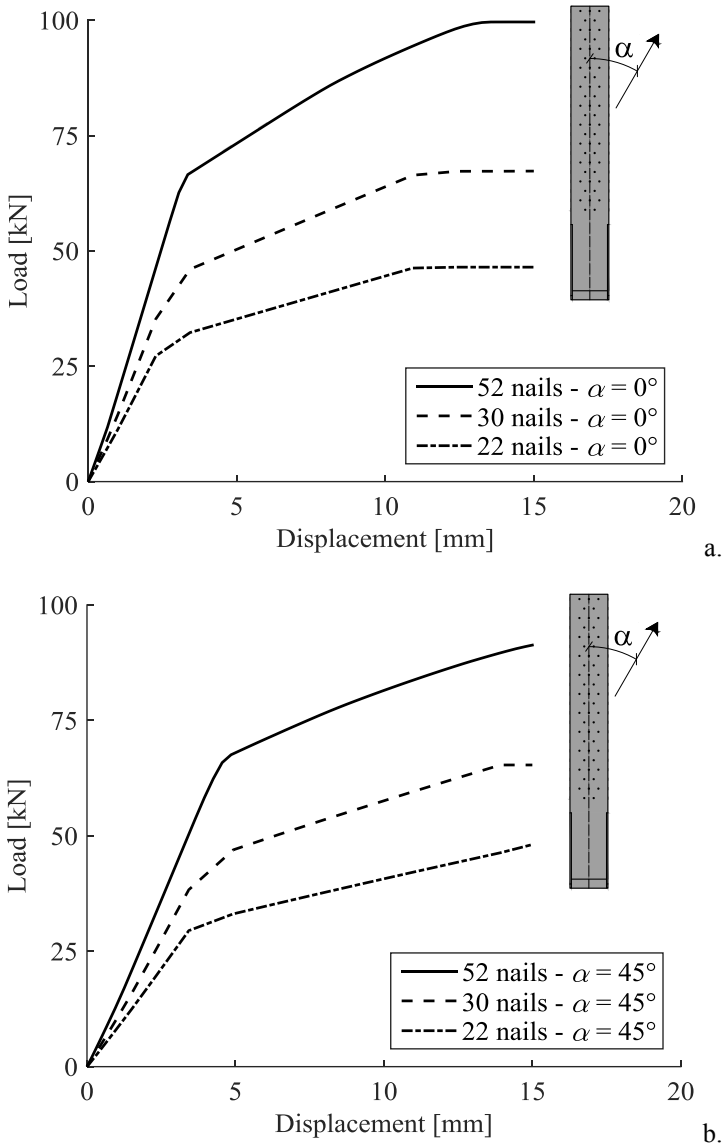

Figure 4.13. Load-displacement response of the WHT620 hold-down loaded (a) with α =0° and (b) with α =45°, when the number of nails varies from 52 (solid line) to 22 (dash dotted line).

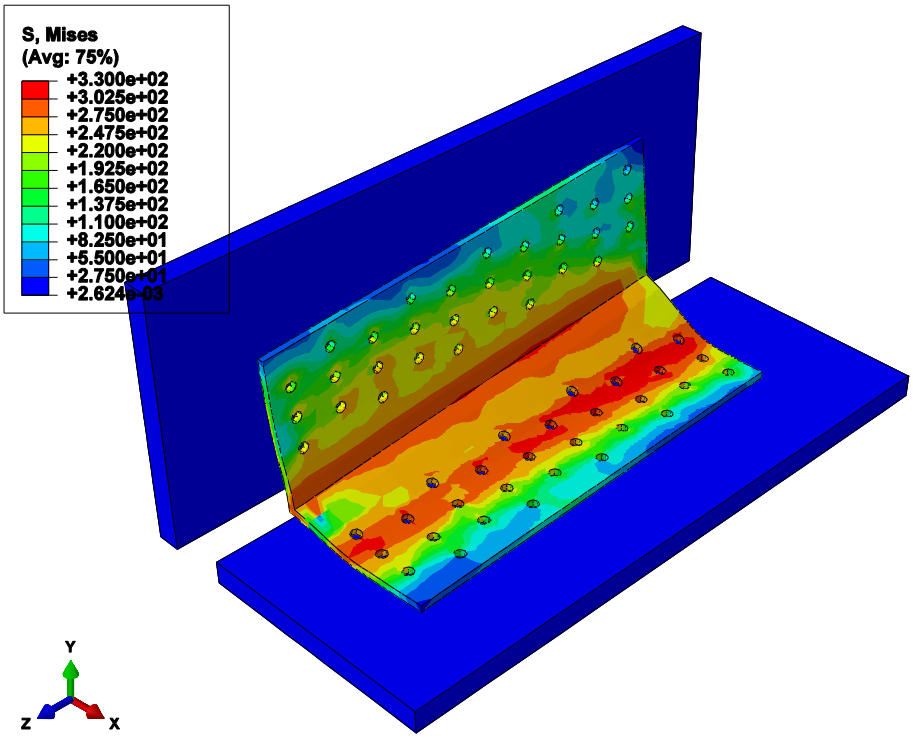

a.

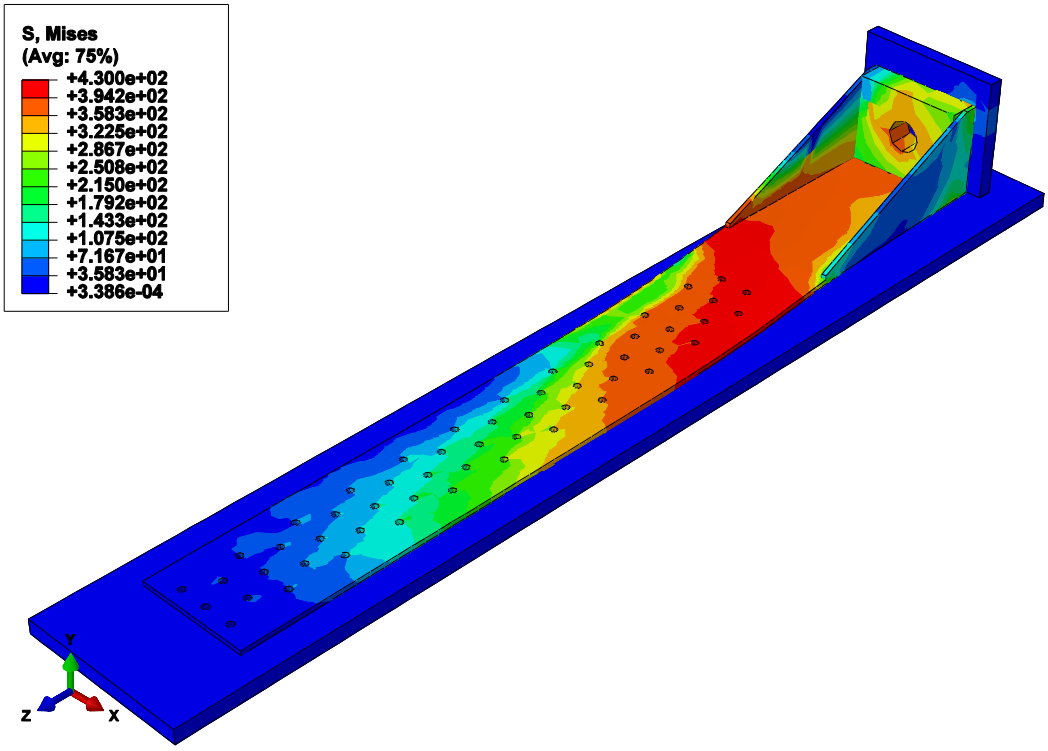

b.

Figure 4.14. Stress distribution in the metal connectors at 15 mm of displacement when α =45° (a) for the TTF200 angle bracket and (b) for the WHT620 hold-down (displayed as contour of Von Mises stresses).

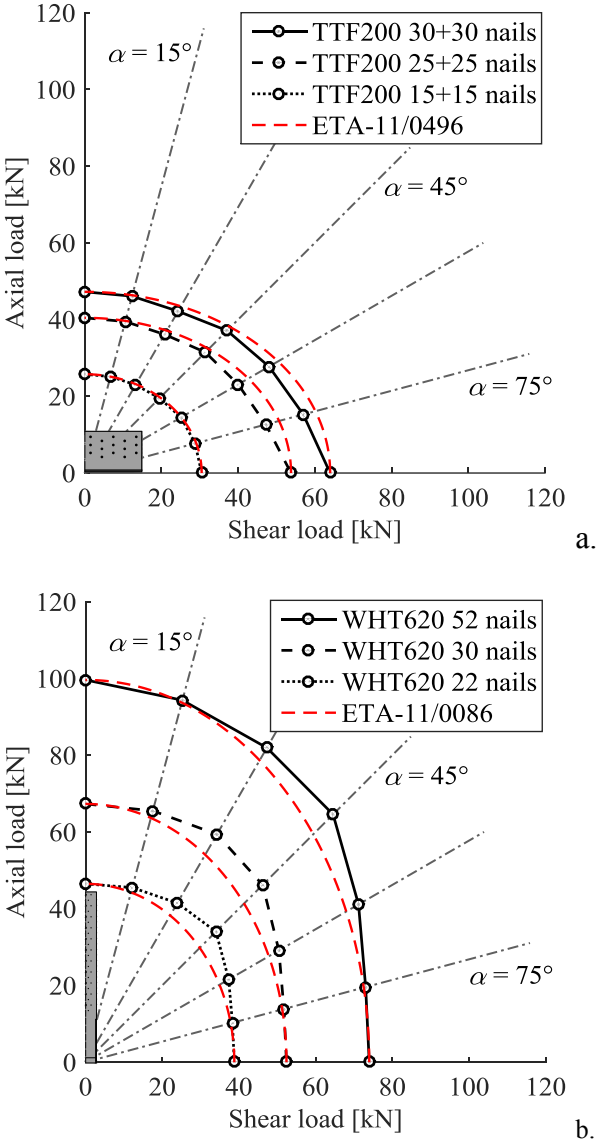

Figure 4.15. Comparison between numerical and analytical strength domains obtained considering different nail patterns (a) for the TTF200 angle bracket and (b) for the WHT620 hold-down.

4.7 CONCLUDING REMARKS

This chapter proposes a numerical model able to predict the mechanical behaviour and the failure mechanisms of wall-to-floor connection systems for CLT structures. Great effort was devoted to the development of a hysteresis model capable to simulate the response of nailed steel-to-timber joints in CLT. Shear and tension tests were reproduced on typical connections with angle brackets and hold-downs; numerical results were then compared to the test data published in literature, leading to limited differences.

Results of the monotonic simulations highlighted that the analytical model prescribed in Eurocode 5 [24] to predict the slip modulus of a nailed steel-to-timber joint leads to an overestimation of the stiffness at the connection level. Moreover, analyses showed that it is necessary to consider the group effect in nailed joints (and to reduce their load-carrying capacity) to obtain reliable predictions of the mechanical behaviour of the connections.

Simulations carried out under cyclic conditions provided an excellent match with the test results taken as a reference in the study, in terms of both load-displacement response and energy dissipation. Finally, the mechanical behaviour under bi-axial loading conditions was investigated by varying the inclination of the external load and the nail pattern used to anchor the metal connectors to the wall and floor panels. Analyses pointed out that the loading direction has a significant influence on the elastic stiffness and the load-carrying capacity, and a quadratic interaction was observed between shear and tension loads.

5 Investigating the hysteretic behaviour of Cross-Laminated Timber wall systems depending on connection properties

SHORT SUMMARY

Cross-Laminated Timber (CLT) wall systems are composed of massive timber panels that are fastened together and to the horizontal elements (the foundations or the intermediate floors) with step joints and mechanical connections. Due to the high in-plane stiffness of CLT, the shear response of such systems markedly depends on the connections used. This chapter proposes a numerical model capable to predict the mechanical behaviour and the failure mechanisms of CLT wall systems. The wall and the element where it is anchored are simulated using 3D solid bodies while the connections are schematized as non-linear hysteretic springs. Typical racking tests of CLT wall systems are reproduced by varying the assumptions used to schematize the mechanical behaviour of the connections. Results are compared to the test data published in literature and the differences are discussed. The influence of the boundary conditions (vertical load applied on top of the wall and friction at its base) and the aspect ratio of the panel are investigated via a parametric numerical study. Finally, the behaviour of a wall system assembled with two CLT panels is analysed, highlighting how the properties of the anchoring connections and of the vertical step joints affect the load-displacement response and the energy dissipation.

The experimental results taken from Gavric et al. were obtained in the framework of the SOFIE research project, funded by the Autonomous Province of Trento (Italy). Tests were carried out at CNR IVALSA (San Michele all'Adige, Italy).

5.1 INTRODUCTION

Cross-Laminated Timber (CLT) structures are made of massive walls and floor panels, fastened together with step joints (e.g. screwed joints) and mechanical connections (e.g. with angle brackets and hold-downs) that transmit the shear and tension loads. Since CLT exhibits a high in-plane stiffness and a linear-elastic behaviour, the dynamic response of

buildings made with CLT panels primarily depends on the properties of the connections used [79]. If well designed, these systems can resist large cyclic displacements, providing the necessary strength, stiffness and energy dissipation under seismic conditions [46].

The hysteretic behaviour of mechanical connections and lateral load-resisting systems made of CLT panels (in this study referred to as 'CLT wall systems') was the focus of a large body or research. Shear and tension tests were performed on wall-to-floor and wall-to-wall connections [7, 39, 47, 48, 99]. Recently, tests carried out under the simultaneous application of lateral and axial loads [68, 70, 83] highlighted that the coupled shear-tension action affects the behaviour of the connections. Finally, racking tests performed on wall systems with different layouts of connections and openings [15, 49, 56, 80, 95, 103] and full-scale tests on multi-storey buildings [10, 38, 55, 81, 104] demonstrated a significant energy dissipation.

Results of these research projects showed that the mechanical behaviour of a CLT wall system is influenced by several factors, including: (*a*) the mechanical properties and the layout of the connections, (*b*) the aspect ratio of the panel, (*c*) the presence of openings and (*d*) the boundary conditions [8, 16, 17, 97].

Determining the load-carrying capacity of CLT wall systems is crucial for both the static and seismic design of CLT structures. Recently, Gavric *et al.* [49] and Flatscher and Schickhofer [40] proposed two advanced calculation models where a displacement-based approach is used to predict the mechanical behaviour of single and segmented CLT wall systems (i.e. systems assembled with multiple wall panels, fastened together with vertical step joints). However, calculation methods have not yet been included either in Eurocode 5 [24] (design under static loads) or in Eurocode 8 [25] (design under seismic loads).

Nowadays, the static design of CLT wall systems is done using force-based methods (see, e.g., Pozza *et al.* [84]), which neglect the connections stiffness and introduce some simplifications on their mechanical behaviour. In particular, hold-downs are assumed to resist only tension and angle brackets only shear (Figure 5.1a). This assumption is realistic

only when the CLT wall is much wider than tall, i.e. if its aspect ratio is greater than one (being the aspect ratio defined as the width of the CLT wall b_{CLT} to its height h_{CLT} ratio).

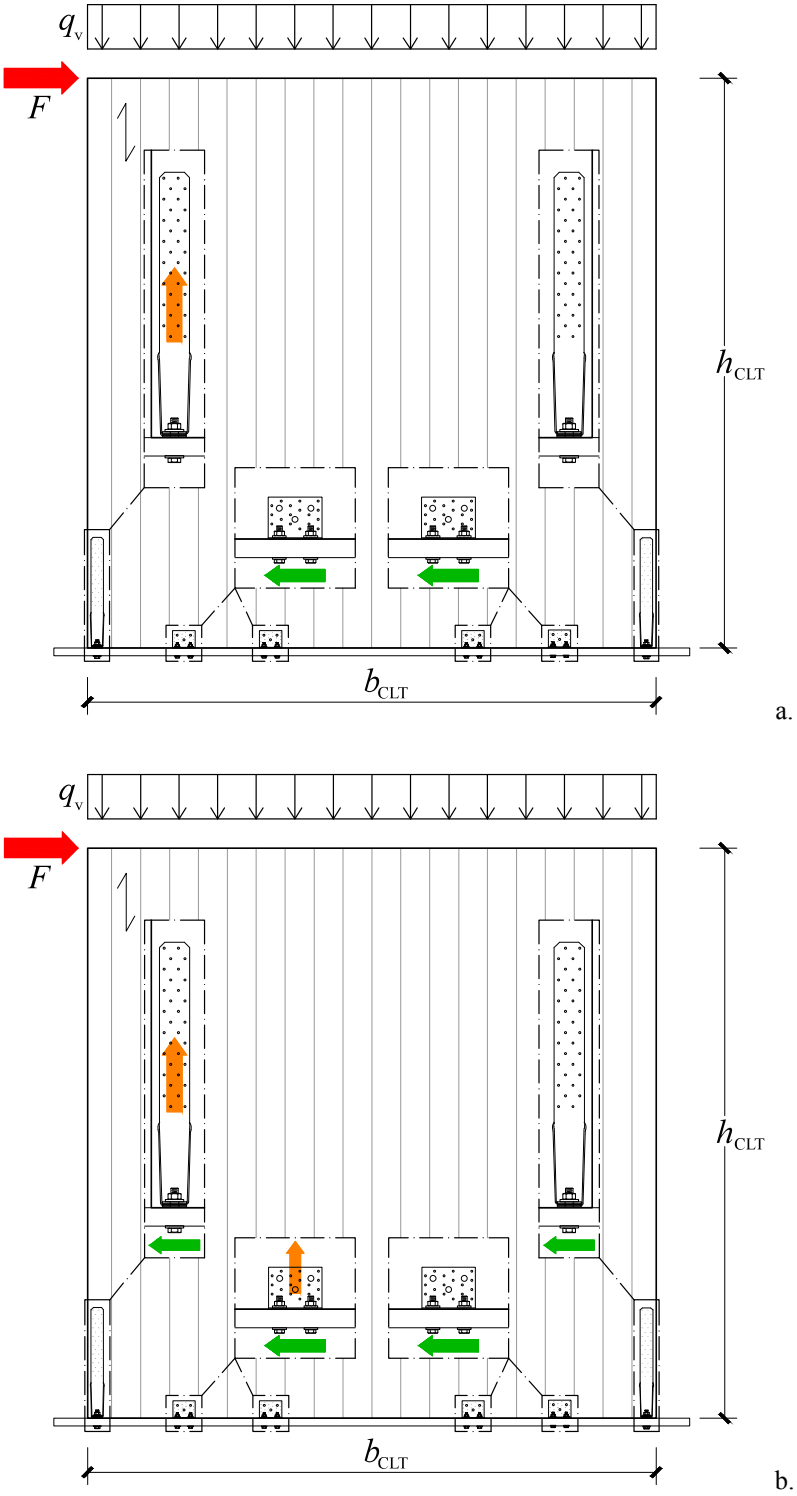

Figure 5.1. Schematics of a CLT wall system subjected to a lateral load (a) when the hold-downs resist only tension and the angle brackets only shear, and (b) when a bi-axial loading condition is considered.

However, several issues arise when the width of the panel is comparable to its height, i.e. if the b_{CLT}/h_{CLT} ratio is close to one. In this situation, angle brackets and hold-downs are simultaneously loaded in shear and tension (Figure 5.1b). As discussed in Gavric *et al.* [47], hold-downs have a relatively weak mechanical behaviour in shear that provides a minor contribution the lateral load-carrying capacity of a wall system. On the contrary, angle brackets might be very stiff in both directions and contribute significantly even in their vertical (axial) direction. Consequently, ignoring the axial contribution of angle bracket connections may lead to inaccurate predictions of the load-carrying capacity.

Regarding the seismic design of CLT structures, Follesa *et al.* [42] recently proposed a revised version of Chapter 8 of Eurocode 8 [25] where a capacity-based design approach is recommended; however, this proposal has not yet been implemented into the standard.

In this chapter, a numerical model capable to predict the mechanical behaviour and the failure mechanisms of CLT wall systems is proposed. The wall and the horizontal element where it is anchored are modelled using solid bodies while the connections are simulated as non-linear hysteretic springs with a user element subroutine taken from Rinaldin *et al.* [86]. In-plane shear tests are reproduced on single and segmented wall systems tested at CNR IVALSA in the framework of the SOFIE research project. Simulations investigated the load-displacement response of a typical wall system by varying the assumptions used to schematize the behaviour of the connections. Experimental and numerical results are compared and critically discussed. The influence of the boundary conditions (vertical load applied on top of the wall and the friction at its base) and the aspect ratio of the panel are analysed via a parametric numerical study. Numerical results are collected in diagrams and compared to the analytical values determined using a simplified approach proposed by Pozza *et al.* [84]. Finally, the behaviour of a wall system assembled with two adjacent walls is investigated. Simulations are carried out by varying the layout of the connections, and their influence on the load-carrying capacity and the energy dissipation is analysed. All the simulations are performed using ABAQUS software package [96].

5.2 MODEL DESCRIPTION

The CLT wall and the element where it is anchored are modelled using 3D solid bodies, meshed with cubic elements with reduced integration (C3D8R). The wall has an elastic orthotropic behaviour with material parameters taken from Brandner *et al.* [6] (moduli of elasticity and shear moduli) and from Ashtari [1] (Poisson's ratios). The horizontal element can be either a CLT floor panel or a rigid foundation (e.g. a concrete basement or a steel profile). In the first case, the same material parameters of the wall are used; in the second case, a linear-elastic isotropic material is considered, with input parameters defined based on the element being analysed. The interaction between the CLT wall and the underlying element is schematized as follows: the normal behaviour is defined by assuming a unilateral hard contact while the tangential behaviour is defined by employing the penalty formulation implemented in ABAQUS [96]. A similar approach is adopted to simulate the contact interaction between adjacent CLT panels.

The mechanical connections are simulated as 2-node non-linear hysteretic springs with three degrees of freedom. Two displacement components simulate the behaviour in the axial and shear direction while the third one reproduces the out-of-plane response. In this study, the wall systems are always subjected to in-plane loads; therefore, the out-of-plane behaviour of the connections is never activated and is disregarded. Each non-linear spring is pinned onto the wall panel (i.e. at the metal connector location) and onto the external surface of the basement (i.e. at the anchoring location), where the boundary conditions of the model are applied.

The displacement components that simulate the mechanical behaviour under shear and tension loads are coupled with the quadratic force-based strength domain reproduced in Equation 5.1. In the expression below, $F_{\mathrm{ax,y}}$ and $F_{\mathrm{sh,y}}$ represent the yield loads in the axial and shear direction while $F_{\mathrm{ax},i}$ and $F_{\mathrm{sh},i}$ are the corresponding loads at the i-th analysis step, respectively. Further information on this quadratic interaction domain and how it affects the response of the non-linear springs are given in Rinaldin *et al.* [86].

$$\left(\frac{F_{\mathrm{ax},i}}{F_{\mathrm{ax,y}}}\right)^2+\left(\frac{F_{\mathrm{sh},i}}{F_{\mathrm{sh,y}}}\right)^2\le 1 \tag{5.1}$$

The inequality given in Equation 5.1 is derived from the strength domain prescribed in the European Technical Assessments (ETAs) of typical connectors for CLT structures (see, e.g., ETA-06/0106 [31] and ETA-11/0086 [33]). However, the ETAs consider the maximum load-carrying capacities in the axial and shear direction instead of the yield loads mentioned before. In this context, it should be mentioned that the adoption of a quadratic interaction relationship between shear and tension components was confirmed by Rinaldin and Fragiacomo [88] and Izzi *et al.* [61] via a parametric numerical study.

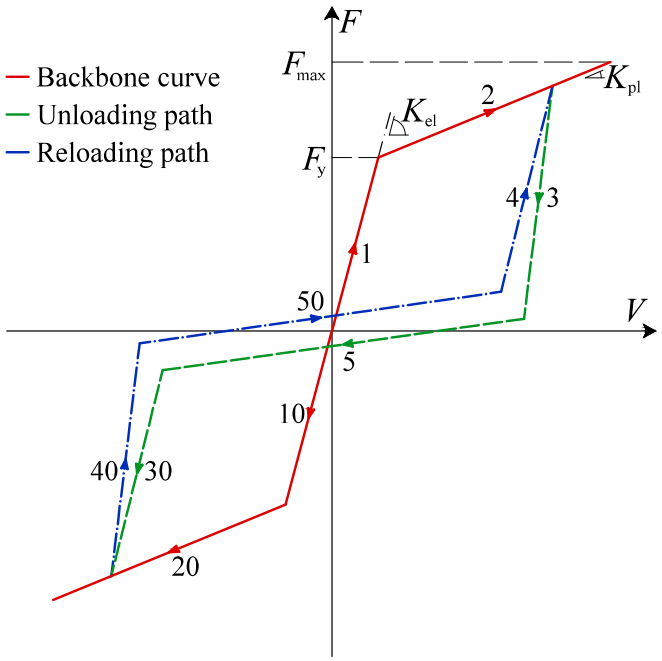

Figure 5.2. Piecewise-linear law of the hysteretic spring (adapted from Rinaldin *et al.* [86]).

Figure 5.2 displays the piecewise-linear law employed in the analyses to schematize the hysteretic behaviour of the connections under shear and tension loads. In Figure 5.2, K_{el} denotes the elastic stiffness of the connection, F_{y} the yield load, K_{pl} the slope of the inelastic branch, and F_{max} the maximum load. It is important to notice that, due to the surface-to-surface contact interaction between the wall and the underlying element, the axial component of the connections can only be loaded in tension. Consequently, the negative part of the corresponding piecewise-linear law is never activated.

The unloading (#3, #5, #30) and reloading (#40, #50, #4) paths should be set according to the mechanical properties of the connection analysed. As discussed in Rinaldin *et al.* [86], the slopes of branches #3 and #4 are expressed as functions of K_{el}; furthermore, the load at the transition point between branches #3 and #5 and between branches #50 and #4 are expressed as percentages of the load attained on the backbone curve. In this study, the unloading and reloading paths are assessed from the reference test data by means of an energetic approach; further details on this method are given in the following section.

5.3 NUMERICAL ANALYSES

Racking tests are reproduced on CLT wall systems tested at CNR IVALSA and published by Gavric *et al.* [49] (Figure 5.3). The first specimen (labelled 'Wall #1') is assembled with a square wall panel while the second one (labelled 'Wall #2') is composed of two adjacent rectangular panels, fastened together with half-lap joints. In both situations, the walls are made of five crosswise laminated board layers with total thickness of 85 mm (5×17 mm). The panels are anchored to a rigid foundation with Rothoblaas WHT540 hold-downs [33] and Simpson Strong-Tie AE116 angle brackets [31], nailed to the timber panel and bolted to the steel basement. In Wall #2, the half-lap joints are assembled with Rothoblaas HBS 8×80 screws [32]. Further details of these systems are given in Table 5.1, where the symbol i_{scr} is used to denote the spacing between two consecutive screws and q_v represents the vertical load applied on top of the wall.

The mechanical properties of the connections are assessed from the experimental tests carried out by Gavric *et al.* [47, 48]. The input parameters required by the hysteretic springs (i.e. K_{el}, F_y, K_{pl}, and F_{max}) are determined from the loading curves using a procedure described in Izzi *et al.* [59]. The unloading and reloading paths are calibrated using an energetic approach. For each test series, the hysteretic springs are used to reproduce the experimental results and, using the same input values governing the hysteresis cycles, the difference of dissipated energy between test data and numerical predictions is minimized (see, e.g., Figure 5.4).

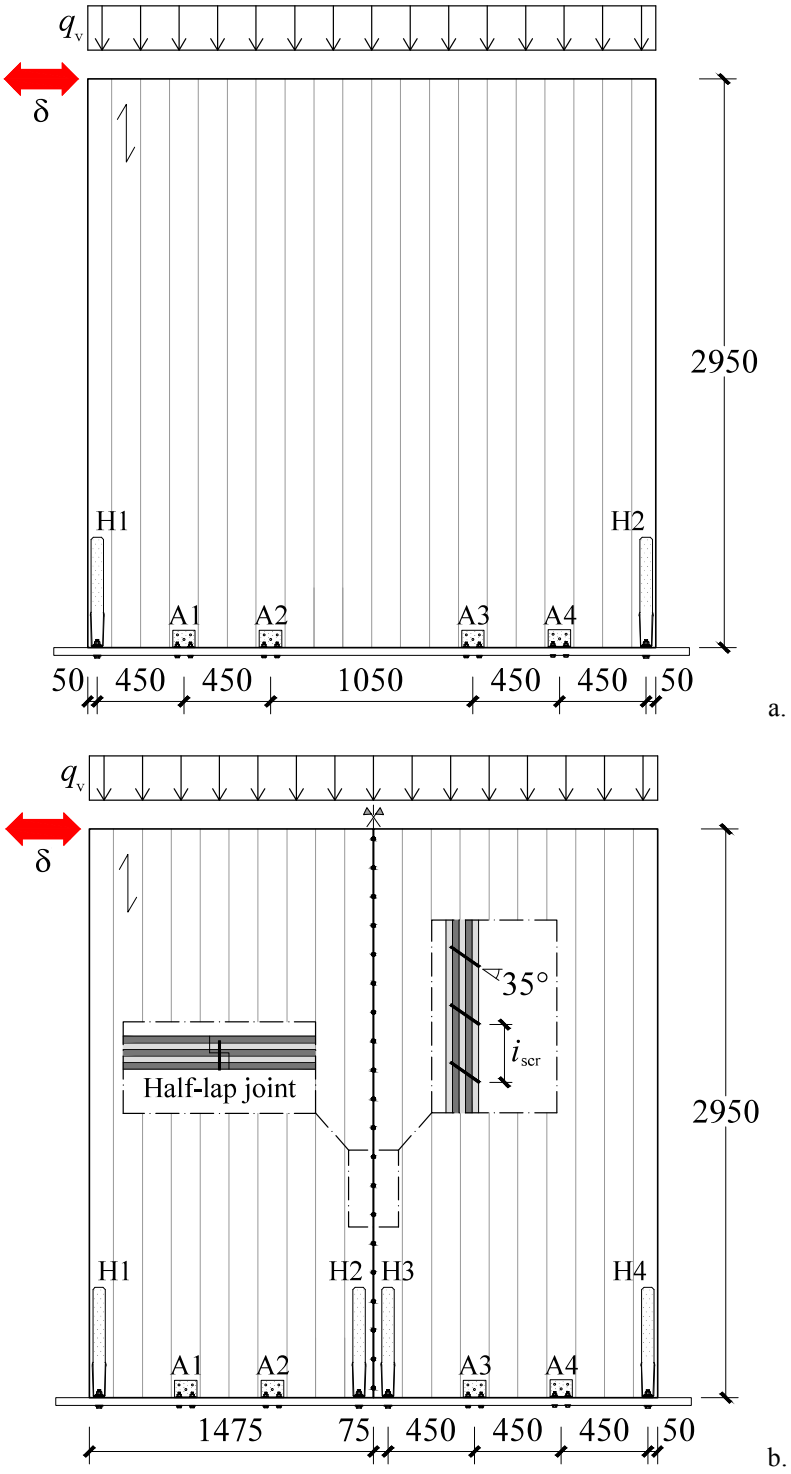

Figure 5.3. Schematics of the CLT wall systems tested by Gavric *et al.* [49] and reproduced in the numerical simulations (dimensions in mm).

Table 5.1. Experimental setup of the CLT wall systems tested by Gavric *et al.* [49].

Wall #	Wall #1	Wall #2-A	Wall #2-B
Wall panel(s)	1 CLT panel 2950×2950 mm^2	2 CLT panels 1475×2950 mm^2	2 CLT panels 1475×2950 mm^2
Angle brackets	4 AE116 (11 nails, 1 bolt)	4 AE116 (11 nails, 1 bolt)	4 AE116 (11 nails, 1 bolt)
Hold-downs	2 WHT540 (12 nails, 1 bolt)	4 WHT540 (12 nails, 1 bolt)	2 WHT540* (12 nails, 1 bolt)
Half-lap joints	None	5 HBS 8×80 (i_{scr} = 500 mm)	20 HBS 8×80 (i_{scr} = 150 mm)
Vertical load q_v	18.5 kN/m	18.5 kN/m	18.5 kN/m

* Hold-downs H2 and H3 were removed.

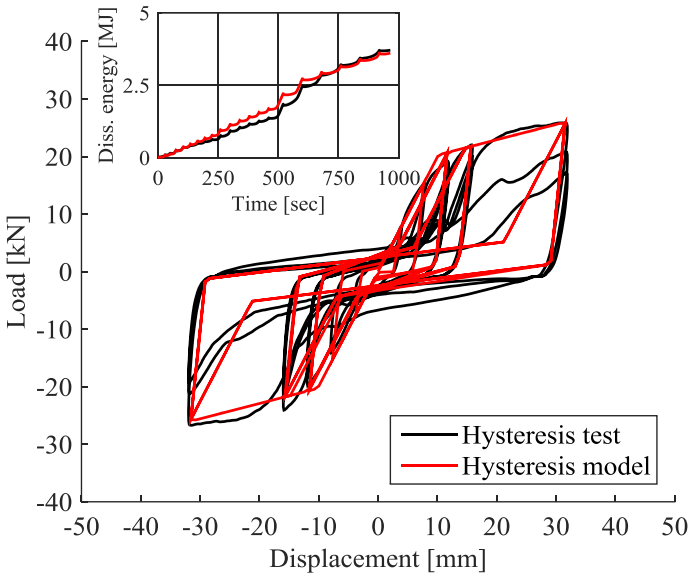

Figure 5.4. Calibration of the non-linear hysteretic spring reproducing an angle bracket connection loaded in shear in terms of force-displacement relationship (with close-up on the history of dissipated energy).

5.3.1 Simulations of Wall #1

The hysteretic behaviour of Wall #1 is investigated by varying the assumptions used to schematize the mechanical behaviour of the connections. For this purpose, four methods are considered (see Table 5.2). Method A is the most accurate since the connections resist both shear and tension loads and the coupled shear-tension interaction is accounted with the quadratic strength domain discussed in Section 5.2. Method B is derived from Method A by neglecting the interaction between the tensile and shear components. Method C is a

further simplification of Method B, since hold-downs are assumed to resist only tension while angle brackets still have both components (uncoupled). Finally, Method D assumes the hold-downs resist only tension and the angle brackets only shear. It should be noticed that Method D employs the same assumptions of the simplified design approach discussed in the introduction, which is adopted by practicing engineers to design the mechanical connections in CLT structures.

Table 5.2. Methods used to schematize the mechanical behaviour of the connections.

Method	Metal connector	Resisting shear	Resisting tension	Interaction*
A	Angle bracket	Yes	Yes	Yes
	Hold-down	Yes	Yes	Yes
B	Angle bracket	Yes	Yes	No
	Hold-down	Yes	Yes	No
C	Angle bracket	Yes	Yes	No
	Hold-down	No	Yes	No
D	Angle bracket	Yes	No	No
	Hold-down	No	Yes	No

* Coupled shear-tension interaction defined according to Equation 1, as discussed in Rinaldin *et al.* [86].

Figures 5.5 and 5.6 provide a comparison between test data and numerical predictions when the mechanical behaviour of the connections is defined according to the afore-mentioned methods. Simulations are carried out using the displacement history extracted from the reference test and neglecting the friction at the base of the CLT panel ($\mu_{fr} = 0$).

Method A provides a correct identification of the mechanical behaviour of the system, although the dissipated energy at the end of the simulation is about 25% lower than in the test. Differences could be due to the simplifications introduced in the analysis to account for the coupled shear-tension interaction. According to Rinaldin *et al.* [86], who published the user element subroutine employed in the simulations, the reduction of strength due to the bi-axial loading condition is activated when the yield load of either the tension or the shear component is first attained. However, cyclic tests carried out by Pozza *et al.* [83] highlighted a continuous interaction among those components and a significant influence on the energy dissipation of the connections. Therefore, to improve the accuracy of the

numerical results, future developments of this study should consider either a force-based strength domain updated at every analysis step or a displacement-based interaction among shear and tension components (see, e.g., Talledo *et al.* [98]).

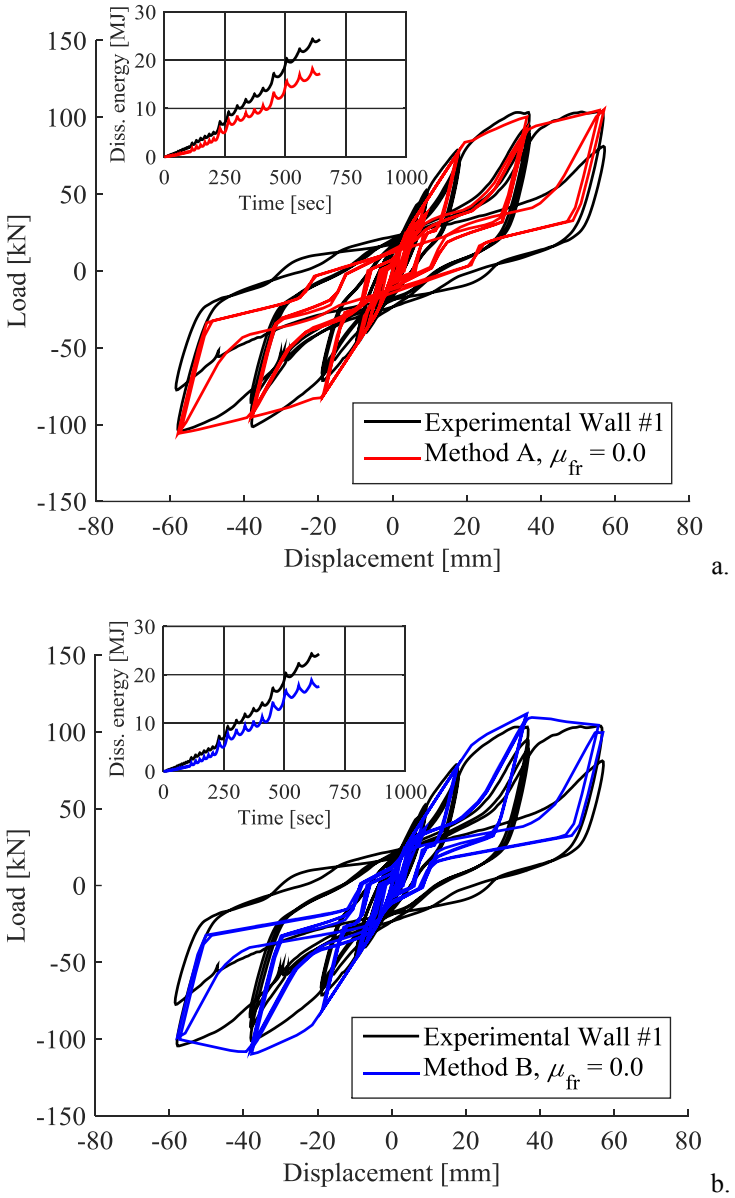

Figure 5.5. Comparison between experimental hysteresis (from Gavric *et al.* [49]) and numerical results for the Wall #1 configuration when the behaviour of the connections is defined according to (a) Method A and (b) Method B (with close-up on the history of dissipated energy).

Methods B and C lead to slightly less accurate predictions of both the maximum load-carrying capacity and the dissipated energy. Moreover, results obtained using Method C confirmed that the shear component of hold-downs provides a minor contribution to the lateral resistance a CLT wall system. Finally, due to the several simplifications introduced

in the analysis, Method D leads to a maximum load-carrying capacity about 25% lower than Method A and to an energy dissipation around 50% lower than in the test.

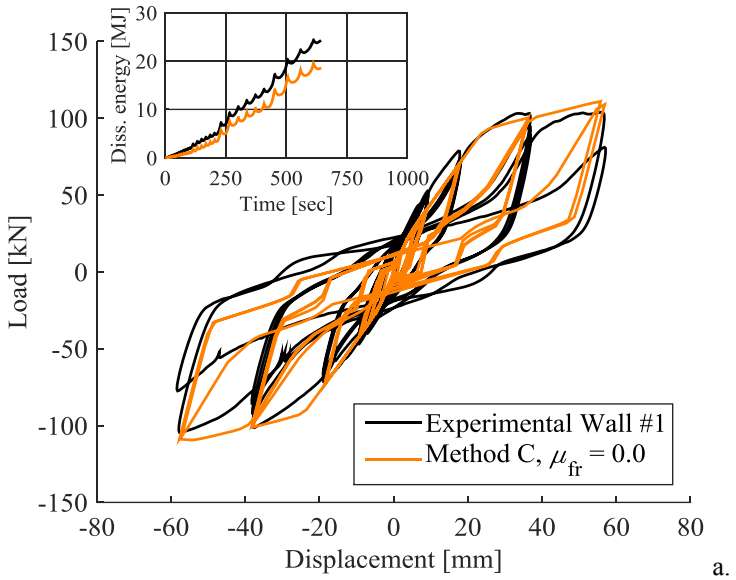

a.

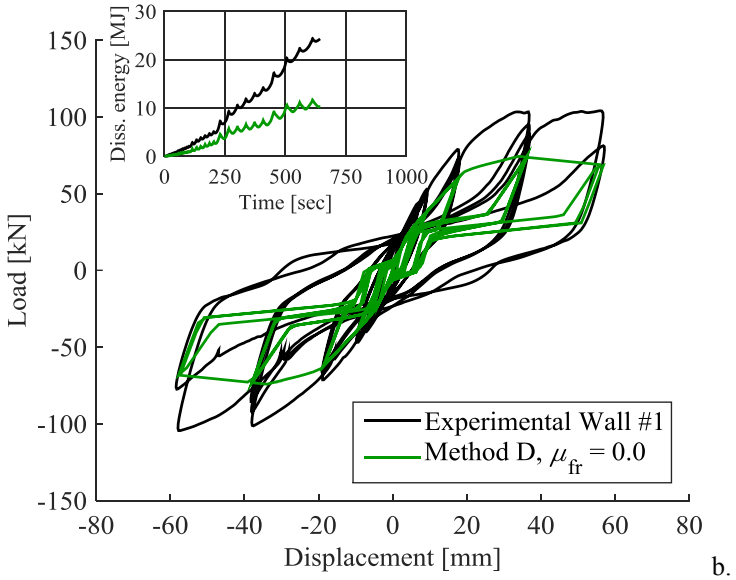

b.

Figure 5.6. Comparison between experimental hysteresis (from Gavric *et al.* [49]) and numerical results for the Wall #1 configuration when the behaviour of the connections is defined according to (a) Method C and (b) Method D (with close-up on the history of dissipated energy).

The friction at the base of the CLT panel is subsequently included in the analysis. The simulation carried out considering Method A is repeated by considering a static friction coefficient μ_{fr} = 0.1 between the bottom edge of the wall and the upper surface of the steel basement. As shown in Figure 5.7, the friction improves the energy dissipation up to 20 mm of displacement, where sliding is the most significant contribution. Rocking is

the most important mechanism at higher displacement amplitudes, leading to a final energy dissipation about 8% higher than the original simulation.

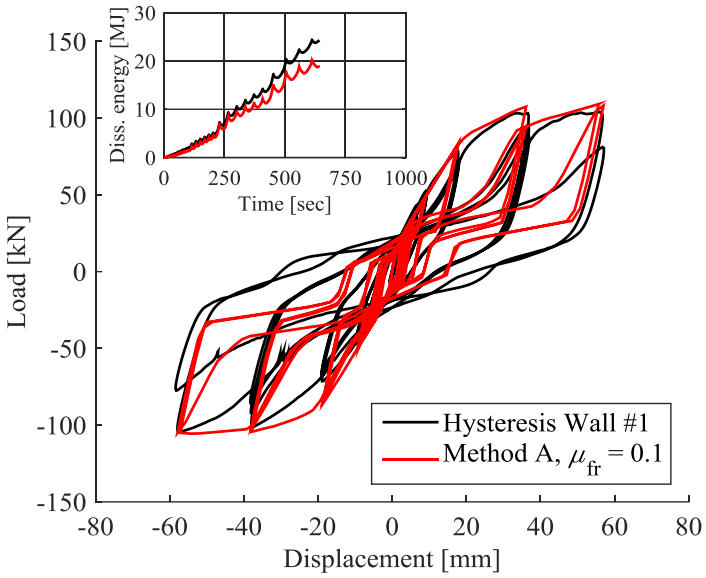

Figure 5.7. Comparison between experimental hysteresis (from Gavric *et al.* [49]) and numerical prediction for the Wall #1 configuration when the behaviour of the connections is defined according Method A and the friction at the base of the CLT panel is taken into account in the analysis with a static friction coefficient μ_{fr} = 0.1 (with close-up on the history of dissipated energy).

Finally, a parametric numerical study is carried out to investigate the influence of the vertical load and the aspect ratio of the CLT panel on the load-carrying capacity. Analyses are carried out by considering a vertical load q_v varying between zero and 40 kN/m and two aspect ratios: b_{CLT}/h_{CLT} = 1 (the same used above) and b_{CLT}/h_{CLT} = 2 (obtained by doubling up the width of Wall #1). Results are compared to the predictions obtained using a simplified approach proposed by Pozza *et al.* [84] (Equation 5.2). Based on the outcome of the previous analysis, although friction is undoubtedly important in cyclic conditions, its contribution is here neglected in order to have a direct comparison between numerical and analytical results.

$$F_{max} = \min\left[\sum_n F_{max,AB,n} \quad \frac{b_{CLT}}{h_{CLT}}\left(F_{max,HD} + \frac{q_v b_{CLT}}{2}\right)\right] \tag{5.2}$$

In Equation 5.2, $F_{max,AB}$ and $F_{max,HD}$ denote the maximum load-carrying capacities of an angle bracket (shear) and a hold-down (tension), n is the number of angle brackets used in the wall system while b_{CLT} and h_{CLT} are the width and the height of the wall.

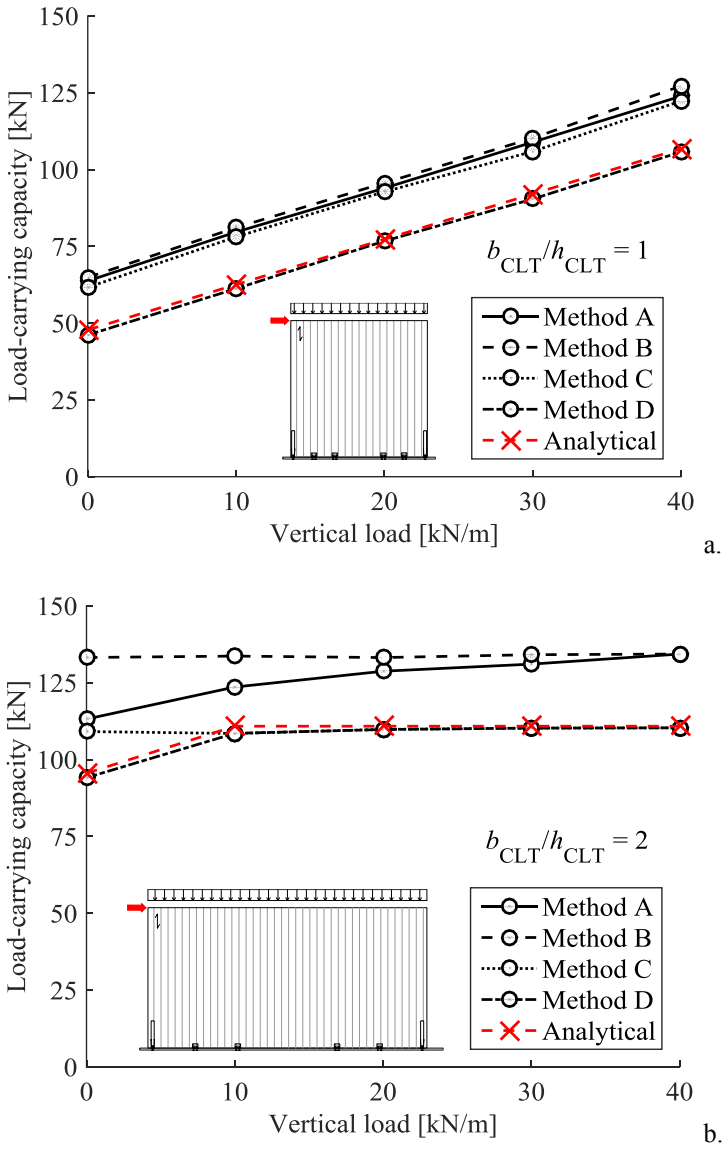

Figure 5.8. Parametric study showing how the vertical load, the aspect ratio of the wall and the method used to schematize the behaviour of the connections affect the maximum load-carrying capacity of a wall system.

Results of this parametric numerical study are displayed in Figure 5.8. Failure occurred by rocking when the aspect ratio is equal to one ($b_{CLT}/h_{CLT} = 1$). In such situation, Method A, B and C lead to similar load-carrying capacities, confirming what observed in the first set of simulations. Furthermore, Method D leads to a good agreement with the analytical values obtained using Equation 5.2. It should be noted that, by neglecting the contribution of angle brackets in the axial direction, Method D leads to load-carrying capacities always 25% lower than Method A.

Failure occurred by sliding when $b_{CLT}/h_{CLT} = 2$, with only two exceptions: Method D and the simplified model proposed by Pozza *et al.* [84], which predicts failure by rocking

when q_v is zero. Good agreement is obtained between Method C, Method D and Equation 5.2 when q_v is greater than 10 kN/m. Method B predicts the highest load-carrying capacity, which is constant for all the load levels considered in the analyses. Method A leads to a maximum load slightly higher than Method C when the load is zero; differences can be attributed to the lateral shear contribution of the hold-downs, which enhances the load-carrying capacity of the system. Finally, the maximum load obtained according to Method A increases when the vertical load augments and is the same value obtained with Method B when q_v = 40 kN/m. This trend is due to the deformed configuration of the system when the maximum load-carrying capacity is attained. In particular, failure occurs for a combination of rocking and sliding when q_v is less than 30 kN/m while only sliding is observed with higher vertical loads.

5.3.2 Simulations of Wall #2

The mechanical behaviour of Wall #2 is investigated by varying the number and layout of the connections. Two configurations are considered, as summarized in Table 5.1. In the first configuration (labelled 'Wall #2-A') each wall panel is anchored to the foundation with two hold-downs and two angle brackets while the vertical step joints are made using five screws. In the second one (labelled 'Wall #2-B'), the number of hold-downs is halved (hold-downs H2 and H3 have been removed) and the number of screws in the vertical joint is increased to twenty. Simulations are carried out by assuming that the behaviour of the connections is defined using Method A and by considering a friction coefficient μ_{fr} = 0.1 between the bottom edge of the walls and the upper surface of the basement. The friction between adjacent wall panels is neglected.

Figure 5.9 shows a comparison between experimental and numerical results when Wall #2-A is considered; analyses are carried out by assuming the same number of screws used in the test (i.e. five) and then by increasing their number to twenty. Figure 5.9a provides a correct identification of the maximum load, although the dissipated energy is about 20% lower than in the reference test. In both simulations, failure occurred by rocking; however, in the second case (Figure 5.9b) the half-lap joints prevent the relative sliding of the

panels. Consequently, the CLT walls behave like a monolithic element and the maximum load is enhanced by the hold-downs H2 and H3 (Figure 5.3b), becoming about 30% higher than in the test. Furthermore, the redistribution of loads within the wall system affects the energy dissipation, which becomes around 20% higher than in the test.

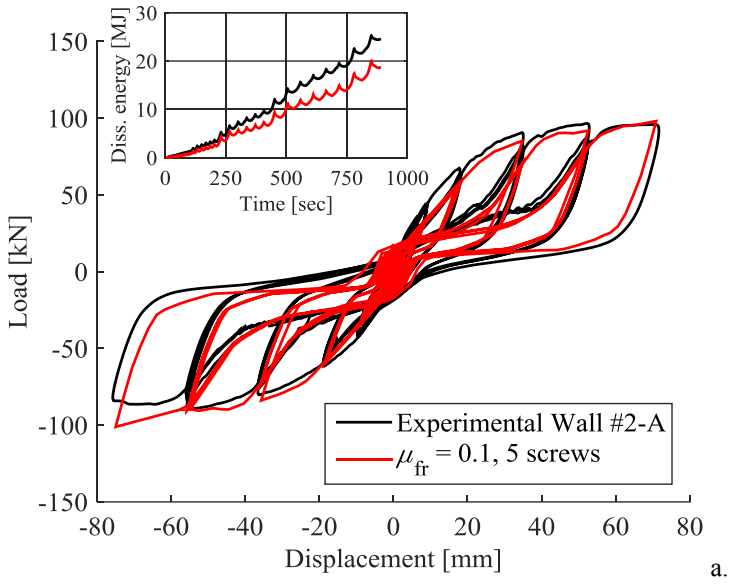

a.

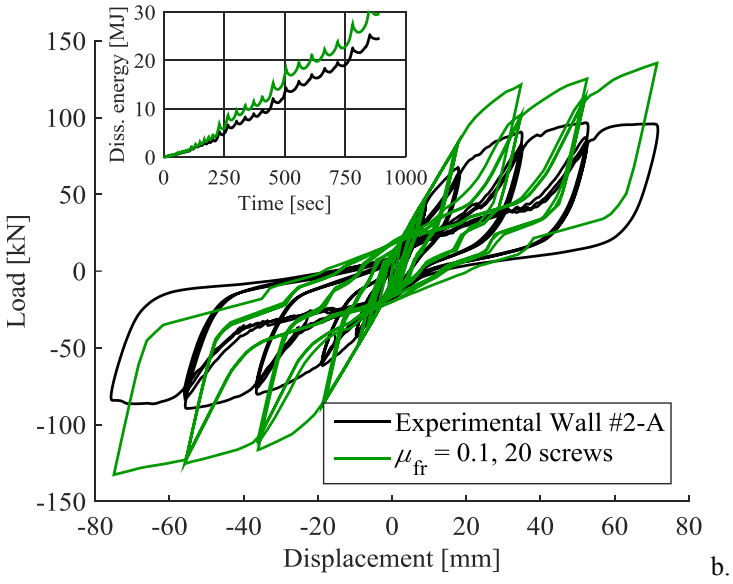

b.

Figure 5.9. Comparison between experimental hysteresis (from Gavric *et al.* [49]) and numerical results for the Wall #2-A configuration (a) when five screws are used in the vertical step joints (b) when their number is increased to twenty (with close-up on the history of dissipated energy).

Figure 5.10 compares test data and numerical results when Wall #2-B is considered; analyses are carried out by assuming the same number of screws used in the test (twenty) and then by reducing their number to ten. Figure 5.10a shows a good agreement between

experimental and numerical results, in terms of both mechanical behaviour and dissipated energy. In Figure 5.10b, due to the presence of fewer screws, the coupling effect of the step joints is less effective and the maximum load-carrying capacity is about 10% lower than in the test. Moreover, the dissipated energy reduces significantly compare to Figure 5.10a, becoming around 35% lower than in the first case.

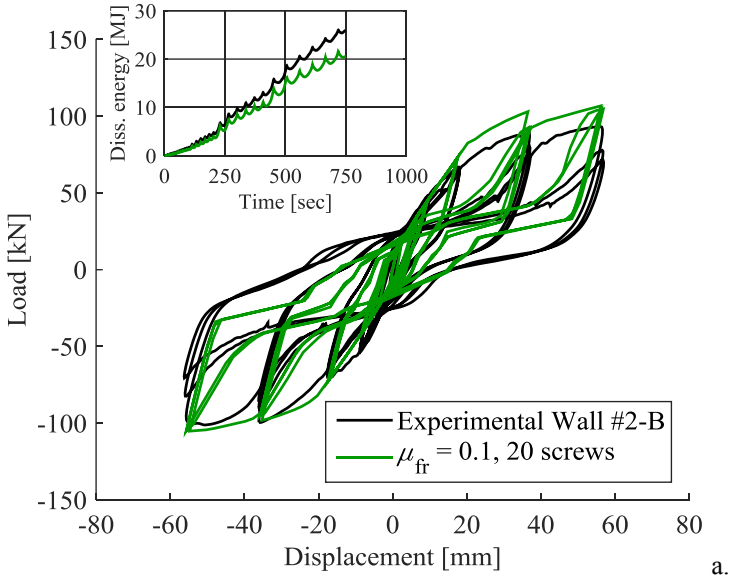

a.

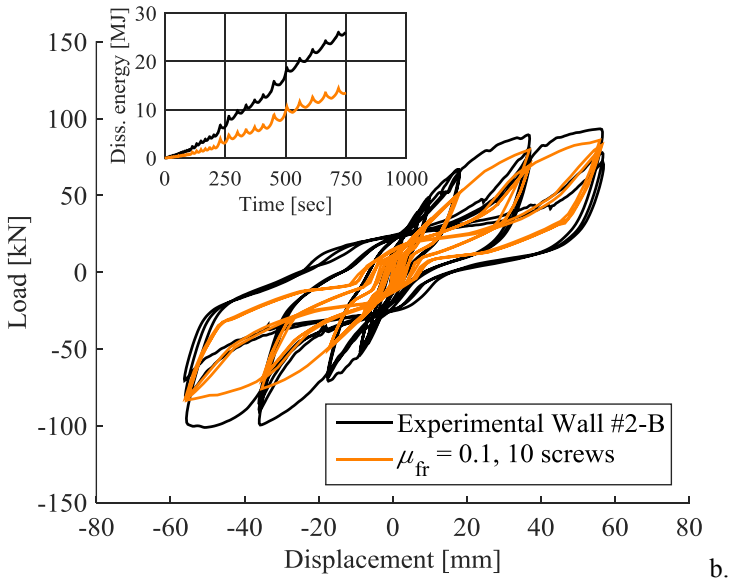

b.

Figure 5.10. Comparison between experimental hysteresis (from Gavric *et al.* [49]) and numerical results for the Wall #2-B configuration (a) when twenty screws are used in the vertical step joints (b) when their number is reduced down to ten (with close-up on the history of dissipated energy).

Finally, to gain a better insight into the behaviour of segmented CLT wall systems, a parametric numerical study is carried out by varying the layout of the connections and the

load applied on top of the walls. Racking tests are reproduced on Wall #2-A and #2-B by considering five layouts of the connections (uncoupled walls, five/ten/twenty screws in the vertical step joints and a monolithic panel) and two vertical loads (18.5 kN/m and 40.0 kN/m). Analyses are performed under monotonic conditions, by considering an ultimate displacement of 80 mm and the same assumptions adopted in the cyclic simulations (i.e. Method A and a static friction coefficient μ_{fr} = 0.1). Results of this study are shown in Figure 5.11 (Wall #2-A) and Figure 5.12 (Wall #2-B).

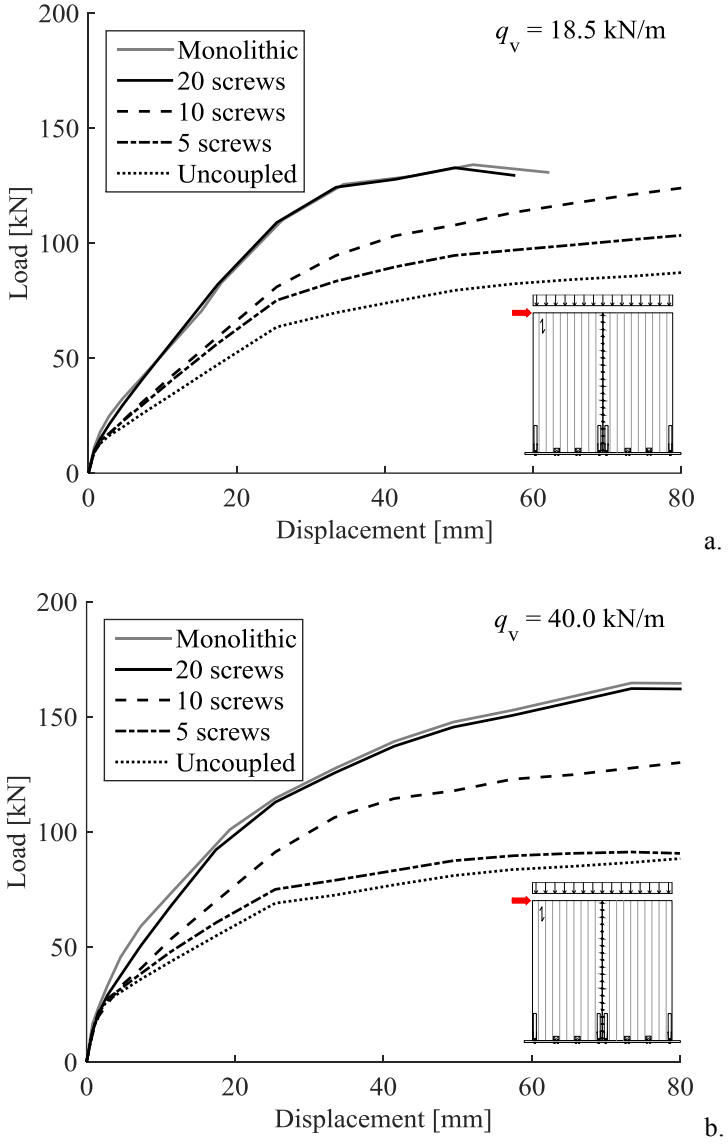

Figure 5.11. Load-displacement response of Wall #2-A when the coupling effect provided by the vertical step joints is varied from two uncoupled walls (i.e. no screws in the vertical joint) to a monolithic panel, (a) if q_v = 18.5 kN/m and (b) if q_v = 40.0 kN/m.

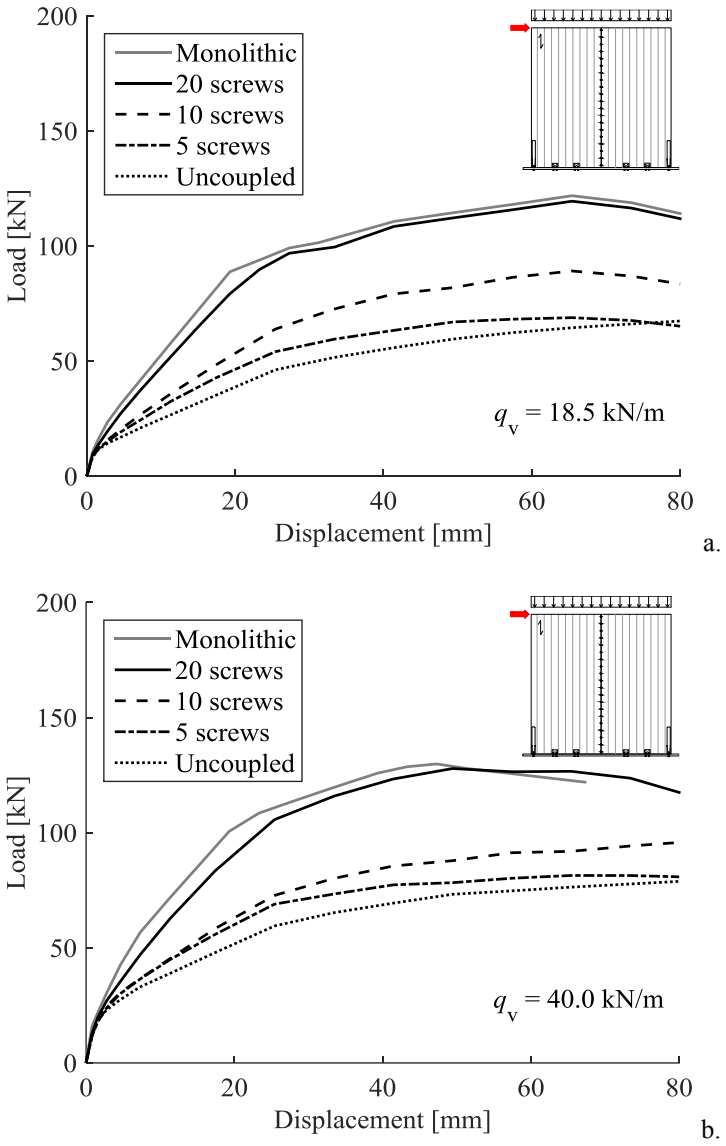

Figure 5.12. Load-displacement response of Wall #2-B when the coupling effect provided by the vertical step joints is varied from two uncoupled walls (i.e. no screws in the vertical joint) to a monolithic panel, (a) if q_v = 18.5 kN/m and (b) if q_v = 40.0 kN/m.

Parametric analyses carried out with q_v = 18.5 kN/m confirmed the outcome of the cyclic simulations, i.e. that the panels behave as a monolithic element when twenty screws are considered while a partially coupled behaviour is attained in the other two situations.

In Wall #2-A, if q_v is increased to 40.0 kN/m, the simulations with ten and twenty screws show an increase of both the stiffness and the maximum load-carrying capacity. On the contrary, if five screws are used, results highlight a higher stiffness and a slightly lower load-carrying capacity. This is due to a redistribution of forces in the anchoring connections and a reduction of the load transferred to the hold-downs.

In Wall #2-B, if q_v is increased to 40.0 kN/m, a general increase of both the stiffness and the maximum load-carrying capacity is observed. It should be also noticed that results obtained with five and ten screws lead to a similar load-displacement response up to 25 mm of drift. In particular, if five screws are used, the half-lap joints are not able to prevent the relative sliding of the panels; consequently, each wall is independent and the load-carrying capacity is significantly influenced by the stabilizing effect of the vertical load. If ten screws are used, the behaviour is coupled and overall the load-carrying capacity is affected by the properties and the position of the anchoring connections.

5.4 CONCLUDING REMARKS

This chapter presents a numerical model capable to predict the mechanical behaviour and the failure mechanisms of CLT wall systems. Racking tests were reproduced on typical CLT wall systems, by varying the assumptions used to schematize the behaviour of the connections. Results highlighted that is necessary to consider the axial contribution of angle brackets to obtain realistic predictions of the load-carrying capacity and the friction at the base of the walls to obtain reliable predictions of the energy dissipation.

The influence of the vertical load applied on top of the walls and the aspect ratio of the panels were analysed via a parametric numerical study. Failure occurred by rocking when the aspect ratio of the wall b_{CLT}/h_{CLT} is equal to one while sliding occurred if b_{CLT}/h_{CLT} is equal to two. Results were compared to the analytical values obtained using a simplified approach proposed by Pozza *et al.* [84]. It was demonstrated that the simplified method provides load-carrying capacities about 25% lower than the numerical simulations.

Finally, the hysteretic behaviour of wall systems assembled with two adjacent panels was investigated, varying the layout of the anchoring connections and of the vertical step joints. Simulations showed that the vertical step joints affect the load distribution within the wall system and the energy dissipation. If those step joints are capable of preventing the relative sliding of the walls, the system behaves as a monolithic element. However, if the relative sliding between the CLT wall panels is not prevented, the load-displacement response markedly depends on the property and position of the anchoring connections.

6 Summary and recommendations for future research

6.1 MAIN CONTRIBUTIONS

This PhD thesis focused on the mechanical characterization of typical connection systems for Cross-Laminated Timber (CLT) structures; the research work aimed at gaining a better understanding on how the connections influence the seismic behaviour of a CLT building. To achieve this objective, several milestone were reached.

Experimental testing

An experimental programme was carried out on nailed steel-to-timber joints in CLT. The ultimate tensile strength and the yield moment of the nails were determined by performing tension tests and bending tests. Furthermore, withdrawal tests and shear tests were carried out to investigate the mechanical behaviour of single fastener joints.

Average and characteristic values of the strength capacities were assessed from the test data and compared to the analytical predictions determined according to current structural design codes and literature.

Analytical modelling

The test results obtained on single fastener joints were used to propose simplified design principles for nailed joints in CLT. In particular, to fulfil the requirements of the capacity-based design, the overstrength factor and the strength degradation factor were evaluated and conservative values were recommended.

A simplified design method for nailed steel-to-timber joints in CLT was proposed, to predict their average mechanical properties (shear capacity and slip modulus) and load-displacement response. Great effort was devoted to the development of a hysteresis model capable to simulate the response under cyclic conditions.

Numerical modelling

Several numerical procedures capable to predict the mechanical and hysteretic behaviour at different building levels were developed. Firstly, the research focused on the behaviour of joints with dowel-type fasteners. A numerical model was proposed, where the joint is

schematized as an elasto-plastic beam in a non-linear medium with a compression-only behaviour. In contrast with the differential approach adopted by most of the hysteresis models published in literature, the major advantage of this model is the use of basic input parameters (geometrical data of the fastener and average density of timber) and simplified mechanical relationships (elasto-plastic relationships). Simulations were carried out on a nailed steel-to-timber joint in CLT and results provided an accurate match with the test data obtained on similar systems.

The focus was then shifted to typical wall-to-floor connections for CLT structures. The connectors were modelled using 3D solid bodies while the nailed joints were schematized as non-linear springs. Shear and tension tests were reproduced on typical connections and results were compared to the experimental data obtained on similar test setups, leading to limited differences. Furthermore, the mechanical behaviour when shear and tension loads are applied simultaneously was investigated. Results pointed out that the loading direction has a significant effect on the stiffness and the load-carrying capacity of the connections. Moreover, a quadratic interaction domain was observed between shear and axial loads.

Finally, the hysteretic behaviour of CLT wall systems was investigated. Racking tests were reproduced on typical wall systems by varying the assumptions used to schematize the behaviour of the connections. Results highlighted that it is necessary to consider the contribution of angle brackets in the axial direction to obtain realistic predictions of the load-carrying capacity. Furthermore, simulations pointed out that is important to consider the friction at the base of the walls to obtain accurate predictions of the dissipated energy. The mechanical behaviour of segmented CLT wall systems was then analysed. Numerical results showed that the vertical step joints between adjacent wall panels have a significant influence on the mechanical behaviour and the energy dissipation of a wall system.

6.2 RECOMMENDATIONS FOR FUTURE RESEARCH

CLT structures are relatively new building systems and there is still a significant amount of further research required. Some specific aspects that have been identified from this research work are listed below:

- Development of analytical predictive models for typical connections used in CLT structural systems, so as to provide input information for analytical and numerical models of CLT buildings;
- Continuation of work on the development of non-linear spring elements, to improve the reliability of the numerical analyses, with specific attention to the mechanical behaviour under the simultaneous presence of shear and tension loads;
- Parametric studies on long monolithic and segmented walls systems, coupled with vertical step joints, to understand the differences in behaviour when the layout and the position of the connections is varied;
- Parametric studies on wall systems with openings, to gain a better understanding of the behaviour when the in-plane stiffness of the wall panel is reduced;
- Parametric studies on multi-storey wall systems, to highlight the influence of the horizontal floors on the mechanical behaviour and the energy dissipation;
- Analyses of the interaction among different structural systems, with specific focus on hybrid solutions and/or mixed solutions, e.g. CLT wall systems and light-frame constructions, or CLT structural systems and reinforced concrete walls.

References

1. Ashtari S (2012) In-plane stiffness of Cross-Laminated Timber floors. *MS Thesis*. University of British Columbia, Vancouver, Canada.
2. Blaß HJ, Bienhaus A, Krämer V (2001) Effective bending capacity of dowel-type fasteners. *International RILEM Symposium on Joints in Timber Structures*, Cachan, France.
3. Blaß HJ, Uibel T (2007) *Tragfähigkeit von stiftförmigen Verbindungsmitteln in Brettsperrholz*. **8**, Karlsruher Berichte zum Ingenieurholzbau, Karlsruhe, Germany, doi: 10.5445/KSP/1000006318.
4. Blaß HJ, Schädle P (2011) Ductility aspects of reinforced and non-reinforced timber joints. *Engineering Structures,* **33**(11): 3018-3026, doi: 10.1016/j.engstruct.2011.02.001.
5. Blaß HJ, Colling F (2015) Load-carrying capacity of dowelled connections. *INTER 2015 Meeting*, Šibenik, Croatia, Paper 48-7-3.
6. Brandner R, Flatscher G, Ringhofer A, Schickhofer G, Thiel A (2016) Cross laminated timber (CLT): overview and development. *European Journal of Wood and Wood Products,* **74**(3): 331-351, doi: 10.1007/s00107-015-0999-5.
7. Casagrande D, Polastri A, Sartori T, Loss C, Chiodega M (2016) Experimental campaign for the mechanical characterization of connection systems in the seismic design of timber buildings. *World Conference on Timber Engineering (WCTE)*, Vienna, Austria.
8. Casagrande D, Doudak G, Mauro L, Polastri A (2017) Analytical approach to establish the elastic behaviour of multi-panel CLT shear-walls subjected to lateral loads. *Journal of Structural Engineering (under review)*.
9. Ceccotti A, Fragiacomo M, Giordano S (2007) Long-term and collapse tests on a timber-concrete composite beam with glued-in connection. *Materials and Structures,* **40**(1): 15-25, doi: 10.1617/s11527-006-9094-z.
10. Ceccotti A, Sandhaas C, Okabe M, Yasumura M, Minowa C, Kawai N (2013) SOFIE project - 3D shaking table test on a seven-storey full-scale cross-laminated building. *Earthquake Engineering & Structural Dynamics,* **42**(13): 2003-2021, doi: 10.1002/eqe.2309.
11. Chui YH, Ni C (1997) Load-embedment response of timber to reversed cyclic load. *Wood and Fiber Science,* **29**(2): 148-160.

12. Chui YH, Ni C, Jiang L (1998) Finite-element model for nailed wood joints under reversed cyclic load. *Journal of Structural Engineering,* **124**(1): 96-103, doi: 10.1061/(ASCE)0733-9445(1998)124:1(96).
13. Coste G (2010) The assessment and applications of a new connector type for use in timber structural systems. *PhD Thesis*. Edinburgh Napier University, Edinburgh, United Kingdom.
14. Domínguez M, González Fueyro JL, Cabezas JA (2017) Accounting of the thread embedment in timber structures dowel-type joints. Load-slip relationship. *Proceedings of the Institution of Mechanical Engineers, Part C: Journal of Mechanical Engineering Science* **231**(1): 150-160, doi: 10.1177/0954406216663578.
15. Dujic B, Pucelj J, Zarnic R (2004) Testing of racking behavior of massive wooden wall panels. *37th CIB-W18 Meeting*, Edinburgh, Scotland, Paper 37-15-2.
16. Dujic B, Aicher S, Zarnic R (2005) Racking of wooden walls exposed to different boundary conditions. *38th CIB-W18 Meeting*, Karlsruhe, Germany, Paper 38-15-6.
17. Dujic B, Klobcar S, Zarnic R (2007) Influence of openings on shear capacity of wooden walls. *40th CIB-W18 Meeting*, Bled, Slovenia, Paper 40-15-6.
18. Ehlbeck J, Larsen HJ (1993) Eurocode 5 - Design of Timber Structures: Joints. *International Workshop on Wood Connectors*, Madison, Wisconsin, USA.
19. EN 383 (2007) Timber structures. Test methods. Determination of embedment strength and foundation values for dowel type fasteners. CEN, Brussels, Belgium.
20. EN 384 (2016) Structural timber. Determination of characteristic values of mechanical properties and density. CEN, Brussels, Belgium.
21. EN 409 (2009) Timber structures. Test methods. Determination of the yield moment of dowel type fasteners. CEN, Brussels, Belgium.
22. EN 1380 (2009) Timber structures. Test methods. Load bearing nails, screws, dowels and bolts. CEN, Brussels, Belgium.
23. EN 1382 (2016) Timber structures. Test methods. Withdrawal capacity of timber fasteners. CEN, Brussels, Belgium.
24. EN 1995-1-1:2004/A2 (2014) Eurocode 5: Design of timber structures. Part 1-1: General. Common rules and rules for buildings. CEN, Brussels, Belgium.
25. EN 1998-1:2004/A1 (2013) Eurocode 8: Design of structures for earthquake resistance. Part 1: General rules, seismic actions and rules for buildings. CEN, Brussels, Belgium.

26. EN 12512:2001/A1 (2005) Timber structures. Test methods. Cyclic testing of joints made with mechanical fasteners. CEN, Brussels, Belgium.

27. EN 13183-1 (2002) Moisture content of a piece of sawn timber - Part 1 - Determination by oven dry method. CEN, Brussels, Belgium.

28. EN 14358 (2016) Timber structures. Calculation and verification of characteristic values. CEN, Brussels, Belgium.

29. EN 26891 (1991) Timber structures. Joints made with mechanical fasteners. General principles for the determination of strength and deformation characteristics CEN, Brussels, Belgium.

30. ETA-04/0013 (2015) European Technical Assessment. Nails and screws for use in nailing plates in timber structures. ETA-Denmark, Nordhavn, Denmark.

31. ETA-06/0106 (2014) European Technical Assessment. Three-dimensional nailing plate (timber-to-timber/timber-to-concrete angle bracket). ETA-Denmark, Nordhavn, Denmark.

32. ETA-11/0030 (2016) European Technical Assessment. Screws for use in timber constructions. ETA-Denmark, Nordhavn, Denmark.

33. ETA-11/0086 (2015) European Technical Assessment. Three-dimensional nailing plate (Angle brackets and hold-downs for timber-to-timber or timber-to-concrete or steel connections). ETA-Denmark, Nordhavn, Denmark.

34. ETA-11/0496 (2014) European Technical Assessment. Three-dimensional nailing plate (Angle bracket for timber-to-timber or timber-to-concrete or steel connections). ETA-Denmark, Nordhavn, Denmark.

35. ETA-13/0523 (2013) European Technical Assessment. Annular ring shank nails and connector screws. ETA-Denmark, Nordhavn, Denmark.

36. Fahrni R (2016) Finite-element modeling of timber connections. *MS Thesis*. ETH Zurich, Zurich, Switzerland.

37. Flatscher G (2010) Außergewöhnliche Einwirkung „Erdbeben“ - Überlegungen zur versuchstechnischen Erfassung der Verbindungstechnik im Holz-Massivbau. *Masterarbeit*. Technische Universität Graz, Graz, Austria.

38. Flatscher G, Schickhofer G (2015) Shaking-table test of a cross-laminated timber structure. *Proceedings of the ICE - Structures and Buildings,* **168**(11): 878-888, doi: 10.1680/stbu.13.00086.

39. Flatscher G, Bratulic K, Schickhofer G (2015) Experimental tests on cross-laminated timber joints and walls. *Proceedings of the ICE - Structures and Buildings,* **168**(11): 868-877, doi: 10.1680/stbu.13.00085.

40. Flatscher G, Schickhofer G (2016) Displacement-based determination of laterally loaded Cross Laminated Timber (CLT) wall systems. *INTER 2016 Meeting*, Graz, Austria, Paper 49-12-1.

41. Foliente GC (1995) Hysteresis modeling of wood joints and structural systems. *Journal of Structural Engineering,* **121**(6): 1013-1022, doi: 10.1061/(ASCE)0733-9445(1995)121:6(1013).

42. Follesa M, Fragiacomo M, Vassallo D, Piazza M, Tomasi R, Rossi S, Casagrande D (2015) A proposal for a new Background Document of Chapter 8 of Eurocode 8. *INTER 2015 Meeting*, Šibenik, Croatia, Paper 48-7-3.

43. Folz B, Filiatrault A (2001) Cyclic analysis of wood shear walls. *Journal of Structural Engineering,* **127**(4): 433-441, doi: 10.1061/(ASCE)0733-9445(2001)127:4(433).

44. Fortino S, Mirianon F, Toratti T (2009) A 3D moisture-stress FEM analysis for time dependent problems in timber structures. *Mechanics of Time-Dependent Materials,* **13**: 333-356, doi: 10.1007/s11043-009-9103-z.

45. Foschi RO (2000) Modeling the hysteretic response of mechanical connections for wood structures. *World Conference on Timber Engineering (WCTE)*, Whistler, British Columbia, Canada.

46. Fragiacomo M, Dujic B, Sustersic I (2011) Elastic and ductile design of multi-storey crosslam massive wooden buildings under seismic actions. *Engineering Structures,* **33**(11): 3043-3053, doi: 10.1016/j.engstruct.2011.05.020.

47. Gavric I, Fragiacomo M, Ceccotti A (2015) Cyclic behaviour of typical metal connectors for cross laminated (CLT) structures. *Materials and Structures,* **48**(6): 1841-1857, doi: 10.1617/s11527-014-0278-7.

48. Gavric I, Fragiacomo M, Ceccotti A (2015) Cyclic behavior of typical screwed connections for cross-laminated (CLT) structures. *European Journal of Wood and Wood Products,* **73**(2): 179-191, doi: 10.1007/s00107-014-0877-6.

49. Gavric I, Fragiacomo M, Ceccotti A (2015) Cyclic behavior of CLT wall systems: Experimental tests and analytical prediction models. *Journal of Structural Engineering,* **141**(11): 04015034(1-14), doi: 10.1061/(ASCE)ST.1943-541X.0001246.

50. Glišović I, Boško S, Tatjana K-M (2012) Embedment test of wood for dowel-type fasteners. *Wood Research,* **57**(4): 639-650.

51. González Fueyro JL, Domínguez M, Cabezas JA, Cabezas MP (2009) Design of connections with metal dowel-type fasteners in double shear. *Materials and Structures,* **42**(3): 385-397, doi: 10.1617/s11527-008-9389-3.

52. He M, Lam F, Foschi RO (2001) Modeling three-dimensional timber light-frame buildings. *Journal of Structural Engineering,* **127**(8): 901-913, doi: 10.1061/(ASCE)0733-9445(2001)127:8(901).

53. Hilson BO (1995) Joints with dowel-type fasteners - Theory. *Timber Engineering STEP 1: Basis of design, material properties, structural components and joints*, pp: C3/1-11, Centrum Hout, Almere, The Netherlands.

54. Hong J-P, Barrett D (2010) Three-dimensional finite-element modeling of nailed connections in wood. *Journal of Structural Engineering,* **136**(6): 715-722, doi: 10.1061/ASCE ST.1943-541X.0000160.

55. Hristovski V, Dujic B, Stojmanovska M, Mircevska V (2013) Full-scale shaking-yable tests of XLam panel systems and numerical verification: Specimen 1. *Journal of Structural Engineering,* **139**(11): 2010-2018, doi: 10.1061/(ASCE)ST.1943-541X.0000754.

56. Hummel J, Flatscher G, Seim W, Schickhofer G (2013) CLT wall elements under cyclic loading - Details for anchorage and connection. *COST Action FP1004, Focus solid timber solutions - European Conference on Cross Laminated Timber (CLT)*, pp: 152-165, Graz, Austria.

57. ISO 16670 (2003) Timber Structures. Joints made with mechanical fasteners. Quasi-static reversed-cyclic test method. ISO, Geneva, Switzerland.

58. Ivanov IM (1949) The new measure of the strength of wood and methods of its determination. *Bulletin of the Forest Institute of Academy of Science of USSR,* **4**: 34-45.

59. Izzi M, Flatscher G, Fragiacomo M, Schickhofer G (2016) Experimental investigations and design provisions of steel-to-timber joints with annular-ringed shank nails for Cross-Laminated Timber structures. *Construction and Building Materials,* **122**: 446-457, doi: 10.1016/j.conbuildmat.2016.06.072.

60. Izzi M, Rinaldin G, Polastri A, Fragiacomo M (2016) Numerical modelling of joints with dowel-type fasteners. *European Journal of Wood and Wood Products (under review)*.

61. Izzi M, Polastri A, Fragiacomo M (2017) Modelling the mechanical behaviour of typical wall-to-floor connection systems for Cross-Laminated Timber structures. *Engineering Structures (under review)*.

62. Johansen KW (1949) Theory of timber connections. *International Association of Bridge and Structural Engineering,* **9**: 249-262, doi: 10.5169/seals-9703.

63. Jorissen A, Fragiacomo M (2011) General notes on ductility in timber structures. *Engineering Structures,* **33**(11): 2987-2997, doi: 10.1016/j.engstruct.2011.07.024.

64. Joyce T, Smith I, Ballerini M (2011) Mechanical behaviour of in-plane shear connections between CLT wall panels. *44th CIB-W18 Meeting*, Alghero, Italy, Paper 44-7-2.

65. Judd JP, Fonseca FS (2005) Analytical model for sheathing-to-framing connections in wood shear walls and diaphragms. *Journal of Structural Engineering,* **131**(2): 345-352, doi: 10.1061/(ASCE)0733-9445(2005)131:2(345).

66. Karagiannis V, Málaga-Chuquitaype C, Elghazouli AY (2016) Modified foundation modelling of dowel embedment in glulam connections. *Construction and Building Materials,* **102**: 1168-1179, doi: 10.1016/j.conbuildmat.2015.09.021.

67. Kuenzi EW (1955) *Theoretical design of nailed or bolted joint under lateral load*. United States Department of Agriculture, Forest Service, Forest Laboratory Products, Report No: D1951 (revised March 1955), Madison, Wisconsin, USA.

68. Laggner TM, Flatscher G, Schickhofer G (2016) Combined loading of self-tapping screws. *World Conference on Timber Engineering (WCTE)*, Vienna, Austria.

69. Li M, Foschi RO, Lam F (2012) Modeling hysteretic behavior of wood shear walls with a protocol-independent nail connection algorithm. *Journal of Structural Engineering,* **138**(1): 99-108, doi: 10.1061/(ASCE)ST.1943-541X.0000438.

70. Liu J, Lam F (2016) Experimental test of Cross Laminated Timber connections under bi-directional loading. *World Conference on Timber Engineering (WCTE)*, Vienna, Austria.

71. Mack JJ (1966) The strength and stiffness of nailed joints under short-duration loading. *Division of Forest Products, Technological Paper n. 40*, Commonwealth Scientific and Industrial Research Organization, Melbourne Australia.

72. Meghlat EM, Oudjene M, Ait-Aider H, Batoz JL (2013) A new approach to model nailed and screwed timber joints using the finite element method. *Construction and Building Materials,* **41**: 263-269, doi: 10.1016/j.conbuildmat.2012.11.068.

73. Muñoz W, Mohammad M, Salenikovich A, Quenneville P (2008) Need for a harmonized approach for calculations of ductility of timber assemblies. *41st CIB-W18 Meeting*, St. Andrews, Canada, Paper 41-15-1.

74. Muñoz W, Mohammad M, Salenikovich A, Quenneville P (2008) Determination of yield point and ductility of timber assemblies: in search for a harmonised approach. *World Conference on Timber Engineering (WCTE)*, Miyazaki, Japan.

75. ÖNORM B 1995-1-1 (2014) Eurocode 5. Bemessung und Konstruktion von Holzbauten. Teil 1-1: Allgemeines. Allgemeine Regeln und Regeln für den Hochbau. Nationale Festlegungen zur Umsetzung der ÖNORM EN 1995-1-1 nationale Erläuterungen und nationale Ergänzungen. ÖN, Wien, Austria.

76. Oudjene M, Meghlat EM, Ait-Aider H, Batoz JL (2013) Non-linear finite element modelling of the structural behaviour of screwed timber-to-concrete composite connections. *Composite Structures,* **102**: 20-28, doi: 10.1016/j.compstruct.2013.02.007.

77. Pedersen MU (2002) Dowel type timber connections - Strength modelling. *PhD Thesis*. Technical University of Denmark, Copenhagen, Denmark.

78. Plesnik T, Erochko J, Doudak G (2016) Nailed connection behavior in light-frame wood shear walls with an intermediate layer of insulation. *Journal of Structural Engineering,* **142**(7): 04016045(1-9), doi: 10.1061/(ASCE)ST.1943-541X.0001506.

79. Polastri A, Pozza L (2016) Proposal for a standardized design and modeling procedure of tall CLT buildings. *International Journal for Quality Research,* **10**(3): 607-624, doi: 10.18421/IJQR10.03-12.

80. Popovski M, Karacabeyli E (2011) Seismic performance of Cross-Laminated Wood panels. *44th CIB-W18 Meeting*, Alghero, Italy, Paper 44-15-7.

81. Popovski M, Gavric I (2016) Performance of a 2-story CLT house subjected to lateral loads. *Journal of Structural Engineering,* **142**(4): E4015006(1-12), doi: 10.1061/(ASCE)ST.1943-541X.0001315.

82. Porteous J (2003) The structural behaviour of timber joints made with fully overlapping nails. *PhD Thesis*. Napier University, Edinburgh, United Kingdom.

83. Pozza L, Massari M, Savoia M, Ferracuti B (2016) Experimental campaign of mechanical CLT connections subjected to a combination of shear and tension forces. *Structures and Architecture: Beyond their Limits*: 110-118, doi: 10.1201/b20891-13.

84. Pozza L, Scotta R, Trutalli D, Polastri A, Smith I (2016) Experimentally based *q*-factor estimation of cross-laminated timber walls. *Proceedings of the ICE - Structures and Buildings,* **169**(7): 492-507, doi: 10.1680/jstbu.15.00009.

85. Rinaldin G (2012) Modellazione e analisi non lineare di strutture in muratura e legno. *PhD Thesis*. University of Trieste, Trieste, Italy.

86. Rinaldin G, Amadio C, Fragiacomo M (2013) A component approach for the hysteretic behaviour of connections in cross-laminated wooden structures. *Earthquake Engineering & Structural Dynamics,* **42**(13): 2023-2042, doi: 10.1002/eqe.2310.

87. Rinaldin G, Amadio C, Macorini L (2016) A macro-model with nonlinear springs for seismic analysis of URM buildings. *Earthquake Engineering & Structural Dynamics,* **45**(14): 2261-2281, doi: 10.1002/eqe.2759.

88. Rinaldin G, Fragiacomo M (2016) Non-linear simulation of shaking-table tests on 3- and 7-storey X-Lam timber buildings. *Engineering Structures,* **113**: 133-148, doi: 10.1016/j.engstruct.2016.01.055.

89. Sandhaas C, Boukes J, Van de Kuilen J-WG, Ceccotti A (2009) Analysis of X-lam panel-to-panel connections under monotonic and cyclic loading. *42nd CIB-W18 Meeting*, Dübendorf, Zürich, Swizerland, Paper 42-12-2.

90. Sandhaas C, Van de Kuilen J-WG, Blaß HJ (2012) Constitutive model for wood based on continuum damage mechanic. *World Conference on Timber Engineering (WCTE)*, Auckland, New Zealand.

91. Sandhaas C (2013) Material model for wood. *Heron*, **53**(2-3), pp: 179-200, Stevin Lab. and Inst. TNO for Bldg Materials and Structures, Delft, The Netherlands.

92. Sandhaas C, Mergny E (2016) Yiel moment of nails. *INTER 2016 Meeting*, Graz, Austria, Paper Note 1.

93. Santos CL, De Jesus AMP, Morais JJL, Lousada JLPC (2008) Quasi-static mechanical behaviour of a double-shear single dowel wood connection. *Construction and Building Materials,* **23**: 171-182, doi: 10.1016/j.conbuildmat.2008.01.005.

94. Sewata K, Yasumura M (2002) Determination of embedding strength of wood for dowel-type fasteners. *Journal of Wood Science,* **48**(2): 138-146, doi: 10.1007/BF00767291.

95. Shahnewaz M, Tannert T, Alam MS, Popovski M (2016) In-plane stiffness of CLT panels with and without openings. *World Conference on Timber Engineering (WCTE)*, Vienna, Austria.

96. Simulia DS (2012) *ABAQUS 6.12 Documentation*. Providence, Rhode Island, USA.

97. Sustersic I, Fragiacomo M, Dujic B (2016) Seismic analysis of Cross-Laminated multistory timber buildings using code-drescribed methods: Influence of panel size, connection ductility, and schematization. *Journal of Structural Engineering,* **142**(4): E4015012(1-14), doi: 10.1061/(ASCE)ST.1943-541X.0001344.

98. Talledo D, Pozza L, Saetta A, Savoia M (2016) Coupled shear-tension numerical model for modelling of CLT connections. *World Conference on Timber Engineering (WCTE)*, Vienna, Austria.

99. Tomasi R, Smith I (2015) Experimental characterization of monotonic and cyclic loading responses of CLT panel-to-foundation angle bracket connections. *Journal of Materials in Civil Engineering,* **27**(6): 04014189(1-10), doi: 10.1061/(ASCE)MT.1943-5533.0001144.

100. Uibel T, Blaß HJ (2006) Load carrying capacity of joints with dowel type fasteners in solid wood panels. *39th CIB-W18 Meeting*, Florence, Italy, Paper 39-7-5.

101. Whale LRJ, Smith I, Hilson BO (1989) Characteristic properties of nailed and bolted joints under short-term lateral load, Part 4 - The influence of testing mode and fastener diameter upon embedment test data. *Journal of the Institute of Wood Science,* **11**(5): 156-161.

102. Xu J, Dolan JD (2009) Development of nailed wood joint element in ABAQUS. *Journal of Structural Engineering,* **135**(8): 968-976, doi: 10.1061/ ASCE ST.1943-541X.0000030.

103. Yasumura M, Kobayashi K, Okabe M (2016) Failure analysis of CLT shear walls with openings subjected to horizontal and vertical loads. *World Conference on Timber Engineering (WCTE)*, Vienna, Austria.

104. Yasumura M, Kobayashi K, Okabe M, Miyake T, Matsumoto K (2016) Full-scale tests and numerical analysis of low-rise CLT structures under lateral loading. *Journal of Structural Engineering,* **142**(4): E4015007(1-12), doi: 10.1061/(ASCE)ST.1943-541X.0001348.

105. Zhou T, Guan Z (2006) Review of existing and newly developed approaches to obtain timber embedding strength. *Progress in Structural Engineering and Materials,* **8**(2): 49-67, doi: 10.1002/pse.213.